

Aus der Klinik für Neurologie mit Experimenteller Neurologie
der Medizinischen Fakultät Charité – Universitätsmedizin Berlin

DISSERTATION

Einfluss von Indomethazin auf die adulte hippocampale Neurogenese
und viskoelastische Eigenschaften des Gehirns
im MPTP-Mausmodell für Dopamindepletion

zur Erlangung des akademischen Grades
Doctor medicinae (Dr. med.)

vorgelegt der Medizinischen Fakultät
Charité – Universitätsmedizin Berlin

von

Elisabeth Gertrud Hain

aus Stollberg/Erzgeb.

Datum der Promotion: 06.03.2020

Inhaltsverzeichnis

Abkürzungsverzeichnis.....	3
Abstract (deutsch)	5
Abstract (english)	6
1. Einleitung.....	7
2. Material und Methodik.....	8
2.1. Tiere	8
2.2. <i>In-vivo</i> -Behandlungen und Untersuchungen	8
2.2.1. MPTP-Mausmodell für Dopamindepletion	8
2.2.2. 5'-Bromo-2'-desoxyuridin (BrdU)-Injektion	10
2.2.3. Indomethazinbehandlung	10
2.2.4. Magnetresonanz-Elastographie (MRE).....	11
2.3. Versuchsaufbau	12
2.3.1. Studie 1: MRE-Hippocampus-Studie	12
2.3.2. Studie 2: MRE-SN-Studie.....	12
2.3.3. Studie 3: Indomethazin-Studie.....	13
2.4. Perfusion und Probengewinnung	13
2.5. Histologie und Zellquantifizierung	13
2.5.1. Immunhistochemie	13
2.5.2. Immunfluoreszenz	14
2.6. Molekularbiologie	15
2.6.1. Enzymatisches Immunadsorptionsverfahren	15
2.6.2. Quantitative Polymerase-Kettenreaktion.....	15
2.7. Statistische Analyse und Darstellung	16
3. Ergebnisse.....	16
3.1. MRE-Hippocampus-Studie (Studie 1): Transient höhere Elastizität im Hippocampus ist assoziiert mit kurzfristig gesteigerter Neurogenese nach Dopamindepletion	16
3.2. MRE-SN-Studie (Studie 2): Reduktion der Viskoelastizität in der SN ist assoziiert mit dem Verlust dopaminerger Neurone nach MPTP-Behandlung	17
3.3. Indomethazin-Studie (Studie 3): Höhere Überlebensrate neuer Neurone im DG durch Indomethazinbehandlung nach MPTP-Gabe in Zusammenhang mit verringerter zellulärer Inflammation und hochregulierter proneurogener Signalwege.....	18
4. Diskussion	19
4.1. Schlussfolgerung	22
5. Literaturverzeichnis.....	24
Eidesstattliche Versicherung	27
Anteilserklärung an den ausgewählten Publikationen.....	28
Druckexemplare der ausgewählten Publikationen	29
Lebenslauf.....	71
Komplette Publikationsliste.....	73
Danksagung	74

Abkürzungsverzeichnis

%	Prozent
φ	Phasenwinkel
ANOVA	Varianzanalyse, engl. analysis of variance
abs(G*)	Magnitude
BrdU	5'-Bromo-2'-desoxyuridin
°C	Grad Celsius
CD	Cluster-of-Differentiation
cDNA	komplementäre Desoxyribonukleinsäure, engl. complementary deoxyribonucleic acid
COX	Cyclooxygenase
CTR	Kontrolltiere für MPTP
D	dimensional
DAPI	4',6-Diamidin-2-phenylindol
DCX	Doublecortin
DG	Gyrus dentatus
dpi	Tag <i>post injectionem</i> , engl. post-injection day
ELISA	enzymatisches Immunadsorptionsverfahren, engl. enzyme-linked immunosorbent assay
engl.	englisch
F	F-Wert der Varianzanalysen
FLASH	engl. Fast Low Angle Shot
g	Gramm
g	Erdbeschleunigung
G*	komplexes Schermodul
G'	Realteil des komplexen Schermoduls G*
G''	Imaginärteil des komplexen Schermoduls G*
GFP	grün fluoreszierendes Protein
H ₂ O ₂	Wasserstoffperoxid
HCl	Chlorwasserstoff
Hz	Hertz
Iba1	Ionisiertes-Calcium-bindendes-Adaptermolekül-1
IFN	Interferon
IL	Interleukin
i.p.	intraperitoneal
kg	Kilogramm
KG	Körpergewicht
kPa	Kilopascal
LT	Langzeitbehandlung, engl. long-term treatment
μ m	Mikrometer
μ l	Mikroliter
m	Meter
M	Molar

mg	Milligramm
mm	Millimeter
MPTP	1-Methyl-4-phenyl-1,2,3,6-tetrahydropyridin, 1-Methyl-4-phenyl-1,2,3,6-tetrahydropyridin-Hydrochlorid, 1-Methyl-4-(2'-methylphenyl)-1,2,3,6-tetrahydropyridin-Hydrochlorid
MRE	Magnetresonanz-Elastographie
MRT	Magnetresonanztomographie, Magnetresonanztomograph
ms	Millisekunden
MSG	bewegungssensitiver Gradient, engl. motion-sensitizing gradient
mT	Millitesla
n	Anzahl
NaCl	Kochsalzlösung
Nestin-GFP	Expression des grün fluoreszierenden Proteins unter dem Promotor für Nestin
NeuN	engl. Neuronal Nuclei
p	Signifikanzniveau
PBS	phosphatgepufferte Kochsalzlösung, engl. phosphate buffered saline
PBS+	phosphatgepufferte Kochsalzlösung angereichert mit Eselserum
PFA	Paraformaldehyd
RNA	Ribonukleinsäure, engl. ribonucleic acid
s	Sekunde
SN	Substantia nigra
ST	Kurzzeitbehandlung, engl. short-term treatment
TH	Thyrosinhydroxylase
TNF	Tumornekrosefaktor
vehicle	Kontrolltiere für Indomethazin
vs.	versus

Abstract (deutsch)

Die Neurogenese im Gyrus dentatus (DG) des Hippocampus kann durch diverse Faktoren wie eine modulierte Transmitterhomöostase oder Entzündung beeinflusst werden und ist auch in neurodegenerativen Erkrankungen verändert. Mediatoren einer Entzündung sind zum Beispiel Zytokine oder Prostaglandine, wobei letztere durch das Enzym Cyclooxygenase (COX) erzeugt werden. Ob eine COX-Hemmung und dadurch modulierte Entzündungsreaktionen die adulte Neurogenese im DG in neurodegenerativen Erkrankungen beeinflussen, ist bisher unklar. Eine veränderte Neurogenese oder ein neuronaler Zellverlust in neurodegenerativen Erkrankungen könnte außerdem zu einer modifizierten Zusammensetzung des zellulären Netzwerks führen und sich in den viskoelastischen Eigenschaften widerspiegeln, welche durch die Messparameter des neuen bildgebenden Verfahrens Magnetresonanz-Elastographie (MRE) ermittelt werden könnten. Veränderte viskoelastische Parameter des Gehirns wurden bereits in Patienten mit neurodegenerativen Erkrankungen beobachtet, aber bisher gibt es nur wenige Studien zur Untersuchung der zugrundeliegenden zellulären Mechanismen.

In der vorliegenden Arbeit wurden die Veränderungen viskoelastischer Eigenschaften mittels MRE und mögliche basierende zelluläre Mechanismen im Hippocampus (Studie 1) und in der SN (Studie 2) im 1-Methyl-4-phenyl-1,2,3,6-tetrahydropyridin (MPTP)-Mausmodell für Neurodegeneration mit resultierender Dopamindepletion untersucht. Des Weiteren wurde der Einfluss des nichtselektiven COX-Hemmers Indomethazin auf die adulte hippocampale Neurogenese und deren regulatorische Signalwege sowie die Entzündungsreaktionen im DG und SN eruiert (Studie 3). Die hippocampale Neurogenese und zelluläre Entzündungsreaktion wurden unter Zuhilfenahme immunhistochemischer Färbungen beurteilt. Ferner wurden Veränderungen neurogeneserelevanter Signalwege mit Hilfe der quantitativen Polymerase-Kettenreaktion und in Zytokinkonzentrationen mittels enzymatischen Immunadsorptionsverfahrens bestimmt.

Nach MPTP-Behandlung zeigte sich im Hippocampus eine transient höhere Anzahl neuer Vorläuferzellen, welche in einem kurzfristig gesteigerten prozentualen Anteil neuer Neurone resultierte und somit zu einer transient höheren Viskoelastizität führte. In der SN hatte der Verlust dopaminergischer Neurone eine Verringerung viskoelastischer Eigenschaften zur Folge. Die Anzahl neuer reifer Neurone im DG war zu einem späteren Zeitpunkt nach MPTP-Gabe vermindert, welches durch Indomethazinbehandlung, unterstützt durch hochregulierte proneurogene Signalwege, verhindert werden konnte. Dies war zudem mit einer verringerten zellulären Entzündungsreaktion assoziiert.

Zusammenfassend weisen die Ergebnisse darauf hin, dass Neurone zu den biomechanischen Eigenschaften eines Gewebes beitragen. Daher könnte die MRE durch Erfassung verminderter viskoelastischer Eigenschaften bei neurodegenerativen Erkrankungen ein mögliches klinisch diagnostisches Werkzeug sein. Ferner verhinderte der COX-Hemmer Indomethazin eine geschädigte Neurogenese und Entzündung nach Dopamindepletion. Dies trägt dazu bei nichtselektive COX-Hemmer als mögliche Medikamente zur Verbesserung der Neurogenese in neurodegenerativen Erkrankungen in Betracht zu ziehen.

Abstract (english)

Neurogenesis in the dentate gyrus (DG) of the hippocampus can be influenced by diverse factors, such as altered transmitter homeostasis or inflammation, and is also changed in neurodegenerative diseases. Mediators of inflammation are, for example, cytokines or prostaglandins. Last-mentioned mediators are catalyzed by the enzyme cyclooxygenase (COX). However, it is still not clear if COX inhibition and thus modulated inflammatory reactions influence adult neurogenesis in the DG in neurodegenerative diseases. In neurodegenerative diseases, altered neurogenesis or the loss of neurons could also lead to a changed composition of the cellular network and could be displayed in viscoelastic properties, which could be detected by parameters of the novel imaging technique magnetic resonance elastography (MRE). Altered viscoelastic parameters of the brain have already been observed in patients with neurodegenerative diseases, but to date only a few studies have researched the underlying cellular mechanisms.

Here, we investigated the alterations of viscoelastic properties using MRE and possible underlying cellular mechanism in the hippocampus (study 1) and in the SN (study 2) by applying the 1-methyl-4-phenyl-1,2,3,6-tetrahydropyridine (MPTP) mouse model of dopamine depletion. Moreover, we evaluated the influence of the nonselective COX inhibitor indomethacin on adult hippocampal neurogenesis and neurogenic signaling pathways as well as inflammation in the DG and SN (study 3). Hippocampal neurogenesis and cellular inflammation were investigated using immunohistochemical stainings. Furthermore, alterations in neurogenesis-relevant signaling pathways were analyzed using quantitative polymerase chain reaction, and concentrations of cytokines were quantified by enzyme-linked immunosorbent assay.

In the hippocampus, MPTP treatment caused a transiently increased amount of new progenitor cells resulting in a transiently increased percentage of new neurons leading to a temporarily higher viscoelasticity. In the SN, the loss of dopaminergic neurons led to a decrease of viscoelastic properties. At a later time point after MPTP administration, the number of new mature neurons was decreased in the DG. This could be prevented by indomethacin treatment, which was supported by upregulated proneurogenic signaling pathways, and was associated with a decreased cellular inflammation.

In conclusion, the MRE and histological results show that neurons contribute to the biomechanical tissue characteristics. Thus, decreased viscoelastic properties in neurodegenerative diseases observed by MRE may be a potential approach for clinical diagnosis. Furthermore, the COX inhibitor indomethacin prevented impaired adult neurogenesis and inflammation after dopamine depletion. This contributes to the validation of nonselective COX inhibitors as a potential therapeutic drug to restore neurogenesis in neurodegenerative diseases.

1. Einleitung

In mehreren Studien wurde eine Bildung neuer Neurone im Gyrus dentatus (DG) des Hippocampus eines erwachsenen Menschen beobachtet¹⁻³. Dabei befinden sich in der subgranulären Zone des DG die gliaähnlichen Stammzellen Typ-1, welche in der weiteren Proliferation und Differenzierung über die Stadien der Vorläuferzellen Typ-2a sowie Typ-2b in die sogenannten Neuroblasten Typ-3 übergehen. Von hier aus bilden sich proliferationsinaktive, unreife Neurone, die sich in der weiteren Entwicklung zu reifen Neuronen differenzieren⁴. Die Bildung neuer Neurone wird von vielen Faktoren, wie zum Beispiel Entzündungsprozesse oder Transmittersysteme, beeinflusst⁵. In Tierstudien konnte gezeigt werden, dass dopaminerge Fasern von der Substantia nigra (SN) zur subgranulären Zone ziehen und der Verlust dopaminergener Neurone in einer geänderten Bildung neuer Vorläuferzellen und verminderten Überlebensrate neuer Neurone im DG resultiert⁶⁻⁸. Auch in *post-mortem*-Studien zeigten sich im DG von Patienten mit idiopathischem Parkinsonsyndrom weniger Vorläuferzellen⁶, was zu den bekannten kognitiven Einschränkungen von Erkrankten beitragen könnte⁹.

Um eine möglichst frühzeitige Diagnosestellung und einen raschen Therapiebeginn von neurodegenerativen Erkrankungen in Zukunft zu ermöglichen, könnten mit Hilfe einer nichtinvasiven Methode namens Magnetresonanz-Elastographie (MRE), ähnlich wie bei der manuellen Palpation, die viskoelastischen Eigenschaften der zu untersuchenden Areale ermittelt werden^{10,11}. Bei Patienten mit der Parkinson-Krankheit wurde eine reduzierte Viskoelastizität im Nucleus lentiformis und atrophiebedingt im gesamten Gehirn festgestellt^{12,13}. Erste Studien im Tiermodell für Multiple Sklerose und Ischämie haben eine Korrelation von veränderter Viskoelastizität und Zellzusammensetzung gezeigt¹⁴⁻¹⁶. Inwieweit Veränderungen der biomechanischen Parameter in primär neurodegenerativen Erkrankungen, wie dem idiopathischen Parkinsonsyndrom, mit Abweichungen der Zellzusammensetzung von Neuronen, deren Vorläuferzellen sowie Gliazellen, deren Vernetzung und Dichte übereinstimmen, wurde bisher nicht untersucht.

Ein etabliertes Tiermodell für Neurodegeneration mit nachfolgender Dopamindepletion ist die Applikation des Opiumderivats 1-Methyl-4-phenyl-1,2,3,6-tetrahydropyridin (MPTP)¹⁷, welches in den 1980er Jahren Aufmerksamkeit aufgrund irreversibler Parkinsonsyndrome bei akzidentellem Konsum erlangte¹⁸. Die Injektion von MPTP führt zu einem Verlust dopaminergener Neurone in der SN¹⁷ und wird von entzündlichen Prozessen begleitet^{19,20}. Zudem konnten im MPTP-Tiermodell auch hippocampusassoziierte Defizite, zum Beispiel des räumlichen Arbeitsgedächtnisses, festgestellt werden^{21,22}.

Um die MRE als diagnostisches Werkzeug für neurodegenerative Erkrankungen weiter zu etablieren, wurden Messungen der viskoelastischen Parameter in den vulnerablen Gehirnbereichen des MPTP-Tiermodells durchgeführt und eine histologische Aufarbeitung dieser vorgenommen. Hierzu wurde zum einen der Zusammenhang zwischen den biomechanischen Eigenschaften im Hippocampus und die Bildung neuer Neurone und deren Vorläuferzellen untersucht (Studie 1: MRE-Hippocampus-Studie). Zum anderen wurde das Vorhandensein einer Übereinstimmung von viskoelastischer und zellulärer Veränderung in der SN eruiert (Studie 2: MRE-SN-Studie).

Neurodegenerative Erkrankungen werden zudem von entzündlichen Prozessen, zum Beispiel von der Aktivierung mikroglialer Zellen, Infiltration von Lymphozyten oder Freisetzung von

Botenstoffen, wie Zytokine als auch Prostaglandine, begleitet²⁰. Entzündliche Veränderungen beeinflussen selbst auch die adulte Neurogenese²³. Indomethazin, ein nichtselektiver Cyclooxygenase (COX)- Hemmer, konnte in früheren Studien mit Tiermodellen für Ischämie und radioaktiver Bestrahlung die Bildung neuer Neurone im Hippocampus, assoziiert mit einer Verminderung mikroglialer Aktivität, fördern^{24,25}. Ebenso zeigte sich in der SN ein geringerer Verlust dopaminerger Neurone nach MPTP bei präventiver Gabe von Indomethazin²⁶. Daher interessierten wir uns für den Einfluss von Indomethazin auf die Bildung neuer Neurone sowie deren Vorläuferstufen im DG und auf die entzündlichen Veränderungen im Hippocampus und SN im MPTP-Model für neurodegenerative Erkrankungen (Studie 3: Indomethazin-Studie).

2. Material und Methodik

2.1. Tiere

Sechs bis zwölf Wochen alte, weibliche C57Bl/6N-Mäuse (Charles River Laboratories Inc., Deutschland) und transgene C57Bl/6N-Mäuse aus der Forschungseinrichtung für experimentelle Medizin (Berlin, Deutschland), die das grün fluoreszierende Protein (GFP) unter dem Promotor für das Intermediärfilament Nestin (Nestin-GFP) exprimieren, wurden verwendet. Die Koexpression von GFP und Nestin unterstützt Nestin exprimierende Zellen, vornehmlich neuronale Vorläuferzellen, zu identifizieren²⁷. Die Tiere wurden in einem Standardkäfig in einem für Temperatur und Luftfeuchtigkeit kontrollierten Raum mit einem 12-Stunden-Tag/Nacht-Rhythmus sowie freiem Zugang zu Futter und Wasser gehalten. Alle Experimente wurden mit der Genehmigung vom Landesamt für Gesundheit und Soziales, Berlin und in Übereinstimmung mit den Richtlinien des Rates der Europäischen Gemeinschaft vom 22. September 2010 (2010/63/EEC) durchgeführt. Die Mäuse wurden pseudorandomisiert den Gruppen zugeordnet.

2.2. *In-vivo*-Behandlungen und Untersuchungen

2.2.1. MPTP-Mausmodell für Dopamindepletion

Zur Erreichung eines dopaminergen Zellverlustes in der SN erhielten die Mäuse in Studie 1 und 2 das Neurotoxin MPTP-Hydrochlorid (MPTP) und in Studie 3 1-Methyl-4-(2'-methylphenyl)-1,2,3,6-tetrahydropyridin-Hydrochlorid (auch 2'-Methyl-MPTP genannt, ebenso MPTP), gelöst in 0,9 % Kochsalzlösung (NaCl), mit einer Dosis von 20 mg/kg Körpergewicht (KG) an drei aufeinanderfolgenden Tagen intraperitoneal (i.p.). Kontrolltiere für MPTP (CTR) wurden stattdessen mit 0,9 % NaCl behandelt.

Die in den Studien verwendeten Substanzen sind in Tabelle 1 aufgelistet.

Tabelle 1: Liste der verwendeten Substanzen einschließlich verwendeter Dosis und Herstellerangabe

Substanz	Abkürzung	Dosis/ Eigenschaften	Hersteller
1-Methyl-4-phenyl-1,2,3,6-tetrahydropyridin-Hydrochlorid; 1-Methyl-4-(2'-methylphenyl)-1,2,3,6-tetrahydropyridin-Hydrochlorid	MPTP	20 mg/kg KG	Sigma-Aldrich Inc., St. Louis, USA; Geschenk von Prof. Dr. Christian Klein, Medizinische Chemie, Institut für Pharmazie und Molekulare Biotechnologie, Universität Heidelberg, Deutschland

2-Methylbutan		unverdünnt	Sigma-Aldrich Inc., St. Louis, USA
3,3'-Diaminobenzidin		0,025 mg/ml	Sigma-Aldrich Inc., St. Louis, USA
4',6-Diamidin-2-phenylindol	DAPI	1:1000	Thermo Fisher Scientific Inc., Waltham, USA
5'-Bromo-2'-desoxyuridin	BrdU	50 mg/kg KG	Sigma-Aldrich Inc., St. Louis, USA
5'-Bromo-2'-desoxyuridin-Antikörper	anti-BrdU	1:500	AbD Serotec, Kidlington, UK
Alexa-488-gekoppelter Antikörper		1:1000	Invitrogen AG, Carlsbad, USA
Alexa-647-gekoppelter Antikörper		1:300	Dianova GmbH, Hamburg, Deutschland
Aprotinin		1 µl/ml	Sigma-Aldrich Inc., St. Louis, USA
Bio-Plex Pro™ Mouse Cytokine Th17 Panel A 6-Plex Group 1			Bio-Rad Laboratories Inc., Hercules, USA
Biotinylierter Antikörper		1:250	Dianova GmbH, Hamburg, Deutschland
Boratpuffer		0,1 M, pH 8,5	Carl Roth GmbH + Co. KG, Karlsruhe, Deutschland
Chlorwasserstoff	HCl	2 N	Merck KGaA, Darmstadt, Deutschland
Cluster-of-differentiation-68-Antikörper	anti-CD68	1:400	AbD Serotec Kidlington, UK
Doublecortin-Antikörper	anti-DCX	1:100	Santa Cruz Biotechnology Inc., Dallas, USA
Eserum		3 %, 10 %	Sigma-Aldrich Inc., St. Louis, USA
Ethylenclykol		25 %	Carl Roth GmbH + Co. KG, Karlsruhe, Deutschland
Gapdh TaqMan® assay			Applied Biosystems, Foster City, USA
Gli TaqMan® assay			Applied Biosystems, Foster City, USA
Glycerin		25 %	Carl Roth GmbH + Co. KG, Karlsruhe, Deutschland
Grün-fluoreszierendes-Protein-Antikörper	anti-GFP	1:250, 1:200	Novus Biologicals, Abcam plc.
Hes5 TaqMan® assay			Applied Biosystems, Foster City, USA
High Capacity RNA-to-cDNA™ Kit			Applied Biosystems, Foster City, USA
Indomethazin		2,5 mg/kg KG	Chiesi Farmaceutici S.p.A., Parma, Italien
Ionisiertes-Calcium-bindendes-Adaptermolekül-1-Antikörper	anti-Iba1	1:1000	FUJIFILM Wako Chemicals Europe GmbH, Neuss, Deutschland
Isofluran		1,5 – 2 %	AbbVie Inc., North Chicago, USA

Ketaminhydrochlorid/Xylazin	Ketamin/ Xylazin	10 %/ 2 %, 0,1 ml/ 20 g KG	Provet AG, Lyssach, Schweiz
Kochsalzlösung	NaCl	0,9 %	B.Braun Melsungen AG, Melsung, Deutschland
Lef 1 TaqMan® assay			Applied Biosystems, Foster City, USA
Natriumborhydrit		1 mg/ml	Carl Roth GmbH + Co. KG, Karlsruhe, Deutschland
NeuroD6 TaqMan® assay			Applied Biosystems, Foster City, USA
Neuronal Nuclei-Antikörper	anti-NeuN	1:100	Merck Millipore, Billerica, USA
Ngn1 TaqMan® assay			Applied Biosystems, Foster City, USA
Nickelchlorid		0,01 % (0,4mg/ml)	Sigma-Aldrich Inc., St. Louis, USA
Nucleo Spin® RNA/Protein Kit			MACHEREY-NAGEL GmbH & Co. KG
Paraformaldehyd	PFA	4 %	Sigma-Aldrich Inc., St. Louis, USA
Phosphatgepufferter Kochsalzlösung	PBS	0,1M, pH 7,4	Carl Roth GmbH + Co. KG, Karlsruhe, Deutschland
ProTaq®Clear, ProTags®PARAMount			Quartett GmbH, Berlin, Deutschland
Rhodamin-X-gekoppelter Antikörper		1:250	Dianova, Hamburg, Deutschland
Saccharoselösung		20 %	Sigma-Aldrich Inc., St. Louis, USA
TaqMan® Fast Advanced Master Mix			Applied Biosystems, Foster City, USA
Thyrosinhydroxylase- Antikörper	anti-TH	1:10000	Sigma-Aldrich Inc., St. Louis, USA
Triton-X-100		0,1 %	Sigma-Aldrich Inc., St. Louis, USA
Vectastain® ABC Elite Kit	ABC Reagenz		Vector Laboratories Inc., Burlingame, USA
Wasserstoffperoxid	H ₂ O ₂	0,6 %, 0,3 %	Carl Roth GmbH + Co. KG, Karlsruhe, Deutschland

2.2.2. 5'-Bromo-2'-desoxyuridin (BrdU)-Injektion

Um die Zellproliferation und das Überleben neu gebildeter Zellen zu quantifizieren, erhielten die Mäuse, welche für die histologischen Untersuchungen bestimmt waren, in Studie 1 und 3 das Thymidinanalogon BrdU i.p. an drei aufeinanderfolgenden Tagen mit einer Konzentration von 50 mg/kg KG, beginnend am letzten Tag der MPTP- bzw. NaCl-Injektion.

2.2.3. Indomethazinbehandlung

Indomethazin ist ein Analgetikum aus der Gruppe der nichtsteroidalen Antirheumatika. Seine Wirkungsweise beruht auf der nichtselektiven Hemmung der COX-1 und -2, so dass durch die verminderte Bildung von Prostaglandinen eine Ausschüttung entzündungsfördernder Stoffe, wie zum Beispiel Zytokine, moduliert wird²⁸. In Studie 3 erhielten die Tiere der Interventionsgruppen

Indomethazin, gelöst in destilliertem Wasser, i.p. in einer Konzentration von 2,5 mg/kg KG. Kontrolltiere für Indomethazin (vehicle) wurden hingegen mit 0,9 % NaCl behandelt.

2.2.4. Magnetresonanz-Elastographie (MRE)

In den Studien 1 und 2 wurden Messungen viskoelastischer Eigenschaften des Gehirns mittels MRE durchgeführt. Die MRE beruht in diesen Studien auf der Induktion von Scherwellen, Aufnahme der Ausbreitung mittels eines 7 Tesla Magnetresonanztomographen (MRT, Bruker PharmaScan 70/16, Ettlingen, Deutschland) und Auswertung mit Welleninversionsalgorithmen. Während der Messungen waren die Tiere mit Isofluran/Sauerstoff anästhesiert. Wie ausführlich von Riek und Kollegen¹⁴ beschrieben wurden Scherwellen innerhalb des Gehirngewebes mechanisch induziert, indem Vibrationen mit einer Frequenz von 900 Hz durch einen sinusoidalen Strom und einer luftgekühlten Lorentz-Spule im magnetischen Randfeld des MRTs generiert und über einen Beißstab auf das Tier übertragen wurden. Die Bildakquisition erfolgte mit einer FLASH-Sequenz, modifiziert mit einem sinusoidalen, bewegungssensitiven Gradienten (engl. motion-sensitizing gradient, MSG) in Schichtselektionsrichtung mittels ParaVision 4.0 Software (Bruker BioSpin, Ettlingen, Germany). Weitere Parameter waren: 9 Zyklen, 285 mT/m MSG-Amplitude, 116,2 ms Wiederholungszeit, 128 x 128 Matrixgröße, 25 mm Sichtfeld, 2 mm Schichtdicke, 14,3 ms Echozeit, 8 Aufnahmen über einen Zyklus und 20 Minuten Aufnahmezeit. Die viskoelastischen Parameter wurden aus dem komplexen Schermodul G^* , welcher mithilfe einer 2D-Helmholtz-Inversion aus den Wellenbildern bestimmt und räumlich über die relevanten Messbereiche gemittelt wurde, berechnet. Die relevanten Messbereiche: Hippocampus (Studie 1 und 2), gesamtes Gehirn (Studie 1), SN (Studie 2) und Mittelhirn exklusive SN (Studie 2) wurden manuell in einer T1-gewichteten Aufnahme eingezeichnet. Das komplexe Schermodul G^* besteht aus dem Realteil, „storage modulus“, $G' = \text{Re}(G^*)$, Parameter für Elastizität, und dem Imaginärteil, „loss modulus“, $G'' = \text{Im}(G^*)$, Parameter für Viskosität, welcher vor allem aus der Geometrie und Dichte des mechanischen Netzwerks bestimmt wird. Insbesondere in elastischen Geweben kann die Elastizität und Viskosität auch durch die Parameter Magnitude $\text{abs}(G^*)$ und dem Phasenwinkel φ dargestellt werden.

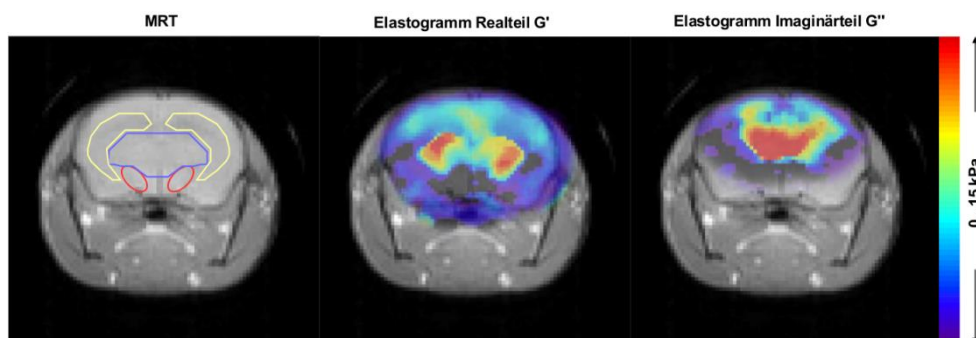


Abbildung 1: Repräsentative Bilder der Magnetresonanz-Elastographie (MRE)-Signale in T1-Wichtung zur Einzeichnung der Messbereiche (rot: Substantia nigra, gelb: Hippocampus, blau: Mittelhirn) und Magnetresonanz-Elastogramme des Realteils G' und Imaginärteils G'' in Kilopascal (kPa). (Modifiziert aus Referenz 29).

2.3. Versuchsaufbau

2.3.1. Studie 1: MRE-Hippocampus-Studie

Mit einer Gruppe unbehandelter, transgener Nestin-GFP-C57Bl/6N-Mäuse (n=5) wurden MRE-Messungen zur Ermittlung der Ausgangswerte viskoelastischer Parameter an Tag -3 *post injectionem* (engl. post-injection day, dpi) durchgeführt. Hiernach wurde diesen Tieren als CTR-Gruppe 0,9 % NaCl i.p. an -2, -1 und 0 dpi injiziert und es erfolgten weitere MRE-Messungen an 3, 6, 10, 14 und 18 dpi. Im weiteren Verlauf wurde denselben Tieren nach Abschluss der Kontrollmessungen MPTP an -2, -1 und 0 dpi i.p. injiziert und es fanden weitere MRE-Messungen an 3, 6, 10, 14 und 18 dpi statt. Parallel zu den Tieren, welche die MRE-Messungen durchliefen, wurden weitere elf Gruppen von transgenen Nestin-GFP-C57Bl/6N-Mäusen (n=5) als histologische Referenzgruppen zu den MRE-Messungen gebildet. Eine Gruppe wurde als Ausgangsgruppe an -3 dpi perfundiert. Die anderen Gruppen wurden entweder mit 0,9 % NaCl oder MPTP i.p. an -2, -1 und 0 dpi behandelt und an den jeweiligen Messtagen (3, 6, 10, 14, 18 dpi) perfundiert. Den Mäusen der histologischen Gruppen wurde zudem zur Identifikation sich teilender Zellen in der unter 2.2.2. beschriebenen Methode BrdU verabreicht, wobei die Tiere der Ausgangsgruppe an -3 dpi zehn Stunden vor Perfusion BrdU erhielten. Das Schema der zeitlichen Abfolge befindet sich in Abbildung 2.

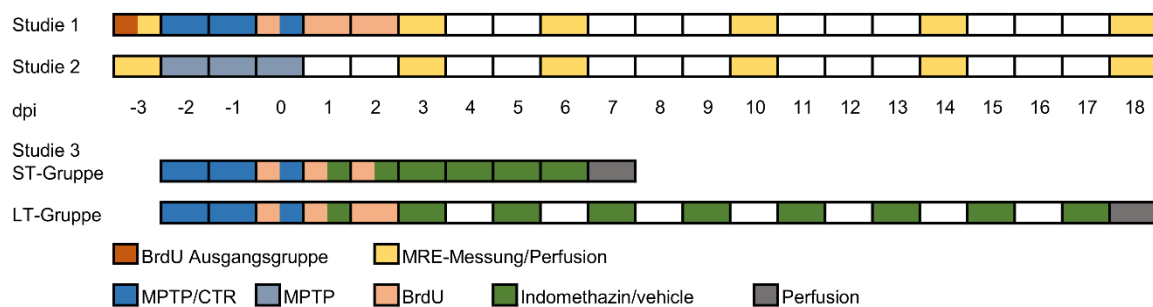


Abbildung 2: Schematischer Versuchsaufbau aller drei Studien. dpi: post-injection day, ST: short-term treatment, LT: long-term treatment, BrdU: 5'-Bromo-2'-desoxyuridin, MRE: Magnetresonanz-Elastographie, MPTP: 1-Methyl-4-phenyl-1,2,3,6-tetrahydropyridin, CTR: Kontrolltiere für MPTP, vehicle: Kontrolltiere für Indomethazin.

2.3.2. Studie 2: MRE-SN-Studie

Mit einer Gruppe von zunächst unbehandelten C57Bl/6N-Mäusen (n=5) wurden MRE-Messungen zur Ermittlung eines Ausgangswertes für die Elastizität G' und Viskosität G'' an -3 dpi durchgeführt. Hiernach wurde diesen Tieren MPTP an -2, -1 und 0 dpi i.p. injiziert und es erfolgten weitere MRE-Messungen an 3, 6, 10, 14 und 18 dpi. Parallel zu den Tieren, die die MRE-Messungen durchliefen, wurden weitere sechs Gruppen von C57Bl/6N-Mäusen (n=5) als histologische Referenz zu den MRE-Messungen gebildet. Von denen wurde eine Gruppe ohne Behandlung an -3 dpi perfundiert. Die anderen Gruppen wurden ebenfalls mit MPTP i.p. an -2, -1 und 0 dpi behandelt und an den korrespondierenden Messtagen (3, 6, 10, 14, 18 dpi) getötet. Das Schema der zeitlichen Abfolge kann aus der Abbildung 2 entnommen werden.

2.3.3. Studie 3: Indomethazin-Studie

Sowohl Wildtyp-C57Bl/6N- als auch transgene Nestin-GFP-C57Bl/6N-Mäuse wurden zunächst in zwei Gruppen aufgeteilt, um entweder das Neurotoxin MPTP oder 0,9 % NaCl i.p. an drei aufeinanderfolgenden Tagen (-2 dpi bis 0 dpi) zu erhalten. Die anschließende Behandlung mit dem Medikament Indomethazin wurde in den Interventionsgruppen der MPTP- und CTR-behandelten Mäusen wie unter 2.2.3. beschrieben durchgeführt. Die Indomethazininjektion erfolgte entweder über sechs aufeinanderfolgende Tage (Kurzzeitbehandlung, engl. short-term treatment, ST) oder über 17 Tage an jedem zweiten Tag (Langzeitbehandlung, engl. long-term treatment, LT). Die Perfusion fand für die ST-Gruppe an 7 dpi und für die LT-Gruppe an 18 dpi statt. Den Mäusen für die histologischen Auswertungen wurde zur Identifikation sich teilender Zellen in der unter 2.2.2. beschriebenen Methode BrdU verabreicht. Die Tiere für die molekularbiologischen Analysen erhielten stattdessen 0,9 % NaCl i.p.. In Abbildung 2 stellt sich die Reihenfolge der Injektionen schematisch dar.

2.4. Perfusion und Probengewinnung

Die Tiere für die histologischen Analysen aller drei Studien wurden zuerst tief mit Ketamin/Xylazin analgosediert, dann transkardial mit phosphatgepufferter Kochsalzlösung (engl. phosphate buffered saline, PBS) und anschließend mit 4 % Paraformaldehyd (PFA) perfundiert. Hiernach wurden die Gehirne entnommen, bei 4 °C über Nacht in PFA post-fixiert und anschließend zur Dehydratation in 30 %-Saccharoselösung gegeben. Nach zwei Tagen wurden die Gehirne in 2-Methylbutan, gekühlt auf -72 °C mit Flüssigstickstoff, gefroren. Die Gehirne wurden mit einem Kryostaten (Leica CM1850 UV, Leica Biosystems GmbH, Wetzlar, Deutschland) koronar in 40 µm dicke Scheiben geschnitten und bei 4 °C in einer kryoprotektiven Lösung (PBS mit 25 % Glycerin und 25 % Ethylenglykol) gelagert.

Den Tieren für die molekularen Analysen der Studie 3 wurde nach tiefer Narkose mit Ketamin/Xylazin zunächst Blut aus der *Vena cava inferior* entnommen. Hiernach erfolgte die transkardiale Perfusion mit PBS. Die herauspräparierten Gehirne wurden auf Trockeneis gefroren. Den Blutproben wurde Aprotinin zur Hemmung der Fibrinolyse hinzugefügt. Die Proben wurden bei 8000 x g für 15 Minuten bei 4 °C zentrifugiert und die Sera abgenommen. Gehirne und Sera wurden bei -80 °C gelagert.

2.5. Histologie und Zellquantifizierung

2.5.1. Immunhistochemie

Zur Quantifizierung BrdU-positiver Zellen, dopaminerger Zellen und, als Ausdruck zellulärer Entzündungsreaktion, Cluster-of-Differentiation (CD) 68-positiver sowie Ionisiertes-Calcium-bindendes-Adaptermolekül (Iba) 1-positiver Zellen wurde in Studie 1 jeder zwölfte, in Studie 2 und 3 jeder sechste Schnitt gefärbt. An den Schnitten für die Färbung von CD68 in Studie 3 wurde zuerst eine Antigendemaskierung mit Natriumborhydrid durchgeführt. Dann wurden die Schnitte aller immunhistochemischen Färbungen mit 0,6 % Wasserstoffperoxid (H₂O₂) behandelt. Für die BrdU-Färbungen in Studie 3 wurden die Schnitte zudem für 30 Minuten mit Chlorwasserstoff (HCl) inkubiert und anschließend mit Boratpuffer und PBS gewaschen. Nach Antigenblockierung mit Eselserum angereichertem PBS (PBS+, bestehend aus PBS mit 0,1 % Triton-X-100 und 3 % oder 10 % Eselserum), erfolgte die Inkubation mit dem Erstantikörper (anti-BrdU, anti-Iba1, anti-

CD68, anti-Thyrosinhydroxylase (TH)) bei 4 °C über Nacht. Am zweiten Tag wurden nach erneuter Waschung die Schnitte zuerst für zwei Stunden mit dem biotinierten Zweitantikörper und danach für eine Stunde mit ABC-Reagenz inkubiert. Als Farbstoff diente 3,3'-Diaminobenzidin, gelöst in PBS, 0,01 % H₂O₂ und 0,04 % Nickelchlorid. Nach Waschung erfolgte die Entwässerung mit einer aufsteigenden Alkoholreihe und ProTaq[®]Clear sowie das Eindeckeln mit ProTaq[®]Paramount.

Zur Quantifizierung der absoluten Zahlen wurde mittels manueller Auszählung auf jedem zwölften (Studie 1) oder sechsten Schnitt (Studie 2 und 3) die Anzahl Iba1-positiver Zellen, amöboider CD68-positiver Zellen als Ausdruck aktivierter Mikroglia und Makrophagen im Körnerzellband, subgranulären Zone, Molekularschicht sowie Hilius, BrdU-positiver, proliferativer Zellen in der Körnerzellschicht und subgranulären Zone des DG in 200-facher Vergrößerung und TH-positiver, dopaminergener Neurone sowie amöboider CD68-positiver Zellen in der SN in 400-facher Vergrößerung an einem Lichtmikroskop (Axioskop HB50/AC, Carl Zeiss Jena GmbH, Jena, Deutschland) ermittelt und zur Berechnung der Gesamtzellzahl mit zwölf oder sechs multipliziert. Die Auszählung der Gesamtzellzahl Iba1- und CD68-positiver Zellen in der SN wurde mittels Stereo Investigator[®] (MBF Bioscience, Williston, USA) an einem Leica DMRA (Leica Biosystems GmbH, Wetzlar, Deutschland) durchgeführt. Nach Festlegung der Zählbereiche in 50- bzw. 40-facher Vergrößerung wurden die Iba1- bzw. alle CD68-positiven Zellen in 400-facher bzw. 200-facher Vergrößerung mit einem Durchmusterungsgitter von 150 µm x 120 µm Größe und einem Zählrahmen von 60 µm x 60 µm Größe markiert. Der Fehlerkoeffizient (Gundersen, m = 1) war ≤0,09. Die Anzahl ramifizierter CD68-positiver Zellen ergab sich aus der Differenz der Zellzahl aller und amöboider CD68-positiver Zellen.

2.5.2. Immunfluoreszenz

Zur Typisierung der sich teilenden Zellen und Einordnung in den Reifeprozess neuer Neurone im DG wurde jeder zwölfte Schnitt dreifach gefärbt für BrdU, Nestin (unter GFP), Doublecortin (DCX) oder BrdU, Nestin (unter GFP), Neuronal Nuclei (NeuN) oder BrdU, DCX und NeuN. Zunächst wurden die Schnitte für die BrdU-Visualisierung für 30 Minuten mit HCl inkubiert und anschließend mit Boratpuffer und PBS gewaschen. Nach Antigenblockierung mit PBS+ erfolgte die Inkubation mit den Erstantikörpern (anti-BrdU, anti-GFP, anti-DCX, anti-NeuN) bei 4 °C für 48 Stunden (Studie 1) oder über Nacht (Studie 3). Am zweiten Färbetag wurden nach erneuter Waschung die Schnitte lichtgeschützt für vier Stunden mit den fluoreszierenden Zweitantikörpern (Rhodamin-X, Alexa-488, Alexa-647) inkubiert.

Zur Quantifizierung aller Zellen jeglichen Typus in der subgranulären Zone und des Körnerzellbandes des DG (Studie 1) sowie in der SN, Mittelhirn exklusive SN und DG (Studie 2) wurde ebenso jeder zwölfte Schnitt mit dem in PBS-gelösten Fluoreszenzfarbstoff 4',6-Diamidin-2-phenylindol (DAPI), welcher alle Zellkerne markiert, für sieben Minuten inkubiert.

Nach Waschung der Schnitte erfolgte die Entwässerung mit einer aufsteigenden Alkoholreihe und ProTaq[®]Clear sowie das Eindeckeln mit ProTaq[®]Paramount.

In Studie 1 wurde zur Quantifizierung BrdU-positiver Zellen des DG die manuell ermittelte Anzahl unter Benutzung eines Fluoreszenzmikroskops (Axioskop HB50/AC, Carl Zeiss Jena GmbH, Jena, Deutschland) bei 400-facher Vergrößerung mit zwölf multipliziert.

Zur Typisierung der proliferierenden Zellen (Studie 1 und 3) wurde in insgesamt 50 zufällig ausgewählten, BrdU-positiven Zellen im DG die Koexpression von Nestin, DCX und/oder NeuN

durch die Bildung von z-Stapeln in der konfokalen Lasermikroskopie (Leica TCS SP2, Leica Biosystems GmbH, Wetzlar, Deutschland) bei 400-facher und 630-facher Vergrößerung analysiert. Eine morphologische Unterscheidung erfolgte zwischen BrdU/Nestin-positiven Typ-1-Zellen, welche ein dreiecksähnliches Soma und einen apikalen Fortsatz haben, und BrdU/Nestin-positiven Typ-2a-Zellen, welche kurze, tangential orientierte Fortsätze besitzen⁴. Zur Ermittlung der absoluten Zellzahlen wurden die prozentualen Werte auf die Zahl aller BrdU-positiven Zellen übertragen. Die Auszählung der DAPI-positiven Zellen wurde nach Markierung der Zählbereiche in 50-facher Vergrößerung bei 400-facher Vergrößerung (Studie 1: Zählrahmen: 30 µm x 30 µm, Durchmusterungsgitter: 120 µm x 100 µm; Studie 2: Zählrahmen: 60 µm x 60 µm; Durchmusterungsgitter: SN: 250 µm x 200 µm, Mittelhirn und Hippocampus: 600 µm x 600 µm) mittels Stereo Investigator® (MBF Bioscience Williston, USA) an einem Leica DMRA (Leica Biosystems GmbH, Wetzlar, Deutschland) durchgeführt. Der Fehlerkoeffizient (Gundersen, m=1) war $\leq 0,09$.

2.6. Molekularbiologie

2.6.1. Enzymatisches Immunadsorptionsverfahren

Zur Bestimmung der Proteinkonzentration der Zytokine: Interleukin (IL)-1 β , IL-6, IL-10, IL-17a, Interferon(IFN)- γ und Tumornekrosefaktor (TNF)- α , in Serum (Studie 3) wurde das enzymatische Immunadsorptionsverfahren (engl. enzyme-linked immunosorbent assay, ELISA) verwendet. Hierzu wurde das Bio-Plex Pro™ Mouse Cytokine TH17 Panel A 6-Plex Group 1 Kit entsprechend dem Herstellerprotokoll Bio-Plex Pro™ Cytokine, Chemokine, and Growth Factor Assays Instruction Manual benutzt. Die Messung und Kalkulation der Fluoreszenzsignale und Konzentrationen erfolgte mit einem Bio-Plex® 200 System (Bio-Rad Laboratories Inc., Hercules, USA).

2.6.2. Quantitative Polymerase-Kettenreaktion

Um Veränderungen in den regulatorischen Signalwegen der Neurogenese zu ermitteln, wurde die Genexpression von *gli1*, *hes5*, *lef1* als Effektorgene des Sonic Hedgehog-, Notch- bzw. Wnt-Signalwegs, und von *neuroD6* sowie *ngn1* als proneurogene Faktoren analysiert. Hierfür wurden Proben von 1 mm Durchmesser von Scheiben des vorderen Hippocampus, welche koronar von Bregma -1,82 bis -2,3 mm mittels Kryostaten (Leica CM1850 UV, Leica Biosystems GmbH, Wetzlar, Deutschland) herausgeschnittenen wurden, für die quantitative Polymerase-Kettenreaktion herausgestanzt. Nach Extraktion und Aufreinigung der Boten-Ribonukleinsäure (engl. ribonucleic acid, RNA) mittels Nucleo Spin® RNA/Protein Kit, erfolgte die Synthese der komplementären Desoxyribonukleinsäure (engl. complementary deoxyribonucleic acid, cDNA) unter Benutzung des High Capacity RNA-to-cDNA™ Kit. Hiernach wurde eine Amplifizierung mit dem TaqMan® Fast Advanced Master Mix unter den Assays für *gli1*, *hes5*, *lef1*, *neuroD6*, *ngn1* und *gapdh* laut TaqMan® Fast Advanced Master Mix Protocol im StepOne™ Real-Time PCR System (Applied Biosystems, Foster City, USA) durchgeführt. *Gapdh* diente als Referenzgen, um die relative Genexpression mittels vergleichender C_T-Methode ($\Delta\Delta C_t$) in der Software StepOne™ (Applied Biosystems, Foster City, USA) zu normieren und die Expressionslevel zu berechnen.

2.7. Statistische Analyse und Darstellung

Die statistischen Auswertungen wurden mit IBM SPSS Statistics (International Business Machines Corporation (IBM), Armonk, USA) Version 19 sowie 25 und GraphPad Prism (GraphPad Software, San Diego, USA) Version 5 sowie 7 durchgeführt. Die Daten wurden mit einer einfaktoriellen oder zweifaktoriellen Varianzanalyse (engl. analysis of variance, ANOVA) mit oder ohne Messwiederholung getestet. Bei statistischer Signifikanz von $p \leq 0,05$ schlossen sich paarweise Vergleiche mit dem Post-hoc-Test nach Bonferroni an. Die Daten wurden als Mittelwert \pm Standardfehler oder Boxplots mit Median, 25. bis 75. Perzentile als Box sowie minimaler und maximaler Wert als Whiskers dargestellt. Die Graphen wurden mit GraphPad Prism (GraphPad Software, San Diego, USA) Version 5 sowie 7 erzeugt. Es erfolgte bei $n=2$ keine statistische Auswertung der DAPI-Zellzählung in Studie 2.

3. Ergebnisse

3.1. MRE-Hippocampus-Studie (Studie 1): Transient höhere Elastizität im Hippocampus ist assoziiert mit kurzfristig gesteigerter Neurogenese nach Dopamindepletion

Es wurden die Parameter der Elastizität: Realteil G' sowie Magnitude $\text{abs}(G^*)$, und der Viskosität: Imaginärteil G'' sowie Phasenwinkel φ , im Hippocampus einschließlich des DG und im gesamten Hirnparenchym in einer Ausgangsgruppe an -3 dpi und in MPTP-behandelten sowie CTR-Tieren an den Tagen 3, 6, 10, 14 und 18 dpi ermittelt. Es zeigte sich ein transienter Anstieg der Viskoelastizität, gleichbedeutend mit einer kurzfristigen Versteifung, nach MPTP-Behandlung im Vergleich zur CTR-Gruppe an 6dpi (G' : $F(5,40) = 3,841$, $p \leq 0,01$; G'' : $F(5,40) = 4,240$, $p \leq 0,01$; $\text{abs}(G^*)$: $F(5,40) = 4,045$, $p \leq 0,01$; MPTP vs. CTR 6 dpi: $p \leq 0,01$). Hier erhöhten sich nach Dopamindepletion die Werte auf $G' = 6,971 (\pm 1,019)$ kPa, $G'' = 1,767 (\pm 0,103)$ kPa und $\text{abs}(G^*) = 7,192 (\pm 1,011)$ kPa. Die Messwerte der CTR-Tiere betragen im Hippocampus $G' = 4,608 (\pm 0,719)$ kPa, $G'' = 1,388 (\pm 0,125)$ kPa und $\text{abs}(G^*) = 4,816 (\pm 0,705)$ kPa. Dies bedeutet eine Erhöhung der Viskoelastizität um 51%, 27% bzw. 49% im Hippocampus sechs Tage nach MPTP-Behandlung. Ferner zeigte sich ein Anstieg der Viskoelastizität über die Zeit (G' : $F(5,40) = 5,239$, $p \leq 0,001$; G'' : ($F(5,40) = 9,699$, $p \leq 0,001$; $\text{abs}(G^*)$ ($F(5,40) = 5,689$, $p \leq 0,001$). Der Phasenwinkel φ war weder durch die Zeit noch durch die MPTP-Behandlung signifikant verändert. Im gesamten Hirnparenchym ließ sich ebenfalls ein kurzfristiger Anstieg der Messparameter an 6 dpi erkennen (G' : $F(5,40) = 4,811$, $p \leq 0,01$; G'' : $F(5,40) = 3,271$, $p \leq 0,05$; $\text{abs}(G^*)$: $F(5,40) = 4,756$, $p \leq 0,01$).

In der histologischen Auswertung des DG MPTP-behandelter Tiere zeigte sich ein transienter Anstieg in den absoluten Zahlen neu generierter BrdU/Nestin-positiver Vorläuferzellen ($F(5,48) = 2,758$, $p \leq 0,05$). In der relativen Anzahl neuer neuronaler Vorläuferzellen aller Tiere ließ sich über die Zeit eine Reduktion finden ($F(5,48) = 9,070$, $p \leq 0,001$), wohingegen die der neu gebildeten BrdU/NeuN-positiven Neurone stieg ($F(5,48) = 41,910$, $p \leq 0,001$). In den paarweisen Vergleichen offenbarte sich in den MPTP-behandelten Tieren eine gesteigerte Proliferation von neuronalen Vorläuferzellen im Vergleich zur CTR-Gruppe an 3 dpi sowohl in den relativen (CTR vs. MPTP 3 dpi: $p \leq 0,05$) als auch in den absoluten Zellzahlen (CTR vs. MPTP 3 dpi: $p \leq 0,001$), wobei sich hier am nachfolgenden Messtag eine Reduktion zeigte (MPTP 3 dpi vs. MPTP 6 dpi: $p \leq 0,01$). An diesem Beobachtungszeitpunkt konnte stattdessen eine höhere relative Anzahl neu generierter BrdU/NeuN-positiver Neurone (CTR vs. MPTP 6 dpi: $p \leq 0,05$) eruiert werden, welche zeitlich zum Anstieg der viskoelastischen Parameter nach MPTP-Behandlung korrespondiert.

Die Anzahl der Iba1-positiven Zellen stieg über die Zeit ($F(5,48) = 9,635$, $p \leq 0,001$). In den paarweisen Vergleichen konnte eine höhere Anzahl von Mikroglia nach MPTP-Gabe an 3 dpi (CTR vs. MPTP 3 dpi: $p \leq 0,05$) gesehen werden. Die Zahl aller DAPI-positiven Zellen im Körnerzellband inklusive der subgranulären Zone war weder durch MPTP-Behandlung noch durch die Zeit verändert.

3.2. MRE-SN-Studie (Studie 2): Reduktion der Viskoelastizität in der SN ist assoziiert mit dem Verlust dopaminerger Neurone nach MPTP-Behandlung

Es wurden die viskoelastischen Parameter in der Ausgangsgruppe an -3 dpi und MPTP-behandelten Tieren an 0, 3, 6, 10, 14 und 18 dpi in der SN, Mittelhirn exklusive der SN und Hippocampus ermittelt.

In der SN ergab sich nach MPTP-Gabe eine Reduktion in den elastischen und viskösen Messparametern (G' : $F(5,29) = 4,274$, $p \leq 0,01$; G'' : $F(5,29) = 8,350$, $p \leq 0,001$). In den paarweisen Vergleichen zeigte sich eine verringerte Elastizität innerhalb der ersten beobachteten Zeitpunkte nach MPTP-Behandlung (3 dpi vs. 6 dpi: $p \leq 0,05$) und eine verminderte Viskosität im Vergleich zur Ausgangsgruppe (-3 dpi vs. 6 dpi: $p \leq 0,001$, -3 dpi vs. 10 dpi: $p \leq 0,05$, -3 dpi vs. 18 dpi: $p \leq 0,01$), so dass durch Gabe von MPTP vor allem die viskösen Eigenschaften der SN abnehmen.

Im Mittelhirn hingegen konnte ein kontinuierlicher Anstieg der Elastizität G' ($F(5,29) = 6,702$, $p \leq 0,001$; -3 dpi vs. 6 dpi und 18 dpi: $p \leq 0,01$; -3 dpi vs. 14 dpi: $p \leq 0,05$) und der Viskosität G'' ($F(5,29) = 6,895$, $p \leq 0,001$; -3 dpi vs. 6 dpi und 18 dpi: $p \leq 0,01$) nach MPTP-Behandlung eruiert werden. Insbesondere die erhöhte Elastizität weist auf eine kontinuierliche Versteifung des Mittelhirns hin.

Im Hippocampus konnte durch Dopamindepletion ein transients Anstieg in den Messparametern der Elastizität G' ($F(5,29) = 11,75$, $p \leq 0,001$; -3 dpi vs. 6 dpi: $p \leq 0,001$) und der Viskosität G'' ($F(5,29) = 8,075$, $p \leq 0,001$; -3 dpi vs. 6 dpi: $p \leq 0,01$) beobachtet werden, welches auf eine kurzfristige Versteifung hindeutet.

In der Ausgangsgruppe zeigte sich eine signifikante Differenz im Messparameter G'' in den drei Arealen ($F(2,14) = 5,396$, $p \leq 0,05$), wobei die paarweisen Vergleiche eine höhere Viskosität im Mittelhirn ($1,836 \pm 0,043$ kPa) als im Hippocampus ($1,426 \pm 0,051$ kPa) ($p \leq 0,05$) offenbarte.

In der histologischen Auswertung der SN offenbarte sich eine Reduktion in der Anzahl TH-positiver, dopaminerger Neurone nach MPTP-Behandlung ($F(5,28) = 7,499$, $p \leq 0,001$) an allen Messtagen im Vergleich zur Ausgangsgruppe (-3 dpi vs. 3 dpi and 6 dpi: $p \leq 0,001$, -3 dpi vs. 10 dpi, 14 dpi und 18 dpi: $p \leq 0,01$). Bereits am ersten Messtag nach der Behandlung (3 dpi) konnte eine Reduktion dopaminerger Neurone um ca. 57% auf 856 Zellen von 2018 Zellen an -3 dpi beobachtet werden.

In der Anzahl der Mikroglia zeigte sich ein Anstieg auf 21732 Iba1-positive Zellen am ersten Messtag nach MPTP-Gabe ($F(5,28) = 5,706$, $p \leq 0,01$; -3 dpi vs. 3 dpi: $p \leq 0,05$). Hiernach kam es zu einer stetigen Erholung bis fast auf den Ausgangswert mit ca. 15000 Zellen, insgesamt Ausdruck einer kurzzeitigen zellulären entzündlichen Reaktion.

Zudem konnte bei jeweils $n=2$ in der SN eine Reduktion DAPI-positiver Zellen von 224700 (± 6967) in der Ausgangsgruppe auf 164083 (± 8417) an 6 dpi festgestellt werden. Danach kam es wieder zu einem leichten Anstieg der Gesamtzellzahl. Ebenso zeigte sich eine Reduktion von 1834800 (± 116400) DAPI-positiven Zellen an -3 dpi auf 1333800 (± 60600) an 6 dpi im Mittelhirn. Im Hippocampus hingegen konnte ein temporärer Anstieg der Gesamtzellzahl von 1385400

(± 155400) Zellen in der Ausgangsgruppe auf 1468200 (± 89400) Zellen an 6 dpi beobachtet werden.

3.3. Indomethazin-Studie (Studie 3): Höhere Überlebensrate neuer Neurone im DG durch Indomethazinbehandlung nach MPTP-Gabe in Zusammenhang mit verringerter zellulärer Inflammation und hochregulierter proneurogener Signalwege

Zur Evaluation des Indomethazineffekts auf die adulte Neurogenese erfolgte die histologische Auswertung von Anzahl und Typisierung BrdU-inkorporierender Zellen. In der LT-Gruppe konnte im DG eine Reduktion neuer reifer BrdU/NeuN-positiver Neurone durch MPTP-Gabe ($F(1,26) = 5,413$, $p \leq 0,05$; CTR + vehicle vs. MPTP + vehicle: $p \leq 0,05$) beobachtet werden, welche durch die Behandlung mit Indomethazin verhindert werden konnte (MPTP + vehicle vs. MPTP + Indomethazin: $p \leq 0,01$). In der Kontrollgruppe ergab sich keine Veränderung durch Indomethazin (CTR + vehicle vs. CTR + Indomethazin: $p = 0,748$).

In der Gesamtzellzahl proliferierender BrdU-positiver Zellen ergaben sich an beiden Beobachtungszeitpunkten keine signifikanten Veränderungen. In den absoluten Zahlen neuronaler Vorläuferzellen zeigte sich ein signifikanter Interaktionseffekt in der Zahl der BrdU/Nestin/DCX-positiven Typ-2b-Zellen in der ST-Gruppe ($F(1,26) = 4,325$, $p \leq 0,05$), wobei die paarweisen Vergleiche keinen signifikanten Unterschied darlegten. Durch MPTP-Behandlung ließ sich jedoch eine Reduktion neuer BrdU/Nestin-positiver Typ-2a-Zellen in der LT-Gruppe ($F(1,28) = 4,893$, $p \leq 0,05$) ermitteln. Keine signifikanten Effekte waren in den absoluten Zahlen der BrdU/Nestin-positiven Typ-1-Zellen, BrdU/Nestin-positiven Typ-2a-Zellen in der ST-Gruppe und BrdU/Nestin/DCX-positiven Typ-2b-Zellen in der LT-Gruppe sowie BrdU/DCX-positiven Typ-3-Zellen, welche ebenso die unreifen Neurone beinhalten, an beiden Zeitpunkten zu sehen.

In der Analyse regulatorischer Signalwege der Neurogenese zeigte sich in der mRNA-Expression von *lef1*, Effektorgen des Wnt-Signalweges, eine Reduktion durch alleinige MPTP- oder Indomethazinbehandlung in den Kontrolltieren der ST-Gruppe ($F(1,16) = 7,067$, $p \leq 0,05$; CTR + vehicle vs. MPTP + vehicle: $p \leq 0,05$; CTR + vehicle vs. CTR + Indomethazin: $p \leq 0,01$). Zu diesem Zeitpunkt stellte sich auch die Expression des antineurogenen Gens *hes5* aus dem Notch-Signalweg, unabhängig von der jeweils anderen Behandlung, durch das Neurotoxin verringert ($F(1,16) = 5,469$, $p \leq 0,05$), aber durch das Medikament erhöht ($F(1,16) = 5,482$, $p \leq 0,05$) dar. Die Indomethazinbehandlung bewirkte zudem eine gesteigerte mRNA-Expression des proneurogenen Gens *neuroD6* in der ST-Gruppe ($F(1,16) = 9,530$, $p \leq 0,01$). Diese war jedoch verringert in der LT-Gruppe ($F(1,16) = 13,548$, $p \leq 0,01$). Es konnte keine mRNA-Expression des Gens *ngn1* in der ST-Gruppe gemessen werden. Es zeigten sich keine signifikanten Effekte in der mRNA-Expression von *ngn1* in der LT-Gruppe und *gli1* an beiden beobachteten Zeitpunkten. Zur Evaluation zellulärer entzündlicher Reaktionen wurde die Anzahl Iba1- und CD68-positiver Zellen bestimmt. Im DG der Tiere konnte eine höhere Anzahl amöboider CD68-positiver Zellen, Ausdruck aktivierter Mikroglia und Makrophagen, in beiden Messzeiträumen in nur mit MPTP-behandelten Tieren im Vergleich zur Kontrolle beobachtet werden (ST: $F(1,28) = 7,923$, $p \leq 0,01$; CTR + vehicle vs. MPTP + vehicle: $p \leq 0,001$; LT: $F(1,26) = 5,860$, $p \leq 0,05$; CTR + vehicle vs. MPTP + vehicle: $p \leq 0,05$). In der ST-Gruppe konnte dies durch die Indomethazinbehandlung verhindert werden (MPTP + vehicle vs. MPTP + Indomethazin: $p \leq 0,01$). Keine signifikanten Unterschiede stellten sich in der Anzahl ramifizierter CD68-positiver und aller CD68-positiver Zellen dar.

In der Menge Iba1-positiver Zellen konnte in der ST-Gruppe eine Interaktion der Faktoren ($F(1,28)=4,497$, $p\leq 0,05$) ohne signifikante paarweise Vergleiche ermittelt werden.

Neben der zellulären Komponente wurden zudem die Konzentrationen von Zytokinen im Serum gemessen. Hier konnte in der LT-Gruppe eine Konzentrationserhöhung des antiinflammatorischen ILs-10 ($F(1,31) = 4,432$, $p\leq 0,05$; CTR + vehicle vs. MPTP + vehicle: $p\leq 0,05$) und des proinflammatorischen ILs-17a ($F(1,29) = 7,825$, $p\leq 0,01$; CTR + vehicle vs. MPTP + vehicle: $p\leq 0,01$) nach MPTP-Gabe ermittelt werden. Indomethazinbehandlung hingegen verhinderte dies (MPTP + vehicle vs. MPTP + Indomethazin IL-10 und IL-17a: $p\leq 0,01$). Es zeigten sich keine signifikanten Unterschiede in den Konzentrationen der proinflammatorischen Zytokine IL-1 β , IL-6, IFN- γ , und TNF- α an beiden beobachteten Zeitpunkten.

In der SN wurde der Effekt der Indomethazinbehandlung auf die Anzahl dopaminerger Neurone und ebenso auf die zelluläre entzündliche Reaktion eruiert. Durch MPTP-Gabe zeigte sich eine Reduktion TH-positiver, dopaminerger Neurone an beiden Zeitpunkten (ST: $F(1,26) = 8,609$, $p\leq 0,01$; LT: $F(1,33) = 11,303$, $p\leq 0,01$). Die Indomethazinbehandlung hatte hier keinen Effekt (ST: $F(1,26) = 2,573$, $p=0,121$; LT: $F(1,33) = 3,189$, $p=0,083$). In der Auswertung Iba1-positiver Zellen stellte sich nach Dopamindepletion mehr Mikroglia dar (ST: $F(1,28) = 7,715$, $p\leq 0,01$; CTR + vehicle vs. MPTP + vehicle: $p\leq 0,01$; LT: ($F(1,26) = 5,800$, $p\leq 0,05$; CTR + vehicle vs. MPTP + vehicle: $p\leq 0,05$), wohingegen die nachfolgende Indomethazingabe dem entgegenwirkte (MPTP + vehicle vs. MPTP + Indomethazin: ST $p\leq 0,001$, LT $p\leq 0,05$). In der ST-Gruppe wurde auch eine verringerte Anzahl der amöboiden CD68-positiven Zellen durch Indomethazingabe allein ($F(1,28) = 14,753$, $p\leq 0,001$) ermittelt. Ansonsten ergaben sich in den Zahlen der CD68-positiven Zellen in der SN keine Effekte.

4. Diskussion

In den drei Studien konnte in einem neurotoxininduzierten Tiermodell für Neurodegeneration dargelegt werden, dass insbesondere Neurone zu den viskoelastischen Eigenschaften von Gehirngewebe beitragen und das Überleben neuer Neurone durch Indomethazin, begleitet von antiinflammatorischen Effekten, gefördert wird.

In der MRE-Hippocampus-Studie (Studie 1) konnte drei Tage nach MPTP-Gabe eine temporär gesteigerte Bildung von zunächst neuronalen Vorläuferzellen beobachtet werden. Der kurzzeitige Anstieg neuronaler Vorläuferzellen im DG nach MPTP-Behandlung wurde bereits in einer früheren Studie beobachtet und kann als temporärer, endogener, reaktiver Versuch des Hippocampus mittels Regeneration einem neuronalen Verlust entgegenzuwirken interpretiert werden³⁰. In der jetzigen Studie ergab sich nachfolgend durch die weitere Differenzierung auch ein Anstieg in der relativen Zahl neuer Neurone an 6 dpi, welches ebenso das Bild eines kurzzeitigen Regenerationseffektes unterstützt.

An 6 dpi war zudem ein temporärer Anstieg der viskoelastischen Parameter mittels MRE zu verzeichnen. Trotzdem sich die Dichte neuer Neurone nur um 10 % steigerte, fand durch die mögliche Integration dieser im DG in das bestehende biomechanische Gerüst insbesondere eine Erhöhung der Elastizität, d.h. Versteifung, um fast 50 % sechs Tage nach induzierter Dopamindepletion statt. Hingegen sah man keine Veränderungen der viskoelastischen Parameter zeitgleich mit dem temporären Anstieg neuer neuronaler Vorläuferzellen an 3 dpi. Insgesamt kann dies auf eine Sensitivität des Elastizitätsparameters G' in Bezug auf Neurone,

welche zur biomechanischen Matrix beitragen, hindeuten. Zudem lässt sich vermuten, dass sich die biomechanischen Eigenschaften der Vorläuferzellen von denen der Neurone unterscheiden. Bisher wurde zumindest eine höhere Steifigkeit in Neuronen im Vergleich zu Gliazellen gesehen³¹. Die hier gemessene höhere Elastizität durch neue Neurone ist passend zu dem bisher beobachteten Gegensatz, dass ein Verlust dieser im Tiermodell der Ischämie in einer verringerten Steifigkeit resultiert¹⁶. Dies zeigt insgesamt eine wichtige Funktion der Neurone im biomechanischen Gerüst des Gehirns.

Dass Neurone eine Schlüsselrolle bezüglich Viskoelastizität in neurodegenerativen Erkrankungen innehalten, ergab sich ebenso aus den Erkenntnissen der MRE-SN-Studie (Studie 2). Hier zeigte sich sechs Tage nach MPTP-Gabe eine Verringerung der Viskosität und im geringen Maße der Elastizität ohne vollständige Wiederherstellung über die Zeit im primär betroffenen Areal der Parkinson-Erkrankung, der SN. Ein größerer Effekt auf die Viskosität deutet insbesondere auf eine Veränderung auf Ebene der Geometrie und Dichte des mechanischen Netzwerks hin, hier beruhend auf den Verlust von Neuronen und deren Fortsätze. Eine verringerte Anzahl TH-positiver, dopaminergener Neurone war bereits drei Tage nach MPTP-Behandlung zu erkennen. Dies ist darauf zurückzuführen, dass eine reduzierte TH-Aktivität innerhalb der Zellen früher einsetzt als die eigentliche Zerstörung der Neurone¹⁷. Folglich resultierte erst der tatsächliche Verlust von dopaminergen Neuronen und Zellfortsätzen an 6 dpi in einer verringerten Viskosität.

Im Mittelhirn konnte ein Anstieg der Viskoelastizität nach MPTP-Gabe beobachtet werden. Jedoch zeigt sich in der Gesamtzellzahl im Gegensatz dazu eine Reduktion. Möglicherweise sind andere Prozesse, welche eine Veränderung der Komplexität des mechanischen Netzwerks hervorrufen, zum Beispiel Veränderungen in Vernetzungen und Verzweigungen, Intermediärfilamente sowie die Interaktion mit der extrazellulären Matrix^{15,32,33}, verantwortlich. Die höhere Viskosität im Mittelhirn im Vergleich zum Hippocampus in der Ausgangsgruppe könnte sich ebenso durch die hier vorhandenen Leitungsbahnen der weißen Substanz erklären, da die weiße Substanz allgemein mehr Steifigkeit aufweist als die graue Substanz¹¹.

Im Hippocampus war in Studie 2 ebenso wie in Studie 1 ein temporärer Anstieg der Elastizität und Viskosität zu verzeichnen. In Studie 1 konnte keine Korrelation mit der Gesamtzellzahl des Körnerzellbandes inklusive der subgranulären Zone beobachtet werden. In Studie 2 ergaben sich hingegen Hinweise auf einen Zusammenhang zwischen höherer Viskoelastizität und Gesamtzellzahl des DG, was jedoch bei hier nichterfolgter statistischer Auswertung weiter untersucht werden muss.

Insgesamt konnte in beiden Studien im DG und in der SN nach MPTP-Behandlung, welche bekanntermaßen eine zelluläre entzündliche Reaktion in beiden Regionen verursacht^{26,34,35}, eine kurzfristige Vermehrung Iba1-positiver Mikroglia eruiert werden, welche sich aber jedoch nicht in den MRE-Parametern widerspiegelte. In dem Model für experimentelle autoimmune Enzephalomyelitis konnte im Zerebellum eine Korrelation von gesteigerter F8/40-Expression, einem Marker für Makrophagen, und verringerter Elastizität nach 21 Tagen gezeigt werden³⁶. Daher ist in kleinen Regionen, wie Hippocampus und SN, die MRE eher geeignet viskoelastische Eigenschaften basierend auf der neuronalen Komponente darzustellen als kurzzeitige mikrogliale Reaktionen. Nichtsdestotrotz hängen die biomechanischen Eigenschaften nicht nur von der Anzahl eines Typs neuraler Zellen ab, sondern auch von anderen Zelltypen, dem Netzwerk, Verzweigungen und Interaktion mit der Extrazellulärmatrix. Unter anderem müsste der Einfluss

langanhaltender, entzündlicher Prozesse insbesondere in kleinen Arealen auf viskoelastische Eigenschaften untersucht werden. Bezüglich der Diagnostik neurodegenerativer Erkrankungen konnte im gesamten Gehirn oder in ausgewählten Regionen von Patienten mit der Parkinson-Krankheit, Alzheimer-Krankheit, progressiven supranukleären Blickparese oder Multiplen Sklerose eine verminderte Viskoelastizität beobachtet werden^{12,37-39}. Zusammen mit unseren Studien kann der neuronale Verlust als Ursache vermutet werden. Studien mit humanem Gewebe zur Korrelation von MRE-Parametern und histologischen Untersuchungen wurden bisher jedoch nicht durchgeführt.

Im Hinblick auf den MPTP-induzierten Effekt auf die Überlebensrate neu gebildeter Neurone im Hippocampus zeigte sich in der Indomethazin-Studie (Studie 3) als auch in vorherigen Studien^{30,40}, dass trotz kurzfristig höherer Bildung die neu generierten Neurone mittelfristig nicht mehr fortbestanden. Wie auch in Studie 1 gezeigt, rief MPTP eine transiente zelluläre entzündliche Reaktion im DG hervor und Inflammation selbst verhindert ebenso wie Dopamindepletion eine regelhafte Neurogenese^{24,40}. Die Gabe des COX-Hemmers Indomethazin förderte die Überlebensrate neuer reifer Neurone im DG in der LT-Gruppe nach MPTP und zeigte damit einen proneurogenen Effekt in einem Modell für Neurodegeneration. Dies ist übereinstimmend mit der erhöhten Anzahl neuer Neurone nach Ischämie und radioaktiver Bestrahlung durch Indomethazin, begleitet von einer reduzierten mikroglialen Aktivität^{24,25}. In unserer Studie stellte sich der antiinflammatorische Effekt von Indomethazin in der reduzierten Anzahl amöboider CD68-positiver Zellen, welche reaktive Mikroglia und Makrophagen beinhalten, dar. Ähnlich wie in einer anderen Studie²², zeigte sich in den verschiedenen Stadien der Neurogenese 18 Tage nach MPTP, unabhängig von der Indomethazinbehandlung, eine verringerte Anzahl neuer Typ-2a-Vorläuferzellen. Dies verdeutlicht insbesondere den bereits erwähnten nur kurzzeitigen Anstieg von Vorläuferzellen³⁰ (Studie 1). Indomethazin selbst oder nach MPTP-Gabe hatte keinen negativen Einfluss auf die neuronalen Vorstufen und unterstützte somit eine physiologische neuronale Zelldifferenzierung bis hin zu einer regelrechten Anzahl reifer Neurone.

In der Analyse neurogeneserelevanter Signalwege konnte eine reduzierte Expression von *lef1*, ein Effektorgen des Wnt/ β -Catenin-Signalwegs, nach MPTP-Gabe in der ST-Gruppe beobachtet werden. In einer *in-vitro*-Studie wurde ebenso eine Verminderung von β -Catenin in neuronalen Vorläuferzellen der subventrikulären Zone nach Hinzufügen von MPTP und mikroglialen Zellen gesehen⁴¹. Zudem ist eine verringerte Aktivierung des Wnt-Signalwegs ebenso mit einer verminderten Anzahl neuer Typ-3-Zellen und unreifen Neuronen bekannt⁴². Daher führte das herunterregulierte Wnt-Signal vermutlich zu einer geringeren Überlebensrate reifer Neurone in der LT-Gruppe. Eine signifikante Erhöhung durch Indomethazin in den MPTP-behandelten Tieren konnte nicht beobachtet werden. Ferner offenbarte sich eine verringerte *lef1*-Expression in den gesunden Tieren durch Indomethazin. Bisher ergaben sich Hinweise, dass eine indomethazinbedingte verminderte Wnt-Signalübertragung zumindest in Krebszellen ein unkontrolliertes Tumorwachstum hemmt⁴³. In dieser Studie konnte jedoch kein negativer Effekt von Indomethazin auf die neu gebildeten Zellen und deren Differenzierung gesehen werden. In der ST-Gruppe war durch Indomethazin die Expression des proneurogenen Gens *neuroD6*, bedeutend für die neuronale Differenzierung, das Überleben der Neurone und der Toleranz gegenüber oxidativem Stress^{44,45}, höher. Dies kann auch zu der höheren Überlebensrate der Neurone bis zum zweiten beobachteten Zeitpunkt beigetragen haben. Ein Effekt der verringerten

Expression von *neuroD6* auf die Neurogenese in der LT-Gruppe nach Indomethazinbehandlung konnte in dem Beobachtungszeitraum dieser Studie nicht eruiert werden. Eine Aktivierung des Notch-Signalwegs hemmt die Weiterdifferenzierung von Vorläuferzellen zu reifen Neuronen⁴⁶. In unseren Untersuchungen offenbarte sich unabhängig von der nachfolgenden Indomethazinbehandlung ein temporärer Anstieg der Expression von *hes5*, Effektorgen des Notch-Signalweges, durch das Neurotoxin MPTP. Die kurzzeitige Indomethazinbehandlung selbst jedoch, unabhängig von der MPTP-Gabe, reduzierte die Expression von *hes5*, so dass die verringerte Aktivierung des Notch-Signalwegs auch zu einer Weiterdifferenzierung zu reifen Neuronen in der LT-Gruppe geführt haben könnte.

Die Konzentrationen von Zytokinen sind sowohl in der zerebrospinalen Flüssigkeit als auch im Serum von Patienten der Parkinson-Krankheit erhöht^{47,48}. Da sich keine Veränderungen der Serumkonzentrationen von den meisten proinflammatorischen und antineurogenen Zytokinen nach MPTP zeigten, jedoch das antiinflammatorische und proneurogene Zytokin IL-10 in der LT-Gruppe höher war, kann ein beginnender Rückgang der Entzündung nach MPTP vermutet werden. Zusammen mit den Ergebnissen zweier anderer Studien^{48,49} muss aber beachtet werden, dass eventuell gesteigerte Zytokinkonzentrationen in C57Bl/6 Mäusen nach MPTP peripher im Serum nicht messbar sind, auch wenn diese in der Zerebrospinalflüssigkeit erhöht waren⁴⁸. Zudem können die höheren Zytokinkonzentration von IL-10 und IL-17a auch von einer entzündlichen Reaktion in peripheren Organen wie des Darms stammen, wo ebenfalls eine Makrophageninfiltration und gestiegene Zytokinlevel nach MPTP gefunden wurden⁵⁰.

In der SN konnte wie bei Kurkowska-Jastrzębska und Kollegen²⁶ kein Erhalt der dopaminergen Neurone durch therapeutische Indomethazingabe beobachtet werden. In früheren Studien zu Indomethazin oder anderen COX-2-Hemmern wurde hingegen bei Verabreichung vor MPTP-Gabe ein neuroprotektiver Effekt mit einhergehender verringerter Entzündung eruiert^{26,34}. Zwar konnte in der hier durchgeführten Studie ebenso eine Reduktion der zellulären Entzündungsreaktion in der Anzahl der Iba1-positiven Zellen festgestellt werden, aber die dopaminerge Neurodegeneration ist hier am ehesten auf die direkte Neurotoxizität von MPTP zurückzuführen⁵¹.

In Humanstudien wird ein reduziertes Risiko für die Entwicklung einer Parkinson-Krankheit durch die Einnahme von nichtsteroidalen Antiphlogistika angenommen, wohingegen es bisher keinen Anhaltspunkt für eine Verhinderung des Krankheitsfortschritts gibt⁵². Eventuell kann aber durch eine Verringerung der entzündlichen Vorgänge doch einem weiteren Verlust dopaminergener Neurone entgegengewirkt werden, auch wenn sich dies im hier verwendeten Tiermodell nicht zeigte. In Studie 3 konnte trotz Dopaminepletion eine regelhafte hippocampale Neurogenese mit reduzierter zellulärer Entzündung durch Indomethazinbehandlung festgestellt werden. Dies legt eine Beeinflussung der Neurogenese eher durch Entzündung als durch eine veränderte Transmitterhomöostase nahe. Ferner könnte, da eine gestörte Neurogenese im DG von Patienten mit idiopathischem Parkinsonsyndrom bekannt ist⁶, eine Indomethazinbehandlung durch Förderung einer regelrechten Neurogenese als möglicher Therapieansatz hippocampusassoziierter kognitiver Einschränkungen in Betracht kommen.

4.1. Schlussfolgerung

Unter Anwendung des MPTP-Mausmodells für Neurodegeneration mit resultierender Dopaminepletion konnte gezeigt werden, dass (1) Veränderungen in den biomechanischen

Eigenschaften mit histologischen Prozessen, insbesondere die Neuronenzahl betreffend, in kleinen, spezifischen Regionen einhergehen. Dies trägt insgesamt zur Weiterentwicklung der MRE als mögliches neues nichtinvasives diagnostisches Werkzeug neurodegenerativer Erkrankungen bei. Zudem konnte (2) nach dopaminergem Zellverlust in der SN ein proneurogener Effekt im Sinne einer gesteigerten Überlebensrate reifer Neurone im DG durch Indomethazinbehandlung, begleitet von reduzierter zellulärer Entzündung und proneurogenen Signalwegen, festgestellt werden. Daher repräsentiert Indomethazin einen möglichen Therapieansatz die Neurogenese in neurodegenerativen Erkrankungen zu verbessern.

5. Literaturverzeichnis

1. Eriksson PS, Perfilieva E, Björk-Eriksson T, Alborn AM, Nordborg C, Peterson DA, Gage FH. Neurogenesis in the adult human hippocampus. *Nat Med.* 1998 Nov;4(11):1313-7.
2. Spalding KL, Bergmann O, Alkass K, Bernard S, Salehpour M, Huttner HB, Boström E, Westerlund I, Vial C, Buchholz BA, Possnert G, Mash DC, Druid H, Frisén J. Dynamics of hippocampal neurogenesis in adult humans. *Cell.* 2013 Jun 6;153(6):1219-1227. doi: 10.1016/j.cell.2013.05.002.
3. Boldrini M, Fulmore CA, Tartt AN, Simeon LR, Pavlova I, Poposka V, Rosoklija GB, Stankov A, Arango V, Dwork AJ, Hen R, Mann JJ. Human Hippocampal Neurogenesis Persists throughout Aging. *Cell Stem Cell.* 2018 Apr 5;22(4):589-599.e5. doi: 10.1016/j.stem.2018.03.015.
4. Kempermann G, Jessberger S, Steiner B, Kronenberg G. Milestones of neuronal development in the adult hippocampus. *Trends Neurosci.* 2004 Aug;27(8):447-52.
5. Kempermann G. Seven principles in the regulation of adult neurogenesis. *Eur J Neurosci.* 2011 Mar;33(6):1018-24. doi: 10.1111/j.1460-9568.2011.07599.x. Review.
6. Höglinger GU, Rizk P, Muriel MP, Duyckaerts C, Oertel WH, Caille I, Hirsch EC. Dopamine depletion impairs precursor cell proliferation in Parkinson disease. *Nat Neurosci.* 2004 Jul;7(7):726-35. Epub 2004 Jun 13.
7. Höglinger GU, Arias-Carrión O, Ipach B, Oertel WH. Origin of the dopaminergic innervation of adult neurogenic areas. *J Comp Neurol.* 2014 Jul 1;522(10):2336-48. doi: 10.1002/cne.23537.
8. Zhang T, Hong J, Di T, Chen L. MPTP Impairs Dopamine D1 Receptor-Mediated Survival of Newborn Neurons in Ventral Hippocampus to Cause Depressive-Like Behaviors in Adult Mice. *Front Mol Neurosci.* 2016 Oct 13;9:101. eCollection 2016.
9. Muslimovic D, Post B, Speelman JD, Schmand B. Cognitive profile of patients with newly diagnosed Parkinson disease. *Neurology.* 2005 Oct 25;65(8):1239-45.
10. Muthupillai R, Lomas DJ, Rossman PJ, Greenleaf JF, Manduca A, Ehman RL. Magnetic resonance elastography by direct visualization of propagating acoustic strain waves. *Science.* 1995 Sep 29;269(5232):1854-7.
11. Kruse SA, Rose GH, Glaser KJ, Manduca A, Felmlee JP, Jack CR Jr, Ehman RL. Magnetic resonance elastography of the brain. *Neuroimage.* 2008 Jan 1;39(1):231-7. Epub 2007 Aug 29.
12. Lipp A, Trbojevic R, Paul F, Fehlner A, Hirsch S, Scheel M, Noack C, Braun J, Sack I. Cerebral magnetic resonance elastography in supranuclear palsy and idiopathic Parkinson's disease. *Neuroimage Clin.* 2013 Sep 20;3:381-7. doi: 10.1016/j.nicl.2013.09.006. eCollection 2013.
13. Lipp A, Skowronek C, Fehlner A, Streitberger KJ, Braun J, Sack I. Progressive supranuclear palsy and idiopathic Parkinson's disease are associated with local reduction of in vivo brain viscoelasticity. *Eur Radiol.* 2018 Aug;28(8):3347-3354. doi: 10.1007/s00330-017-5269-y. Epub 2018 Feb 19.
14. Riek K, Millward JM, Hamann I, Mueller S, Pfueller CF, Paul F, Braun J, Infante-Duarte C, Sack I. Demyelination reduces brain parenchymal stiffness quantified in vivo by magnetic resonance elastography. *Neuroimage Clin.* 2012 Sep 12;1(1):81-90. doi: 10.1016/j.nicl.2012.09.003. eCollection 2012.
15. Schregel K, Wuerfel E, Garteiser P, Gemeinhardt I, Prozorovski T, Aktas O, Merz H, Petersen D, Wuerfel J, Sinkus R. Demyelination reduces brain parenchymal stiffness quantified in vivo by magnetic resonance elastography. *Proc Natl Acad Sci U S A.* 2012 Apr 24;109(17):6650-5. doi: 10.1073/pnas.1200151109. Epub 2012 Apr 5.
16. Freimann FB, Müller S, Streitberger KJ, Guo J, Rot S, Ghori A, Vajkoczy P, Reiter R, Sack I, Braun J. MR elastography in a murine stroke model reveals correlation of macroscopic viscoelastic properties of the brain with neuronal density. *NMR Biomed.* 2013 Nov;26(11):1534-9. doi: 10.1002/nbm.2987. Epub 2013 Jun 20.
17. Jackson-Lewis V, Jakowec M, Burke RE, Przedborski S. Time course and morphology of dopaminergic neuronal death caused by the neurotoxin 1-methyl-4-phenyl-1,2,3,6-tetrahydropyridine. *Neurodegeneration.* 1995 Sep;4(3):257-69.
18. Langston JW, Ballard P, Tetrud JW, Irwin I. Chronic Parkinsonism in humans due to a product of meperidine-analog synthesis. *Science.* 1983 Feb 25;219(4587):979-80.
19. Brochard V, Combadière B, Prigent A, Laouar Y, Perrin A, Beray-Berthet V, Bonduelle O, Alvarez-Fischer D, Callebert J, Launay JM, Duyckaerts C, Flavell RA, Hirsch EC, Hunot S. Infiltration of CD4+ lymphocytes into the brain contributes to neurodegeneration in a mouse model of Parkinson disease. *J Clin Invest.* 2009 Jan;119(1):182-92. doi: 10.1172/JCI36470. Epub 2008 Dec 22.
20. Lull ME, Block ML. Microglial activation and chronic neurodegeneration. *Neurotherapeutics.* 2010 Oct;7(4):354-65. doi: 10.1016/j.nurt.2010.05.014.
21. Deguil J, Chavant F, Lafay-Chebassier C, Pérault-Pochat MC, Fauconneau B, Pain S. Neuroprotective effect of PACAP on translational control alteration and cognitive decline in MPTP parkinsonian mice. *Neurotox Res.* 2010 Feb;17(2):142-55. doi: 10.1007/s12640-009-9091-4. Epub 2009 Jul 21.

22. Klein C, Rasińska J, Empl L, Sparenberg M, Poshtiban A, Hain EG, Iggena D, Rivalan M, Winter Y, Steiner B. Physical exercise counteracts MPTP-induced changes in neural precursor cell proliferation in the hippocampus and restores spatial learning but not memory performance in the water maze. *Behav Brain Res.* 2016 Jul 1;307:227-38. doi: 10.1016/j.bbr.2016.02.040. Epub 2016 Mar 21.
23. Kohman RA, DeYoung EK, Bhattacharya TK, Peterson LN, Rhodes JS. Wheel running attenuates microglia proliferation and increases expression of a proneurogenic phenotype in the hippocampus of aged mice. *Brain Behav Immun.* 2012 Jul;26(5):803-10. doi: 10.1016/j.bbi.2011.10.006. Epub 2011 Oct 25.
24. Monje ML, Toda H, Palmer TD. Inflammatory blockade restores adult hippocampal neurogenesis. *Science.* 2003 Dec 5;302(5651):1760-5. Epub 2003 Nov 13.
25. Kluska MM, Witte OW, Bolz J, Redecker C. Neurogenesis in the adult dentate gyrus after cortical infarcts: effects of infarct location, N-methyl-D-aspartate receptor blockade and anti-inflammatory treatment. *Neuroscience.* 2005;135(3):723-35. Epub 2005 Sep 8.
26. Kurkowska-Jastrzebska I, Babiuch M, Joniec I, Przybyłkowski A, Członkowski A, Członkowska A. Indomethacin protects against neurodegeneration caused by MPTP intoxication in mice. *Int Immunopharmacol.* 2002 Jul;2(8):1213-8.
27. Yamaguchi M1, Saito H, Suzuki M, Mori K. Visualization of neurogenesis in the central nervous system using nestin promoter-GFP transgenic mice. *Neuroreport.* 2000 Jun 26;11(9):1991-6.
28. Kalinski P. Regulation of immune responses by prostaglandin E2. *J Immunol.* 2012 Jan 1;188(1):21-8. doi: 10.4049/jimmunol.1101029.
29. Hain EG, Klein C, Munder T, Braun J, Riek K, Mueller S, Sack I, Steiner B. Dopaminergic Neurodegeneration in the Mouse Is Associated with Decrease of Viscoelasticity of Substantia Nigra Tissue. *PLoS One.* 2016 Aug 15;11(8):e0161179.
30. Lesemann A, Reinel C, Hühnchen P, Pilhatsch M, Hellweg R, Klaisle P, Winter C, Steiner B. MPTP-induced hippocampal effects on serotonin, dopamine, neurotrophins, adult neurogenesis and depression-like behavior are partially influenced by fluoxetine in adult mice. *Brain Res.* 2012 May 31;1457:51-69. doi: 10.1016/j.brainres.2012.03.046. Epub 2012 Mar 27.
31. Lu YB, Franze K, Seifert G, Steinhäuser C, Kirchhoff F, Wolburg H, Guck J, Janmey P, Wei EQ, Käs J, Reichenbach A. Viscoelastic properties of individual glial cells and neurons in the CNS. *Proc Natl Acad Sci U S A.* 2006 Nov 21;103(47):17759-64. Epub 2006 Nov 8.
32. Klein C, Hain EG, Braun J, Riek K, Mueller S, Steiner B, Sack I. Enhanced adult neurogenesis increases brain stiffness: in vivo magnetic resonance elastography in a mouse model of dopamine depletion. *PLoS One.* 2014 Mar 25;9(3):e92582. doi: 10.1371/journal.pone.0092582. eCollection 2014.
33. Lu YB, Iandiev I, Hollborn M, Körber N, Ulbricht E, Hirrlinger PG, Pannicke T, Wei EQ, Bringmann A, Wolburg H, Wilhelmsson U, Pekny M, Wiedemann P, Reichenbach A, Käs JA. Reactive glial cells: increased stiffness correlates with increased intermediate filament expression. *FASEB J.* 2011 Feb;25(2):624-31. doi: 10.1096/fj.10-163790. Epub 2010 Oct 25.
34. Vijitruth R, Liu M, Choi DY, Nguyen XV, Hunter RL, Bing G. Cyclooxygenase-2 mediates microglial activation and secondary dopaminergic cell death in the mouse MPTP model of Parkinson's disease. *J Neuroinflammation.* 2006 Mar 27;3:6.
35. Costa G, Simola N, Morelli M. MDMA administration during adolescence exacerbates MPTP-induced cognitive impairment and neuroinflammation in the hippocampus and prefrontal cortex. *Psychopharmacology (Berl).* 2015 Jan;232(1):315-6.
36. Millward JM, Guo J, Berndt D, Braun J, Sack I, Infante-Duarte C. Tissue structure and inflammatory processes shape viscoelastic properties of the mouse brain. *NMR Biomed.* 2015 Jul;28(7):831-9. doi: 10.1002/nbm.3319. Epub 2015 May 12.
37. Wuerfel J, Paul F, Beierbach B, Hamhaber U, Klatt D, Papazoglou S, Zipp F, Martus P, Braun J, Sack I. MR-elastography reveals degradation of tissue integrity in multiple sclerosis. *Neuroimage.* 2010 Feb 1;49(3):2520-5. doi: 10.1016/j.neuroimage.2009.06.018. Epub 2009 Jun 16.
38. Murphy MC, Huston J 3rd, Jack CR Jr, Glaser KJ, Manduca A, Felmlee JP, Ehman RL. Decreased brain stiffness in Alzheimer's disease determined by magnetic resonance elastography. *J Magn Reson Imaging.* 2011 Sep;34(3):494-8. doi: 10.1002/jmri.22707. Epub 2011 Jul 12.
39. Streitberger KJ, Sack I, Krefting D, Pfüller C, Braun J, Paul F, Wuerfel J. Brain viscoelasticity alteration in chronic-progressive multiple sclerosis. *PLoS One.* 2012;7(1):e29888. doi: 10.1371/journal.pone.0029888. Epub 2012 Jan 20.
40. Schlachetzki JC, Grimm T, Schlachetzki Z, Ben Abdallah NM, Eittle B, Vöhringer P, Ferger B, Winner B, Nuber S, Winkler J. Dopaminergic lesioning impairs adult hippocampal neurogenesis by distinct modification of α -synuclein. *J Neurosci Res.* 2016 Jan;94(1):62-73. doi: 10.1002/jnr.23677. Epub 2015 Oct 9.
41. L'Episcopo F, Tirolo C, Testa N, Caniglia S, Morale MC, Deleidi M, Serapide MF, Pluchino S, Marchetti B. Plasticity of subventricular zone neuroprogenitors in MPTP (1-methyl-4-phenyl-1,2,3,6-

- tetrahydropyridine) mouse model of Parkinson's disease involves cross talk between inflammatory and Wnt/ β -catenin signaling pathways: functional consequences for neuroprotection and repair. *J Neurosci*. 2012 Feb 8;32(6):2062-85. doi: 10.1523/JNEUROSCI.5259-11.2012.
42. Lie DC, Colamarino SA, Song HJ, Désiré L, Mira H, Consiglio A, Lein ES, Jessberger S, Lansford H, Dearie AR, Gage FH. Wnt signalling regulates adult hippocampal neurogenesis. *Nature*. 2005 Oct 27;437(7063):1370-5.
43. Zheng Q, Zhang Y, Ren Y, Wu Y, Yang S, Zhang Y, Chen H, Li W, Zhu Y. Antiproliferative and apoptotic effects of indomethacin on human retinoblastoma cell line Y79 and the involvement of β -catenin, nuclear factor- κ B and Akt signaling pathways. *Ophthalmic Res*. 2014;51(2):109-15. doi: 10.1159/000355844. Epub 2013 Dec 19.
44. Schwab MH, Bartholomae A, Heimrich B, Feldmeyer D, Druffel-Augustin S, Goebbels S, Naya FJ, Zhao S, Frotscher M, Tsai MJ, Nave KA. Neuronal basic helix-loop-helix proteins (NEX and BETA2/Neuro D) regulate terminal granule cell differentiation in the hippocampus. *J Neurosci*. 2000 May 15;20(10):3714-24.
45. Uittenbogaard M, Baxter KK, Chiaramello A. The neurogenic basic helix-loop-helix transcription factor NeuroD6 confers tolerance to oxidative stress by triggering an antioxidant response and sustaining the mitochondrial biomass. *ASN Neuro*. 2010 May 24;2(2):e00034. doi: 10.1042/AN20100005.
46. Grandbarbe L, Bouissac J, Rand M, Hrabé de Angelis M, Artavanis-Tsakonas S, Mohier E. Delta-Notch signaling controls the generation of neurons/glia from neural stem cells in a stepwise process. *Development*. 2003 Apr;130(7):1391-402.
47. Hirsch EC, Hunot S. Neuroinflammation in Parkinson's disease: a target for neuroprotection? *Lancet Neurol*. 2009 Apr;8(4):382-97. doi: 10.1016/S1474-4422(09)70062-6.
48. Manocha GD, Floden AM, Puig KL, Nagamoto-Combs K, Scherzer CR, Combs CK. Defining the contribution of neuroinflammation to Parkinson's disease in humanized immune system mice. *Mol Neurodegener*. 2017 Feb 14;12(1):17. doi: 10.1186/s13024-017-0158-z.
49. Yasuda Y, Shimoda T, Uno K, Tateishi N, Furuya S, Yagi K, Suzuki K, Fujita S. The effects of MPTP on the activation of microglia/astrocytes and cytokine/chemokine levels in different mice strains. *J Neuroimmunol*. 2008 Nov 15;204(1-2):43-51. doi: 10.1016/j.jneuroim.2008.08.003.
50. Côté M, Poirier AA, Aubé B, Jobin C, Lacroix S, Soulet D. Partial depletion of the proinflammatory monocyte population is neuroprotective in the myenteric plexus but not in the basal ganglia in a MPTP mouse model of Parkinson's disease. *Brain Behav Immun*. 2015 May;46:154-67. doi: 10.1016/j.bbi.2015.01.009. Epub 2015 Jan 27.
51. Przedborski S, Vila M. The 1-methyl-4-phenyl-1,2,3,6-tetrahydropyridine mouse model: a tool to explore the pathogenesis of Parkinson's disease. *Ann N Y Acad Sci*. 2003 Jun;991:189-98.
52. Rees K, Stowe R, Patel S, Ives N, Breen K, Clarke CE, Ben-Shlomo Y. Non-steroidal anti-inflammatory drugs as disease-modifying agents for Parkinson's disease: evidence from observational studies. *Cochrane Database Syst Rev*. 2011 Nov 9;(11):CD008454. doi: 10.1002/14651858.CD008454.pub2.

Eidesstattliche Versicherung

„Ich, Elisabeth Gertrud Hain, versichere an Eides statt durch meine eigenhändige Unterschrift, dass ich die vorgelegte Dissertation mit dem Thema: „Einfluss von Indomethazin auf die adulte hippocampale Neurogenese und viskoelastische Eigenschaften des Gehirns im MPTP-Mausmodell für Dopamindepletion“ selbstständig und ohne nicht offengelegte Hilfe Dritter verfasst und keine anderen als die angegebenen Quellen und Hilfsmittel genutzt habe.

Alle Stellen, die wörtlich oder dem Sinne nach auf Publikationen oder Vorträgen anderer Autoren beruhen, sind als solche in korrekter Zitierung kenntlich gemacht. Die Abschnitte zu Methodik (insbesondere praktische Arbeiten, Laborbestimmungen, statistische Aufarbeitung) und Resultaten (insbesondere Abbildungen, Graphiken und Tabellen) werden von mir verantwortet.

Meine Anteile an etwaigen Publikationen zu dieser Dissertation entsprechen denen, die in der untenstehenden gemeinsamen Erklärung mit der Betreuerin, angegeben sind. Für sämtliche im Rahmen der Dissertation entstandenen Publikationen wurden die Richtlinien des ICMJE (International Committee of Medical Journal Editors; www.icmje.org) zur Autorenschaft eingehalten. Ich erkläre ferner, dass mir die Satzung der Charité – Universitätsmedizin Berlin zur Sicherung Guter Wissenschaftlicher Praxis bekannt ist und ich mich zur Einhaltung dieser Satzung verpflichte.

Die Bedeutung dieser eidesstattlichen Versicherung und die strafrechtlichen Folgen einer unwahren eidesstattlichen Versicherung (§156,161 des Strafgesetzbuches) sind mir bekannt und bewusst.“

Berlin, 11.05.2019

Anteilerklärung an den ausgewählten Publikationen

Elisabeth Gertrud Hain hatte folgenden Anteil an den folgenden Publikationen:

Publikation 1:

Klein C, Hain EG, Braun J, Riek K, Mueller S, Steiner B, Sack I. Enhanced adult neurogenesis increases brain stiffness: in vivo magnetic resonance elastography in a mouse model of dopamine depletion. PLoS One. 2014 Mar 25;9(3):e92582.

Beitrag im Einzelnen: Durchführung der Tierbehandlungen und -experimente, Gewebepräparation, Immunhistochemie und Immunfluoreszenz, Erhebung und Auswertung der histologischen Daten, Revision des Manuskripts.

Publikation 2:

Hain EG, Klein C, Munder T, Braun J, Riek K, Mueller S, Sack I, Steiner B. Dopaminergic Neurodegeneration in the Mouse Is Associated with Decrease of Viscoelasticity of Substantia Nigra Tissue. PLoS One. 2016 Aug 15;11(8):e0161179.

Beitrag im Einzelnen: Studienplanung und Studiendesign, Planung und Durchführung der Tierbehandlungen und -experimente, Gewebepräparation, Immunhistochemie und Immunfluoreszenz, Erhebung und Auswertung der histologischen Daten, statistische Auswertung und grafische Aufarbeitung der histologischen und MRE-Daten in SPSS und GraphPad Prism, Schreiben und Revision des Manuskripts.

Publikation 3:

Hain EG, Sparenberg M, Rasińska J, Klein C, Akyüz L, Steiner B. Indomethacin promotes survival of new neurons in the adult murine hippocampus accompanied by anti-inflammatory effects following MPTP-induced dopamine depletion. J Neuroinflammation. 2018 May 26;15(1):162.

Beitrag im Einzelnen: Studienplanung und Studiendesign, Planung und Durchführung der Tierbehandlungen, Gewebepräparation, Immunhistochemie und Immunfluoreszenz, Erhebung und Auswertung der Daten, statistische Auswertung und grafische Aufarbeitung der Daten in SPSS und GraphPad Prism, Schreiben und Revision des Manuskripts.

Unterschrift, Datum und Stempel PD Dr. med. Barbara Steiner

Unterschrift Elisabeth Gertrud Hain

Enhanced Adult Neurogenesis Increases Brain Stiffness: *In Vivo* Magnetic Resonance Elastography in a Mouse Model of Dopamine Depletion

Charlotte Klein¹, Elisabeth G. Hain¹, Juergen Braun², Kerstin Riek³, Susanne Mueller⁴, Barbara Steiner^{1*}, Ingolf Sack^{3,9}

1 Department of Neurology, Charité - University Medicine Berlin, Berlin, Germany, **2** Institute of Medical Informatics, Charité - University Medicine Berlin, Berlin, Germany, **3** Department of Radiology, Charité - University Medicine Berlin, Berlin, Germany, **4** Center for Stroke Research Berlin, Berlin, Germany

Abstract

The mechanical network of the brain is a major contributor to neural health and has been recognized by *in vivo* magnetic resonance elastography (MRE) to be highly responsive to diseases. However, until now only brain softening was observed and no mechanism was known that reverses the common decrement of neural elasticity during aging or disease. We used MRE in the 1-methyl-4-phenyl-1,2,3,6-tetrahydropyridine hydrochloride (MPTP) mouse model for dopaminergic neurodegeneration as observed in Parkinson's disease (PD) to study the mechanical response of the brain on adult hippocampal neurogenesis as a robust correlate of neuronal plasticity in healthy and injured brain. We observed a steep transient rise in elasticity within the hippocampal region of up to over 50% six days after MPTP treatment correlating with increased neuronal density in the dentate gyrus, which could not be detected in healthy controls. Our results provide the first indication that new neurons reactively generated following neurodegeneration substantially contribute to the mechanical scaffold of the brain. Diagnostic neuroimaging may thus target on regions of the brain displaying symptomatically elevated elasticity values for the detection of neuronal plasticity following neurodegeneration.

Citation: Klein C, Hain EG, Braun J, Riek K, Mueller S, et al. (2014) Enhanced Adult Neurogenesis Increases Brain Stiffness: *In Vivo* Magnetic Resonance Elastography in a Mouse Model of Dopamine Depletion. PLoS ONE 9(3): e92582. doi:10.1371/journal.pone.0092582

Editor: Friedemann Paul, Charité University Medicine Berlin, Germany

Received: October 26, 2013; **Accepted:** February 24, 2014; **Published:** March 25, 2014

Copyright: © 2014 Klein et al. This is an open-access article distributed under the terms of the Creative Commons Attribution License, which permits unrestricted use, distribution, and reproduction in any medium, provided the original author and source are credited.

Funding: The work was supported by the German Research Foundation (Sa 901/4 to IS) and by the Else Kroener Fresenius Foundation (P21/10//A141/09 to BS). The funders had no role in study design, data collection and analysis, decision to publish, or preparation of the manuscript.

Competing Interests: The authors have declared that no competing interests exist.

* E-mail: barbara.steiner@charite.de

⁹ These authors contributed equally to this work.

Introduction

Magnetic resonance elastography (MRE) has been developed over the last few years as a non-invasive tool to evaluate the elasticity of biological tissues [1]. The presence of the skull has always prevented manual palpation of the brain, but MRE now offers the possibility to assess brain consistency under physiological and pathological conditions by *in-vivo* imaging [2–7]. In the brain, the viscoelastic properties are determined by neurons, glial cells [8] and extracellular matrix in addition to fluid flow of interstitial fluid, CSF and blood [9]. Disruption of this complex system by pathological processes provokes mechanical responses, which are influential to the progression of the disease but also of potential value for its diagnosis and clinical assessment. However, the biophysical mechanisms behind an alteration of the mechanical properties of tissue are entirely unknown in the brain.

It has just recently been discovered that brain elasticity is reduced in the course of physiological aging [10] and in diseases such as normal pressure hydrocephalus (NPH) [11], Alzheimer's disease (AD) [12] and multiple sclerosis (MS) [13,14]. First steps to correlate these findings with the histopathology have been taken quite recently by Schregel and colleagues inducing reversible toxic demyelination in the mouse [15] and by Riek and co-workers who studied the effect of inflammation in a mouse model of

experimental autoimmune encephalitis (EAE) [16]. Both groups observed a marked decrease of viscoelastic constants similar to what has been detected in patients with NPH, AD and MS. Of particular interest is a very recent study by Freimann and co-workers demonstrating a clear correlation of brain tissue softening with reduced neuronal density after middle cerebral artery occlusion (MCAO) in mice, which is a commonly used stroke model [17]. It is remarkable that all pathophysiological processes studied by cerebral MRE so far exhibited a rather unspecific reduction in either elasticity or viscosity or both. Inversely, no neural alteration has been observed associated with an increase of viscoelastic constants. Potentially, such a disease-related process would appear highly significant in diagnostic MRE since it would be distinguishable from the general pattern of tissue softening reported in the literature. Based on previous work that showed the correlation between neuronal density and macroscopic brain stiffness by inducing neuronal loss [17], we hypothesize that the generation of new neurons would increase the macroscopic elasticity of the brain. Given that this hypothesis is corroborated, our study would provide an indication about the close relationship between brain mechanical constants and neuronal network density.

The generation of new neurons should be apparent in regions with high cellular turnover. In the adult brain, new nerve cells are

generated in the subgranular zone (SGZ) of the hippocampal dentate gyrus (DG) at substantial levels throughout lifetime. Here, neural precursor cells characterized by the expression of the intermediate filament nestin [18] continuously proliferate and mature into functionally integrated cells in the granular cell layer (GCL) via a multistep process termed adult neurogenesis [19–21]. It has been shown that a homeostasis of neurotransmitters such as dopamine plays a key role in the regulation of adult neurogenesis and the maintenance of a so-called neurogenic niche. Alterations in dopamine levels as observed in Parkinson's disease (PD) and its animal models result in significant quantitative changes of newly generated neural precursor cells and mature neurons in the DG [22–30].

Therefore, we applied MRE to such a mouse model of dopamine depletion, which is induced by the neurotoxin 1-methyl-4-phenyl-1,2,3,6-tetrahydropyridine hydrochloride (MPTP) leading to degeneration of dopaminergic neurons in the substantia nigra pars compacta (SNpc) with a subsequent dopamine deficit in the striatum, hippocampus and other brain areas that are innervated by dopaminergic fibers from the SNpc [31–35]. Cellular changes in the DG of the hippocampus as a consequence of the induced dopamine deficit were visualized by labelling newly generated cells in the SGZ with specific mitotic and neuronal markers, and characterized and quantified using confocal microscopy. To also determine alterations in the total cell number, cells of the GCL in the DG including the SGZ were counted using stereological microscopy. Hence, this animal model of dopamine depletion provides the possibility to examine how alterations of the neuronal matrix in certain brain areas resulting from a dopamine deficit relate to MRE measurements, and to expand the utility of MRE as a tool to monitor cellular changes in the pathology of neurodegenerative diseases.

Materials and Methods

Animals

A total of 60 eight to ten weeks old female transgenic C57Bl/6 mice (Forschungseinrichtung für experimentelle Medizin, FEM, Berlin, Germany), expressing the green fluorescent protein (GFP) under the nestin promoter, were group-housed ($n=5$) in a temperature- and humidity-controlled colony room and maintained on a light/dark cycle of 12/12 h (lights on at 6 am) with ad libitum access to rodent lab chow and water. All experiments were approved by the local animal ethics committee (Landesamt für Gesundheit und Soziales, Berlin) and were carried out in accordance with the European Communities Council Directive of 24 November 1986 (86/609/EEC).

Group Design and Experimental Procedure

The mice were randomly assigned to four groups in total - three for histology and one for MRE. The MRE group ($n=5$) was investigated first without any modifications for obtaining reference (baseline) data; then MRE was applied at five time-points after NaCl treatment at 3, 6, 10, 14 and 18 days post injection (dpi), followed by MPTP treatment and MRE measurements again at 3, 6, 10, 14 and 18 dpi. The last MRE measurement of NaCl-treated mice (18 dpi) also served as baseline data of MPTP-treated mice.

The histology groups (not investigated by MRE) comprised untreated mice (baseline; $n=5$) and treated animals either with MPTP (MPTP; $n=25$) or with NaCl (Control, CTR; $n=25$). The treated groups (MPTP and CTR) were further subdivided into groups of five, which were sacrificed at 3, 6, 10, 14 and 18 days after the MPTP/NaCl treatment period. Figure 1a summarizes the timeline of the injections, MRE experiments and histology.

MPTP Model

1-methyl-4-phenyl-1,2,3,6-tetrahydropyridine hydrochloride (MPTP, Sigma-Aldrich, Steinheim, Germany) was dissolved in 0.9% NaCl.

For lesioning, a protocol previously applied was followed [27,28]. Briefly, mice received three single intraperitoneal (i.p.) injections of MPTP (20 mg/kg body weight; in total 60 mg/kg) on three consecutive days every 24 hours. Control animals were treated with injections of 0.9% NaCl instead for the same time period. Control mice of the baseline group remained untreated.

BrdU Injections

Bromodesoxyuridine (BrdU, Sigma-Aldrich, Steinheim, Germany), used here as the mitotic marker to label proliferating cells, was dissolved in 0.9% NaCl and filtered. Animals received three single i.p. injections of BrdU (50 mg/kg body weight; in total 150 mg/kg) on three consecutive days every 24 h. BrdU treatment started at the final day of MPTP-injections.

Magnetic Resonance Elastography (MRE)

Mechanical stimulation. Mouse brains were mechanically stimulated as previously illustrated [16]. A schematic of the experimental setup is shown in Figure 1b. Briefly, the vibration source was an electromagnetic coil, attached to a carbon fiber piston, the end of which was mounted to the respiratory mask with a bite-bar transducer. The transducer was gimbaled through a rubber bearing and retaining bracket at the temperature-controlled mouse bed. The entire setup was held in the centre of the magnet bore by a plastic disk. Vibrations were produced by applying a sinusoidal current of 900 Hz frequency to an air-cooled Lorentz coil in the fringe field of the MRI scanner. Frequency amplitude and number of sinusoidal oscillation cycles were controlled by an arbitrary function generator connected via an audio amplifier to the driving coil. The main polarization of the vibration was transverse to the principal axis of the magnet field, with amplitudes in the order of tens of micrometers.

Data acquisition and analysis. As previously described [16,17], all measurements were performed on a 7 tesla scanner (Bruker PharmaScan 70/16, Ettlingen, Germany) running ParaVision 4.0 software and using a 20 mm diameter 1H-RF-quadratur mouse head volumecoil. The vibration was initiated by a trigger pulse from the control unit of the scanner, the timing of which was defined by a customized FLASH sequence. The imaging sequence was modified for MRE by sinusoidal motion sensitizing gradient (MSG) in the through-plane direction, as described elsewhere [16]. The MSG strength was 285 mT/m with a frequency of 900 Hz and 9 periods. To compensate for static phase contributions, phase difference images were calculated from two images differing in the sign of the MSG. Further imaging parameters were: a 128×128 matrix, 25 mm FoV, 14.3 ms echo time (TE), 116.2 ms repetition time (TR), eight dynamic scans over a vibration period, one transverse 2-mm slice, and an acquisition time of 20 min.

Complex wave images (Figure 2) corresponding to the harmonic drive frequency were calculated by temporal Fourier transformation of the unfolded phase-difference images and filtered for suppressing noise and compression wave components [16,36]. The pre-processed 2D scalar wave fields were analyzed for the complex shear modulus G^* by algebraic Helmholtz inversion [37]. Then, G^* was spatially averaged over two regions of interest (ROI's), i) the whole brain parenchyma displayed in the image and ii) the hippocampal area (Figure 2), manually segmented by delineating its anatomical structure from MRE magnitude images. The tabulated spatially averaged G^* -values are represented by the real

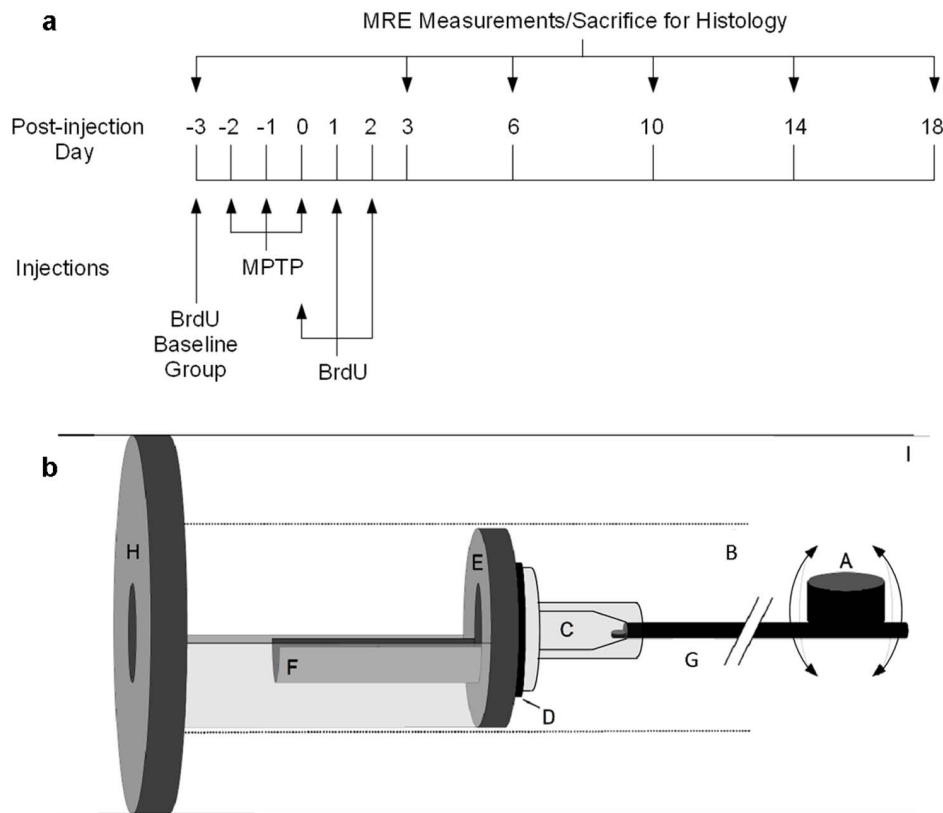


Figure 1. Timeline of the study design and schematic of the mouse MRE apparatus. The timeline (a) of MPTP and BrdU injections, time-points of MRE measurement and sacrifice for histology. A schematic (b) of the mouse MRE apparatus: (A) driving coil, (B) magnet bore, (C) respiratory mask, (D) rubber bearing, (E) retaining bracket, (F) mouse bed, (G) carbon fiber piston, (H) plastic disk, and (I) Lorentz coil (modified from [16]). doi:10.1371/journal.pone.0092582.g001

part of the complex shear modulus G^* , $G' = \text{Re}(G^*)$, known as storage modulus, the imaginary part $G'' = \text{Im}(G^*)$, which is the loss modulus, the magnitude $|G^*| = \text{abs}(G^*)$ and the loss tangent given by $\phi = \arctan(G''/G')$. The storage, loss and magnitude moduli are expressed in kilopascals (kPa) while ϕ is given in radians. In general, G' relates to the elastic properties of a material, while G'' is a measure of viscosity, which is determined by the density and geometry of the mechanical network in biological tissues. In materials with dominating elastic behaviour, the parameters $|G^*|$ and ϕ represent similar properties as G' and G'' . However, in highly crosslinked biological tissues, the phase angle ϕ better represents geometrical changes in the mechanical network than G'' [38].

Perfusion and Tissue Processing

Mice of the histology groups were sacrificed according to the corresponding MRE measurement time-points as depicted in Figure 1a.

They were deeply anesthetized with an overdose of ketamine (ketamine hydrochloride, 100 mg/ml, WDT) and sacrificed by transcardial perfusion with 1 M phosphate buffered saline (PBS) and 4% paraformaldehyde (PFA). Brains were removed and post-fixed overnight in PFA at 4°C and then transferred into 30% sucrose for dehydration for 48 h. Brains were frozen in 2-methyl butane cooled with liquid nitrogen, cut into 40 μm thick coronal sections (Bregma -0.1 mm to -4.04 mm) using a cryostat (Leica CM 1850 UV) and stored in cryoprotectant-containing 24-well plates at 4°C until histological analysis.

Immunohistochemistry

Immunohistochemistry for the Iba1 antigen as a marker for microglia and macrophages was performed following a well-established staining protocol [28]. Briefly, free-floating 1-in-12 section series were treated with 0.6% H_2O_2 to deactivate endogenous tissue peroxidases. After 30 min background blocking with PBS enriched with 3% donkey serum (PBS+), sections were incubated with primary anti-Iba1 (rabbit, 1:1000, Wako) antibody overnight at 4°C. The next day, after washing with PBS and blocking with PBS+, sections were incubated with biotinylated secondary antibody (anti-rabbit, 1:250, dianova) for 2 h at room temperature (RT). ABC reagent (Vectastain ABC Elite Kit, Vector Laboratories) was applied for 1 h. Finally, sections were incubated with Diaminobenzidine (DAB)/peroxidase (Sigma, Germany) in a solution containing 0.3% H_2O_2 and 0.01% nickel chloride for at least 5 min at RT. Sections were mounted on microscope slides and coverslipped for later quantification.

Immunofluorescence

For triple-labelling, free-floating 1-in-12 section series were rinsed and incubated as described above except for H_2O_2 pre-treatment but 1 h PBS+ blocking instead. Anti-BrdU (rat, 1:500, AbD Serotex) anti-GFP (chicken, 1:250, Novus Biologicals) and anti-NeuN (mouse, 1:100, Millipore) were used as primary antibodies. BrdU denotes newly generated cells, while BrdU/Nestin (Nestin/GFP) and BrdU/NeuN denote new neural precursor cells and new neurons, respectively. After incubation for 48 h at 4°C, RhodamineX (anti-rat, 1:250, dianova), Alexa 488 (anti-chicken, 1:1000, Invitrogen) and Alexa 647 (anti-mouse,

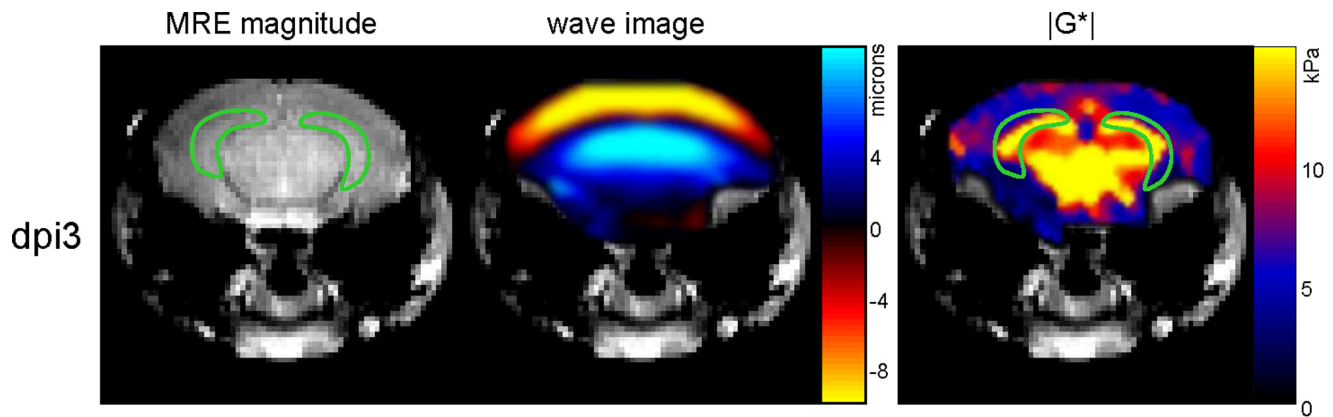


Figure 2. Representative images of the magnitude MRE signal, shear waves and the magnitude complex modulus ($|G^*$) in a mouse. The green line demarcates the chosen region of interest in the hippocampus. doi:10.1371/journal.pone.0092582.g002

1:300, dianova.) as secondary antibodies diluted in PBS+ were applied for 4 h at RT. Sections were mounted on microscope slides and coverslipped for later quantification.

For stereological counting of cells in the GCL of the DG including the cells in the SGZ in order to determine its total cell number, separate 1-in-12 series of sections were incubated with the fluorochrome 4',6-diamidino-2-phenylindole (DAPI), which binds to the DNA thereby labeling cell nuclei in general. For this purpose, sections were incubated with PBS-diluted DAPI (1:1000, Thermo Scientific) for 7 min and afterwards mounted on microscope slides and coverslipped for later quantification.

Quantification

Iba1-positive cells of DAB/oxidase-stained 1-in-12 section series (480 μm apart) from all animals were counted throughout the rostrocaudal extent of the GCL/SGZ, molecular layer (ML) and hilus in the hippocampal formation in both hemispheres using the 40 \times objective of a light microscope (Axioskop, Zeiss, Germany). In total, four brain slices per animal containing the hippocampus were analyzed. Resulting absolute cell numbers were then multiplied by twelve to obtain the estimated total number of Iba1-positive cells per brain.

BrdU-positive cells in the fluorescent-stained sections were counted as described for Iba1 but in the GCL/SGZ only using a fluorescence microscope (Axioskop, Zeiss, Germany).

Double-labeled cells were quantified by analyzing 50 BrdU-positive cells spread throughout the rostrocaudal extent of the GCL/SGZ of four brain slices per animal for co-expression of BrdU and additional markers (Nestin/GFP and NeuN) using a Leica TCS SP2 confocal microscope (400 \times and 630 \times amplification). All images were taken in a sequential scanning mode (z-stacks) to identify superposed cell bodies or nuclei, which appeared artificially merged. Then, the percentages of Nestin/GFP- and NeuN-positive cells in all 50 BrdU-cells were determined. These ratios along with the total numbers of BrdU-positive cells were then used to calculate the absolute numbers of doubly labeled cells.

For quantification of absolute numbers of DAPI-stained cell nuclei in the GCL, a Leica DMRE microscope and Stereo-Investigator (MicroBrightfield) software were used. The boundaries of the GCL, the region of interest, of five sections per animal were traced at 200 \times magnification and the thickness of the slices (40 μm) was entered to the software program. The software then randomly arranged counting frames (30 μm \times 30 μm \times 30 μm) in a sampling grid (120 μm \times 100 μm), which was placed over the

region of interest. The DAPI-stained cell nuclei were counted at 400 \times amplification in oil in the counting frames and in an Optical Disector height of 20 μm , which started 5 μm below the top surface. The total number of cells in the GCL was automatically calculated based on the counted cell number, slice interval, counting frame size, sampling grid size, slice thickness and Optical Disector height.

Statistical Analysis

To test for normal distribution and homogeneous variances, the Kolmogorov-Smirnov test and the Levené test, respectively, were applied. Since group sizes in this study were completely equal ($n = 5$), for analysis, two-way ANOVAs of the histological data and repeated measures (RM) two-way ANOVAs of the MRE data were conducted, although not all data sets met the assumptions for an ANOVA. In the two-way ANOVA, Treatment represented the between-subjects factor and Time the within-subjects factor. In the RM two-way ANOVA, Time and Treatment by Time represented the within-subjects factors and Treatment the between-subjects factor. Pairwise comparisons applying the Bonferroni test were used to directly compare the two treatment groups within each time-point or the different time-points within each treatment group, respectively. All statistical analysis was conducted using SPSS Statistics 19 for Windows with the level of significance set at 0.05. The diagrams were prepared using GraphPad Prism 5.

Results

MPTP-induced Transient Increase of Brain Elasticity and Viscosity

We investigated how brain viscoelasticity is affected by a MPTP-induced dopamine deficit. MRE was performed one day before MPTP-treatment (to establish a baseline), and 3, 6, 10, 14 and 18 days after treatment cessation to determine viscoelastic changes as a consequence of dopamine depletion. The results of MRE measurements focussing on the hippocampus, the region that contains a highly neurogenic area (SGZ) modulated by dopamine, are shown in Figure 3 (a–d). No influence of time was seen in the control group for any of the MRE parameters. Mean values (\pm standard error of the mean, SEM) in the hippocampal region of controls were 4.608 (\pm 0.719) kPa, 1.388 (\pm 0.125) kPa, 4.816 (\pm 0.705) kPa and 0.549 (\pm 0.073) for G' , G'' abs(G^*) and ϕ , respectively. Similar values were found in the entire brain of the control group with 5.234 (\pm 0.564) kPa, 1.447 (\pm 0.87) kPa, 5.432

(± 0.553) kPa and 0.574 (± 0.034) for G' , G'' , $\text{abs}(G^*)$ and ϕ , respectively. RM two-way ANOVA showed an overall effect of time on G' ($F(5,40) = 5.239$, $p < 0.001$), G'' ($F(5,40) = 9.669$, $p < 0.001$) and $\text{abs}(G^*)$ ($F(5,40) = 5.689$, $p < 0.001$), a treatment by time effect on G' ($F(5,40) = 3.841$, $p < 0.01$), G'' ($F(5,40) = 4.240$, $p < 0.01$) and $\text{abs}(G^*)$ ($F(5,40) = 4.045$, $p < 0.01$) in MPTP-treated mice, but no effect of treatment alone on G' ($F(1,8) = 3.758$, $p = 0.089$), G'' ($F(1,8) = 1.378$, $p = 0.274$) and $\text{abs}(G^*)$ ($F(1,8) = 3.979$, $p = 0.081$). Pairwise comparison between groups at different days using the Bonferroni test revealed a marked temporary MPTP-induced increase at 6 dpi of G' (Figure 3a, $p < 0.01$), G'' (Figure 3b, $p < 0.01$) and $\text{abs}(G^*)$ (Figure 3c, $p < 0.01$) towards 6971 (1019) kPa, 1767 (103) kPa, 7192 (1011) kPa in the hippocampus, which was still significant within the whole-brain region (Figure S1). Relative to baseline values, the changes of G' , G'' and $\text{abs}(G^*)$ at 6 dpi in the hippocampus were 51%, 27%, and 49% and 29%, 16%, and 28% in the whole brain, respectively. Since the phase angle ϕ (Figure 3d) remains unchanged by treatment ($F(1,8) = 0.363$, $p = 0.563$) during the course of measurements ($F(5,40) = 0.573$, $p = 0.720$), the findings suggest that the viscoelasticity of hippocampal tissue is selectively altered transiently after MPTP treatment without influencing the architecture of the cellular matrix.

MPTP-induced Transient Increase of New Neural Precursor Cells and Neurons

Figure 3 (e and f) shows cell numbers of new neurons (BrdU+/NeuN+) and precursor cells (BrdU+/Nestin/GFP+) relative to the total number of BrdU-positive cells in the SGZ and GCL. Analysis by two-way ANOVA revealed a noticeable time effect on both cell types (BrdU+/Nestin/GFP+: $F(5,48) = 9.070$, $p < 0.0001$; BrdU+/NeuN+: $F(5,48) = 41.910$, $p < 0.0001$), but only a marginal interaction of both factors (BrdU+/Nestin/GFP+: $F(5,48) = 2.146$, $p = 0.076$; BrdU+/NeuN+: $F(5,48) = 2.095$, $p = 0.082$). Pairwise comparisons showed that mice treated with MPTP displayed a larger proportion of new precursor cells at 3 dpi (Figure 3e; $p < 0.05$) and of new neurons at 6 dpi (Figure 3f; $p < 0.05$) than controls regarding the total amount of newly generated cells. However, at 18 dpi, referring to the last day of MRE measurement, MPTP treatment appeared to provoke a reduced neurogenesis expressed as a smaller proportion of new neurons compared to controls (Figure 3f; $p < 0.05$).

Absolute numbers of newly generated cells (BrdU+), new neural precursor cells and new neurons are shown in Figure 4 (b–d). Representative confocal images of BrdU and its colocalization with Nestin/GFP or NeuN, respectively, are shown in Figure 5. A two-way ANOVA revealed a strong influence of time on all three cell types (BrdU: $F(5,48) = 19.336$, $p < 0.0001$; BrdU/Nestin: $F(5,48) = 12.542$, $p < 0.0001$; BrdU/NeuN: $F(5,48) = 13.920$, $p < 0.0001$). Furthermore, the ANOVA also showed a treatment by time effect on newly generated precursor cells ($F(5,48) = 2.768$, $p < 0.05$). Pairwise comparison showed that in MPTP-treated mice, compared to controls, an increased proliferation of Nestin/GFP cells occurred until 3 dpi (Figure 4c; $p < 0.001$) with a subsequent drop on 6 dpi ($p < 0.01$, compared to MPTP at 3 dpi; not indicated in the figure) that may suggest a transient reactive proliferation of Nestin/GFP precursor cells in response to the neurotoxin as shown before in previous work from our group (27, 28). The observed course of BrdU-, new Nestin/GFP- und new NeuN-positive cell numbers over time generally parallels the suggested different stages during neuronal development including proliferation, survival and maturation [20].

MPTP-induced Increase of Microglia in the DG Region does not Change the Total Number of Cells in the GCL

The obtained numbers from stereological counting of DAPI-stained GCL/SGZ cells are shown in Figure 4a. Neither an overall effect of treatment ($F(1,48) = 1.052$, $p = 0.31$) or time ($F(5,48) = 0.382$, $p = 0.859$) alone nor an interaction between these factors ($F(5,48) = 0.713$, $p = 0.616$) was found, indicating that the total number of GCL and SGZ cells was not affected by MPTP treatment and there was also no change in the total cell number over time.

Absolute numbers of all Iba1-positive cells in the GCL/SGZ, molecular layer and hilus are shown in Figure 4e. As a two-way ANOVA revealed, only time had an influence on the number of Iba1-positive cells ($F(5,48) = 9.635$, $p < 0.0001$). Pairwise comparisons showed that treatment groups differed at 3 dpi ($p < 0.05$) with MPTP-treated mice displaying more microglia and macrophages in the DG region than their unaffected controls. However, numbers of Iba1-positive cells in mice treated with MPTP stay high, while controls then reach the same level of microglia and macrophages at 6 dpi.

Discussion

MPTP-induced degeneration of dopaminergic neurons affects neurogenesis in the hippocampus [24,28,29] and leads to changes in neural cell proliferation patterns in wide regions of the brain [24,25,27,39]. We observed for the first time that newly generated neurons in the DG potentially integrate with the mechanical scaffold of brain tissue yielding an apparent invigoration of the viscoelastic lattice with 50% increased shear modulus (G') in MPTP-lesioned mice at 6 dpi. In comparison, the neuronal density in the SGZ/GCL changed only by 10% (see Figure 3f) thereby highlighting the sensitivity of macroscopic shear modulus to the number and type of cells engaged in the mechanical tissue matrix. This marked increase of shear elasticity as a result of reactively generated neurons induced by a dopamine deficit is in alignment with observations of [17] who demonstrated that, in contrast to our study, brain stiffness in a murine stroke model is reduced due to neuronal loss. Taken together both studies shed light onto the important role of neurons as a supporting structure of the brain's mechanical scaffold and complements recent results of in vivo MRE in volunteers and patients: A loss of neuronal support in the viscoelastic lattice of the brain may contribute to the disseminated decrease of G' and G'' observed in the aging brain and in patients with NPH, AD and MS [10–14]. Given this pivotal role of neurons for the macroscopic mechanical properties of the brain, it is not surprising that cerebral MRE has been more sensitive to physiological aging than any other MRI method [13,40].

In general, the sensitivity of in vivo MRE arises from the scaling properties of mechanical constants. The shear modulus of a hierarchical system is determined by crosslinks in each existing level within the tissue's architecture towards microscopic interactions of cells [38]. Understanding the macroscopic mechanical response of our mouse model requires both knowledge about single-cell properties and how these properties would integrate into the multi-hierarchical lattice of the brain. Single neurons and glia cells taken from mouse brain tissue investigated by scanning force microscopy showed – similar to the bulk tissue – a higher storage modulus than loss modulus ($G' > G''$) with neurons being generally stiffer than glia cells [41]. This supports our proposed mechanistic explanation that the neuronal network establishes the primary mechanical backbone of the brain. In the bulk tissue, the ratio between elastic and viscose properties (as quantified by our loss tangent $\phi = \arctan(G''/G')$) can give some insight into the

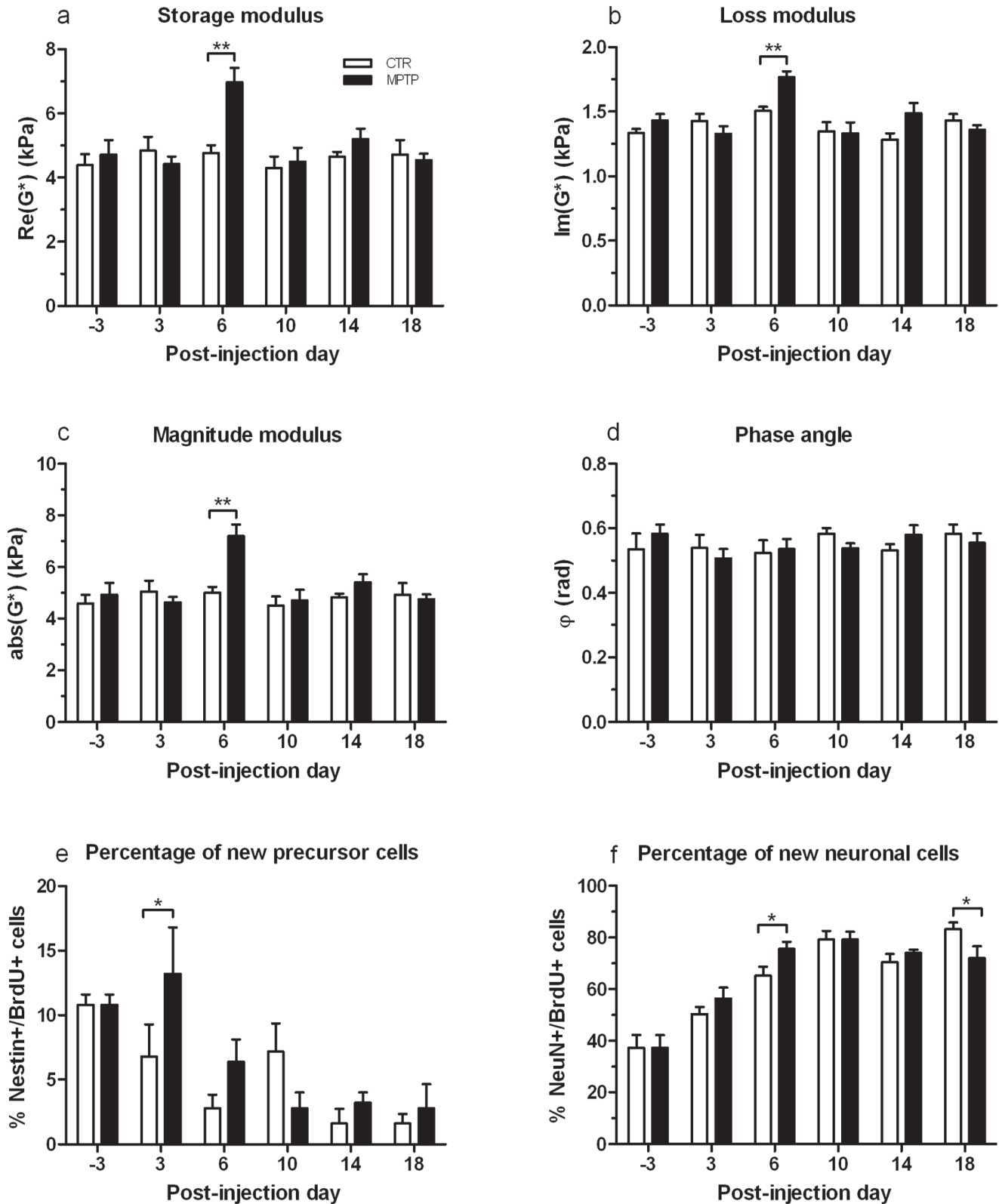


Figure 3. Variation of MRE parameters due to MPTP in the hippocampus of mice and results of cell counts in the DG. MPTP induced a transient increase of brain elasticity and viscosity (a, b and c) at 6 dpi, while the phase angle ϕ (d) remained unchanged (mean \pm SEM). Histologically, a transient MPTP-induced increase of new precursor cells (BrdU+/Nestin/GFP+) at 3 dpi (e) and of new neurons (BrdU+/NeuN+) at 6 dpi (f) as percentage of all newborn cells (BrdU+) was found (mean \pm SEM). * $p < 0.05$, ** $p < 0.01$. doi:10.1371/journal.pone.0092582.g003

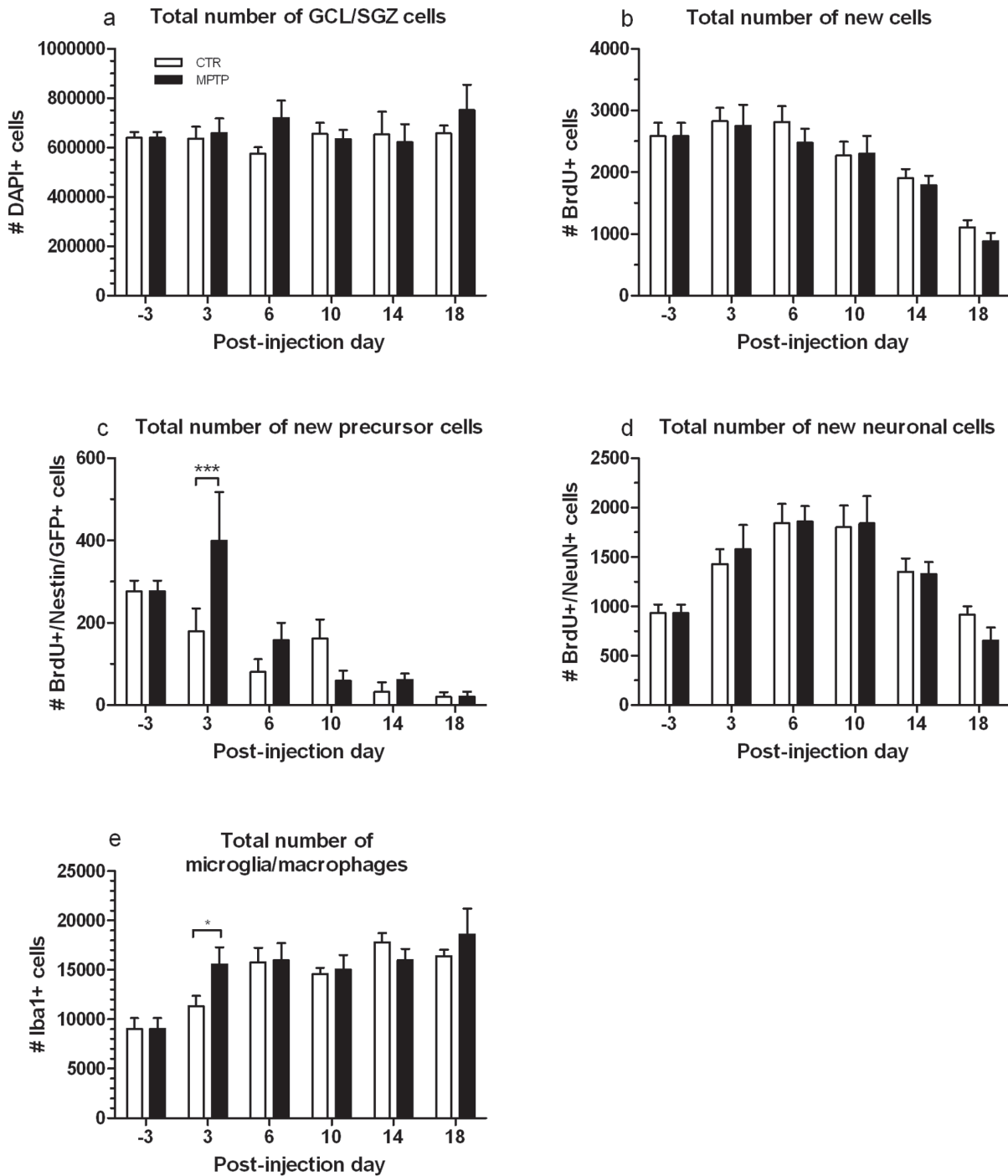


Figure 4. Results of cell counts in the DG. Fluorescence- and DAB-stained brain sections of MPTP-treated and CTR mice at the different time-points of MRE assessment, showing the total number of a) GCL/SGZ cells (DAPI), b) newborn cells (BrdU+), c) new precursor cells (BrdU+/Nestin/GFP+), d) new neuronal cells (BrdU+/NeuN+), and f) microglia and macrophages (Iba1+) in the GCL/SGZ, ML and hilus (mean \pm SEM). * $p < 0.05$, ** $p < 0.01$. doi:10.1371/journal.pone.0092582.g004

alteration of the geometrical arrangement of the mechanical networks. The nonsignificant alteration of ϕ in our data suggests that newly born neurons do not assemble a new network with own geometry at 6 dpi, shortly after their generation. They rather appear isolated yet as differentiation and maturation of newly generated cells into neurons and their functional integration into the present neuronal network by fully developing axons, dendrites

and synaptic links and thus being involved in the structure of the matured viscoelastic lattice takes about four weeks [20,42–45].

There is growing evidence that this process of adult neurogenesis is intimately connected with an intact neurotransmitter homeostasis, since dopamine depletion has been shown to cause disturbances in precursor cell proliferation [24,27–29]. Here, the analyses of newly generated cells in the DG, characterized as cells that incorporated the exogenous mitotic marker BrdU and its co-

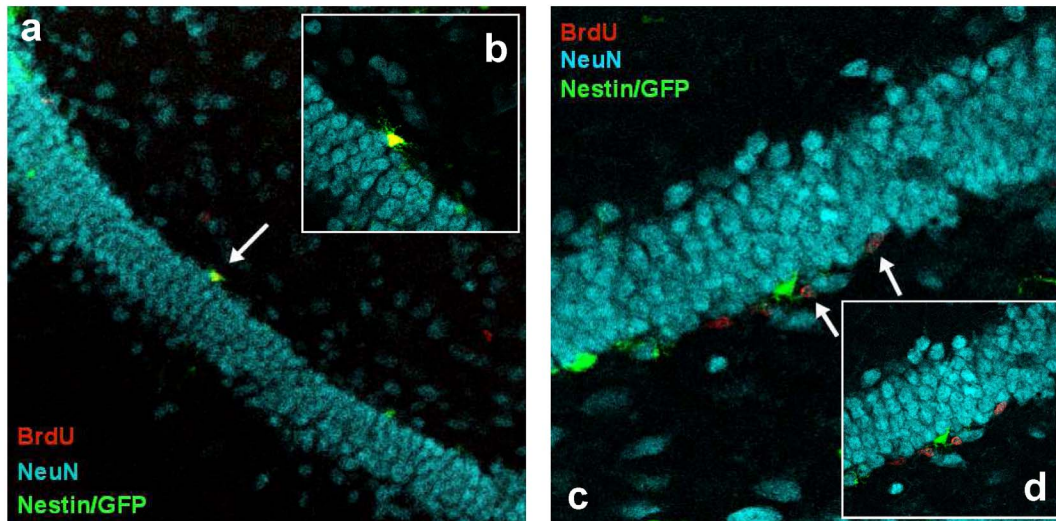


Figure 5. Representative confocal images of double-labeled BrdU⁺/Nestin/GFP⁺ and BrdU⁺/NeuN⁺ cells. Mouse brain sections (40 μ m) fluorescently stained with BrdU (red), NeuN (blue) and Nestin/GFP (green), showing the granular cell layer of the dentate gyrus with a Nestin/GFP-expressing precursor cell that is also positive for BrdU (a, 200 \times magnification and b, 630 \times magnification; arrow) and BrdU-positive cells coexpressing the neuronal marker NeuN (c, 400 \times magnification and d, 630 \times magnification; arrows). doi:10.1371/journal.pone.0092582.g005

localization with Nestin/GFP to identify neural precursor cells, showed a marked transient increase of proliferated Nestin/GFP cells at 3 dpi in MPTP-lesioned mice. It is noteworthy that this rise occurred already at 3 dpi, while the transient gain in viscoelasticity was detected three days later at 6 dpi, which makes the proliferated neural precursor cells an unlikely candidate to account for the augmented stiffness. The observed increased number of proliferated precursor cells is in line with previous findings from our laboratory [27,28] demonstrating an acute and transient rise in new Nestin/GFP-positive cells in the DG and SNpc, respectively, shortly after MPTP treatment. We have previously shown a comparable stimulus-dependent selective regulation of different neural maturation stages in the DG [43,45]. The observed phenomenon possibly reflects a reactive neural precursor cell proliferation that may be, according to studies on other neurodegenerative processes, interpreted as an endogenous regenerative mechanism of the hippocampus to counteract neuronal injury in terms of keeping the endogenous stem-like cell pool at a stable level [46–49]. In the present study, the proportion of new neurons among all BrdU-positive cells at 6 dpi was higher in MPTP-lesioned mice than in unaffected animals. This finding suggests that the previously reactively generated precursor cells mature into neurons, which further supports the intended regenerative potential of the hippocampus. Unlike the Nestin/GFP-positive precursor cells, the increased neuron density three days later at 6 dpi, arisen from the enhanced precursor cell population in the DG, might have provoked the higher viscoelasticity values of the brain tissue at the same time-point. After this cellular gain up to 6 dpi, the proportion of new neurons slightly decreased until 18 dpi. From this, one could hypothesize that the pathological effect of MPTP is partially compensated by a transiently boosted proliferation of precursor cells without an increased net neurogenesis [29,39]. Additionally, although MPTP treatment modulated precursor cell proliferation and neurogenesis, it had no effect on the total amount of newborn BrdU-positive cells in the DG, which is in line with findings from other groups [29,39].

The neurotoxin MPTP is not only known to cause disturbances in neural cell proliferation and differentiation due to dopamine depletion but to also evoke an inflammatory reaction in affected brain areas including accumulation of microglia, lymphocytic infiltration and an increase in cytokine production [50], which might have been also a cause for the observed transient increase in brain elasticity. We addressed this issue by evaluating the number of microglia and macrophages in the DG area, which comprised the GCL/SGZ, molecular layer and hilus. We detected a peak in microglia and macrophages in MPTP-treated at 3 dpi, where no change in MRE measurements was observed. Although it appears unlikely that these inflammation-associated cell types contributed to the noticeable increase in brain viscoelasticity of MPTP-lesioned mice at 6 dpi, we can not preclude an inflammatory rise in extracellular fluid inducing an edematous swelling at a later time-point to be accountable for the observed brain stiffening. Due to the applied fixation method of the brain tissue for histological analysis, by which blood and other fluids are first washed out by PBS and then replaced by PFA, a potential edema is cleared out and not assessable anymore.

The synchrony of the transient MPTP-induced alteration of MRE parameters and neuronal cell density in our mouse model of dopamine depletion highlights the pivotal role of neurogenesis for brain elasticity. It is remarkable that Nestin/GFP-positive precursor cells do not alter MRE constants until their differentiation into NeuN-positive neurons. Hence, their mechanical properties must differ from those of neurons. It has already been demonstrated that neuronal cells are stiffer than glial cells [41], and that the elasticity of reactive glial cells depends on intermediate filament cell content [8]. In future experiments, neurons and neural precursor cells should be studied *in vitro*, applying MRE to analyse their individual mechanical properties and using histological and biomolecular techniques to correlate these mechanical characteristics with their cellular and molecular features. Interestingly, MRE seems to be more sensitive to the process of cell differentiation than histological cell counts and provides additional information about the dissemination of neuronal turnover. Albeit most enhanced in the hippocampus,

we observed a marked increase of G' , G'' and $\text{abs}(G^*)$ throughout the whole brain in a transverse image slice. This apparently diffuse pattern of transiently increased neurogenesis in the hippocampus due to MPTP treatment is a surprising result and motivates further investigations of the correlation between histology and viscoelastic parameters in different regions of the brain. With the current state of the art, MRE can provide consistent quantitative values on a global scale, i.e. considering spatially averaged constants. This permits the detection of diffuse pathology as has been demonstrated for NPH, AD and MS [11–14]. However, fast sampling methods and optimized reconstruction routines are being developed, which expand MRE towards a high resolution imaging modality [7,51,52].

When comparing human MRE with small animal studies, caution has to be taken: The higher dynamic range of MRE in the mouse (900 Hz in our study) compared to ~ 50 Hz in humans may cause a shift in MRE sensitivity towards the loss properties of the tissue. Whether the complex shear modulus of brain tissue at low vibration frequencies would be sensitive to detecting the changes reported in this paper remains to be determined.

In the near future, viscoelastic constants of the brain may provide the missing link between morphometric imaging parameters and neuronal health on the cellular network level. Our results

provide the first indication of the involvement of newly generated neurons into the viscoelastic matrix of the brain, corroborating the hypothesis that the neuronal network effectively contributes to the mechanical scaffold of the brain and therewith encourage further studies on humans for the clinical assessment of neural plasticity and neurodegeneration by MRE.

Supporting Information

Figure S1 Variation of MRE parameters due to MPTP in the whole brain. MPTP induced a transient increase of brain elasticity and viscosity (a, b and c) at 6 dpi, while the phase angle φ (d) remained unchanged (mean \pm SEM). * $p < 0.05$, ** $p < 0.01$ (TIF)

Acknowledgments

We thank Jennifer Altschueler for technical assistance.

Author Contributions

Conceived and designed the experiments: CK KR BS IS. Performed the experiments: CK EH KR SM. Analyzed the data: CK JB IS. Contributed reagents/materials/analysis tools: SM BS IS. Wrote the paper: CK BS IS.

References

- Muthupillai R, Ehman RL (1996) Magnetic resonance elastography. *Nat Med* 2: 601–603.
- Kruse SA, Rose GH, Glaser KJ, Manduca A, Felmlee JP et al. (2008) Magnetic resonance elastography in the brain. *Neuroimage* 39: 231–237.
- Sack I, Beierbach B, Hamberger U, Klatt D, Braun J (2008) Non-invasive measurement of brain viscoelasticity using magnetic resonance elastography. *NMR Biomed* 21: 265–271.
- Green MA, Bilston LE, Sinkus R (2008) In vivo brain viscoelastic properties measured by magnetic resonance elastography. *NMR Biomed* 21: 755–764.
- Clayton EH, Genin GM, Bayly PV (2012) Transmission, attenuation and reflection of shear waves in the human brain. *J R Soc Interface* 9: 2899–2910.
- Weaver JB, Pattinson AJ, McGarry MD, Perreard IM, Swienkowski JG et al. (2012) Brain mechanical property measurement using MRE in intrinsic activation. *Phys Med Biol* 57: 7275–7287.
- Johnson CL, McGarry MD, Gharibans AA, Weaver JB, Paulsen KD et al. (2013) Local mechanical properties of white matter structure in the human brain. *Neuroimage* 79: 145–152.
- Lu Y-B, Iandiev I, Hollborn M, Körber N, Ulbricht et al. (2011) Reactive glial cells: increased stiffness correlates with increased intermediate filament expression. *FASEB J* 25: 624–631.
- Tully B, Ventikos Y (2011) Cerebral water transport using multiple-network poroelastic theory: application to normal pressure hydrocephalus. *J Fluid Mech* 667: 188–215.
- Sack I, Streitberger KJ, Krefling D, Paul F, Braun J (2011) The influence of physiological aging and atrophy on brain viscoelastic properties in humans. *PlosOne* 6: e23451.
- Streitberger K-J, Wiener E, Hoffmann J, Freimann FB, Klatt D et al. (2011) In vivo viscoelastic properties of the brain in normal pressure hydrocephalus. *NMR Biomed* 24: 385–392.
- Murphy MC, Huston III J, Jack Jr CR, Glaser KJ, Manduca A et al. (2011) Decreased brain stiffness in Alzheimer's disease determined by magnetic resonance elastography. *J Magn Reson Imaging* 34: 494–498.
- Streitberger K-J, Sack I, Krefling D, Pfueller C, Braun J et al. (2012) Brain viscoelasticity alteration in chronic-progressive multiple sclerosis. *PlosOne* 7: e29888.
- Wuerfel J, Paul F, Beierbach B, Hamhaber U, Klatt D et al. (2010) MR-elastography reveals degradation of tissue integrity in multiple sclerosis. *Neuroimage* 49: 2520–2525.
- Schregel K, Wuerfel née Tysiak E, Garteiser P, Gemeinhardt I, Prozorowski T et al. (2012) Demyelination reduces brain parenchymal stiffness quantified in vivo by magnetic resonance elastography. *Proc Natl Aca Sci U S A* 109: 6650–6655.
- Riek K, Millward JM, Hamann I, Mueller S, Pfueller CF et al. (2012) Magnetic resonance elastography reveals altered brain viscoelasticity in experimental autoimmune encephalomyelitis. *NeuroImage: Clinical* 1: 81–90.
- Freimann FB, Mueller S, Streitberger K-J, Guo J, Rot S et al. (2013) MR elastography in a murine stroke model reveals correlation of macroscopic viscoelastic properties of the brain with neuronal density. *NMR Biomed* 26: 1534–1539.
- Lendahl U, Zimmermann LB, McKay RDG (1990) CNS stem cells express a new class of intermediate filament protein. *Cell* 60: 585–595.
- Jessberger S, Kempermann G (2003) Adult-born hippocampal neurons mature into activity-dependent responsiveness. *Eur J Neurosci* 18: 2707–2712.
- Kempermann G, Jessberger S, Steiner B, Kronenberg G (2004) Milestones of neuronal development in the adult hippocampus. *Trends Neurosci* 27: 447–452.
- Van Praag H, Schinder AF, Christie BR, Toni N, Palmer TD et al. (2002) Functional neurogenesis in the adult hippocampus. *Nature* 415: 1030–1034.
- Baker SA, Baker KA, Hagg T (2004) Dopaminergic nigrostriatal projections regulate neural precursor proliferation in the adult mouse subventricular zone. *Eur J Neurosci* 20: 575–579.
- Borta A, Hoeglinger GU (2007) Dopamine and adult neurogenesis. *J Neurochem* 100: 587–595.
- Höglinger GU, Rizk P, Muriel MP, Duyckaerts C, Oertel WH et al. (2004) Dopamine depletion impairs precursor cell proliferation in Parkinson disease. *Nature Neurosci* 7: 726–735.
- Freundlieb N, Francois C, Tande D, Oertel WH, Hirsch EC et al. (2006) Dopaminergic substantia nigra neurons project topographically organized to the subventricular zone and stimulate precursor cell proliferation in aged animals. *J Neurosci* 26: 2321–2325.
- Kippin TE, Kapur S, van der Kooy D (2005) Dopamine specifically inhibits forebrain neural stem cell proliferation, suggesting a novel effect of antipsychotic drugs. *Neurobiol Dis* 25: 5815–5823.
- Klaisse P, Lesemann A, Huehnchen P, Hermann A, Storch A et al. (2012) Physical activity and environmental enrichment regulate the generation of neural precursors in the adult mouse substantia nigra in a dopamine-dependent manner. *BMC Neurosci* 13: 1–15.
- Lesemann A, Reinl C, Huehnchen P, Pilhatsch M, Hellweg R et al. (2012) MPTP-induced hippocampal effects on serotonin, dopamine, neurotrophins, adult neurogenesis and depression-like behaviour are partially influenced by fluoxetine in adult mice. *Brain Res* 1457: 51–69.
- Park J-H, Enikolopov G (2010) Transient elevation of adult hippocampal neurogenesis after dopamine depletion. *Exp Neurol* 222: 267–276.
- Yang P, Arnold SA, Habas A, Hetman M, Hagg T (2008) Ciliary neurotrophic factor mediates dopamine D₂ receptor-induced CNS neurogenesis in adult mice. *J Neurosci* 28: 2231–2241.
- Gasbarri A, Sulli A, Packard MG (1997) The dopaminergic mesencephalic projections to the hippocampal formation in the rat. *Prog Neuro-Psychopharmacol & Biol Psychiat* 21: 1–22.
- Gasbarri A, Verney C, Innocenzi R, Campana E, Pacitti C (1994) Mesolimbic dopaminergic neurons innervating the hippocampal formation in the rat: a combined retrograde tracing and immunohistochemical study. *Brain Res* 668: 71–79.
- Kopin IJ (1987) MPTP: An industrial chemical and contaminant of illicit narcotics stimulates a new era in research on parkinson's disease. *Environ Health Perspect* 75: 45–51.
- Scatton B, Simon H, Le Moal M, Bischoff S (1980) Origin of dopaminergic innervation of the rat hippocampus. *Neurosci Lett* 18: 125–131.
- Swanson LW (1982) The projections of the ventral tegmental area and adjacent regions: a combined fluorescent retrograde tracer and immunofluorescence study in the rat. *Brain Res Bull* 9: 321–353.

36. Clayton EH, Garbow JR, Bayly PV (2011) Frequency-dependent viscoelastic parameters of mouse brain tissue estimated by MR elastography. *Phys Med Biol* 56: 2391–2406.
37. Papazoglou S, Hamhaber U, Braun J, Sack I (2008) Algebraic Helmholtz inversion in planar magnetic resonance elastography. *Phys Med Biol* 53: 3147–3158.
38. Posnansky O, Guo J, Hirsch S, Papazoglou S, Braun J et al. (2012) Fractal network dimension and viscoelastic powerlaw behavior: A modeling approach based on a coarse-graining procedure combined with shear oscillatory rheometry. *Phys Med Biol* 57: 4023–4040.
39. Peng J, Xie L, Jin K, Greenberg DA, Andersen JK (2008) Fibroblast growth factor 2 enhances striatal and nigral neurogenesis in the acute 1-methyl-4-phenyl-1,2,3,6-tetrahydropyridine model of parkinson's disease. *Neuroscience* 153: 664–670.
40. Sack I, Beierbach B, Wuerfel J, Klatt D, Hamhaber U et al. (2009) The impact of aging and gender on brain viscoelasticity. *Neuroimage* 46: 652–657.
41. Lu Y-B, Franze K, Seifert G, Steinhäuser C, Kirchhoff F et al. (2006) Viscoelastic properties of individual glial cells and neurons in the CNS. *Proc Natl Acad Sci U S A* 103: 17759–17764.
42. Kronenberg G, Reuter K, Steiner B, Brandt MD, Jessberger S et al. (2003) Subpopulations of proliferating cells of the adult hippocampus respond differently to physiologic neurogenic stimuli. *J Comp Neurol* 467: 455–463.
43. Steiner B, Kronenberg G, Jessberger S, Brandt MD, Reuter K et al. (2004) Differential regulation of gliogenesis in the context of adult hippocampal neurogenesis in mice. *Glia* 46: 41–52.
44. Steiner B, Klempin F, Wang L, Kott M, Kettenmann H et al. (2006) Type-2 cells as link between glial and neuronal lineage in adult hippocampal neurogenesis. *Glia* 54: 805–814.
45. Steiner B, Zurborg S, Hoerster H, Fabel K, Kempermann G (2008) Differential 24 h responsiveness of Prox1-expressing precursor cells in adult hippocampal neurogenesis to physical activity, environmental enrichment, and kainic acid-induced seizures. *Neuroscience* 154: 521–529.
46. Aharoni R, Arnon R, Eilam R (2005) Neurogenesis and neuroprotection induced by peripheral immunomodulatory treatment of experimental autoimmune encephalomyelitis. *J Neurosci* 25: 8217–8228.
47. Arvidsson A, Collin T, Kirik D, Kokaia Z, Lindvall O (2002) Neuronal replacement from endogenous precursors in the adult brain after stroke. *Nat Med* 8: 963–970.
48. Gage FH, Kempermann G, Palmer TD, Peterson DA, Ray J (1998) Multipotent progenitor cells in the adult dentate gyrus. *J Neurobiol* 36: 249–266.
49. Huehnchen P, Prozorovski T, Klaisle P, Lesemann A, Ingwersen J et al. (2011) Modulation of adult hippocampal neurogenesis during myelin-directed autoimmune neuroinflammation. *Glia* 50: 132–142.
50. Kurkowska-Jastrzebska I, Wronska A, Kohutnicka M, Czlonkowski A, Czlonkowska A (1999) The inflammatory reaction following 1-methyl-4-phenyl-1,2,3,6-tetrahydropyridine intoxication in mouse. *Exp Neurol* 156: 50–61.
51. Barnhill E, Kennedy P, Hammer S, van Beek EJ, Brown C et al. (2013) Statistical mapping of the effects of knee extension on thigh muscle viscoelastic properties using magnetic resonance elastography. *Physiol Meas* 34: 1675–1698.
52. Guo J, Hirsch S, Fehlner A, Papazoglou S, Scheel M et al. (2013) Towards an elastographic atlas of brain anatomy. *PlosOne* 8: e71807.

RESEARCH ARTICLE

Dopaminergic Neurodegeneration in the Mouse Is Associated with Decrease of Viscoelasticity of Substantia Nigra Tissue

Elisabeth G. Hain¹, Charlotte Klein¹, Tonia Munder¹, Juergen Braun², Kerstin Riek³, Susanne Mueller⁴, Ingolf Sack³, Barbara Steiner^{1*}

1 Department of Neurology, Charité, University Medicine Berlin, Berlin, Germany, **2** Institute for Medical Informatics, Charité, University Medicine Berlin, Berlin, Germany, **3** Department of Radiology, Charité, University Medicine Berlin, Berlin, Germany, **4** Center for Stroke Research Berlin, Berlin, Germany

* barbara.steiner@charite.de



OPEN ACCESS

Citation: Hain EG, Klein C, Munder T, Braun J, Riek K, Mueller S, et al. (2016) Dopaminergic Neurodegeneration in the Mouse Is Associated with Decrease of Viscoelasticity of Substantia Nigra Tissue. *PLoS ONE* 11(8): e0161179. doi:10.1371/journal.pone.0161179

Editor: Huaibin Cai, National Institutes of Health, UNITED STATES

Received: February 18, 2016

Accepted: August 1, 2016

Published: August 15, 2016

Copyright: © 2016 Hain et al. This is an open access article distributed under the terms of the [Creative Commons Attribution License](https://creativecommons.org/licenses/by/4.0/), which permits unrestricted use, distribution, and reproduction in any medium, provided the original author and source are credited.

Data Availability Statement: All relevant data are within the paper and its Supporting Information files.

Funding: This study was funded by the German Research Foundation (www.dfg.de) to Barbara Steiner: STE 1450/8, and Ingolf Sack: SA901/17. The funder had no role in study design, data collection and analysis, decision to publish, or preparation of the manuscript.

Competing Interests: The authors have declared that no competing interests exist.

Abstract

The biomechanical properties of brain tissue are altered by histopathological changes due to neurodegenerative diseases like Parkinson's disease (PD). Such alterations can be measured by magnetic resonance elastography (MRE) as a non-invasive technique to determine viscoelastic parameters of the brain. Until now, the correlation between histopathological mechanisms and observed alterations in tissue viscoelasticity in neurodegenerative diseases is still not completely understood. Thus, the objective of this study was to evaluate (1) the validity of MRE to detect viscoelastic changes in small and specific brain regions: the substantia nigra (SN), midbrain and hippocampus in a mouse model of PD, and (2) if the induced dopaminergic neurodegeneration and inflammation in the SN is reflected by local changes in viscoelasticity. Therefore, MRE measurements of the SN, midbrain and hippocampus were performed in adult female mice before and at five time points after 1-methyl-4-phenyl-1,2,3,6-tetrahydropyridin hydrochloride (MPTP) treatment specifically lesioning dopaminergic neurons in the SN. At each time point, additional mice were utilized for histological analysis of the SN. After treatment cessation, we observed opposed viscoelastic changes in the midbrain, hippocampus and SN with the midbrain showing a gradual rise and the hippocampus a distinct transient increase of viscous and elastic parameters, while viscosity and—to a lesser extent—elasticity in the SN decreased over time. The decrease in viscosity and elasticity in the SN was paralleled by a reduced number of neurons due to the MPTP-induced neurodegeneration. In conclusion, MRE is highly sensitive to detect local viscoelastic changes in specific and even small brain regions. Moreover, we confirmed that neuronal cells likely constitute the backbone of the adult brain mainly accounting for its viscoelasticity. Therefore, MRE could be established as a new potential instrument for clinical evaluation and diagnostics of neurodegenerative diseases.

Introduction

The macroscopic biomechanical properties of *in vivo* brain tissue are influenced by the cellular composition of the brain given by the number of neurons and glial cells as well as their interactions with the extracellular matrix [1–3]. This composition varies in diverse brain regions and under pathological conditions so that histological differences may be reflected in the biomechanical properties of tissue and can be represented in viscoelastic quantities. Therefore, alterations in viscoelasticity can be considered to be a potential instrument for clinical evaluation and diagnostics.

Magnetic resonance elastography (MRE) attracted attention as an appropriate medical imaging technique to assess biomechanical properties of brain tissue non-invasively and *in vivo* [4]. Biomechanical constants of soft tissues are measured by inducing shear waves and processing the MR images of the propagating shear waves to calculate quantitative values of viscoelasticity such as the complex shear modulus G^* [4,5]. G^* contains the storage modulus G' and the loss modulus G'' . G' gives information about the elasticity of the tissue, which is determined by the number and type of cells in the network. In contrast, G'' gives information about the viscous, dampening properties of the tissue, which depend on the geometry of the network including bonds and branching.

In human MRE studies, it has been found that brain viscoelasticity is reduced during aging [6,7] and under pathological conditions like multiple sclerosis (MS) [8,9], normal pressure hydrocephalus [10], Alzheimer's disease (AD) [11], frontotemporal dementia [12], Glioblastoma [13] and progressive supranuclear palsy [14]. However, the histopathological mechanisms underlying the observed alterations in tissue viscoelasticity are still not completely understood.

With the use of animal models, first steps have been made to elucidate the link between MRE parameters and histology. Millward, Riek and colleagues revealed a correlation between the degree of inflammation, mediated by T-cells and macrophages/microglia, and the viscoelastic constants in a mouse model of MS [15,16]. Schregel and co-workers underlined the decrease of elasticity in a different MS mouse model caused by demyelination and changed extracellular matrix configuration [3].

Aside from inflammation, neuronal alterations have also been observed to play an important role in changed viscoelastic parameters in the MRE. After middle cerebral artery occlusion in mice, the depleted density of neurons correlated directly with reduced elastic properties in the affected brain hemisphere [17]. In addition, mouse models for AD and Parkinson's disease (PD), have been investigated as well. A softening of brain tissue has been observed by MRE in APP-PS1 AD mice [18], but correlating histopathological analyses with particular regard to local changes correlating to region specific changes in MRE are missing. Changes in viscoelasticity and correlating histopathological mechanisms have been observed in previous animal studies in the whole brain [16], in one hemisphere [17] or the cerebellum [15], whereas such investigations in smaller brain regions are still not completed. In the 1-methyl-4-phenyl-1,2,3,6-tetrahydropyridine hydrochloride (MPTP) mouse model reproducing PD-like histopathology, a transient rise in viscoelasticity in the hippocampus has been observed. This was paralleled by a higher density of newly generated neurons, arising from a reactively generated precursor cell population [1]. However, the lesioned substantia nigra (SN) as the mainly affected structure in PD and its models has not been investigated yet in detail. In the work of Klein et al., basic principles in the relation between changes in the number of neurons under neurodegenerative conditions and MRE-measured viscoelastic properties using the MPTP mouse model for PD has been established [1].

PD, however, is initially and mainly characterized by the loss of dopaminergic neurons in the SN, a small region in the midbrain with synaptic connections to the surrounding basal

ganglia and beyond [19]. The neurotoxin MPTP is an established animal model for the histopathology seen in PD patients [20] due to its ability to selectively lesion dopaminergic cells in the SN, which is also accompanied by inflammatory reactions [21,22]. Up to now, Lipp and co-workers demonstrated a reduction of elasticity in the lentiform nucleus as part of the midbrain in humans with PD, whereas the viscoelastic properties of the whole brain were unaffected [14]. However, region specific changes of viscoelasticity due to aging and pathological conditions like neurodegenerative diseases and the analysis of underlying histopathological alterations is still lacking. Thus, we applied the MRE setup to MPTP-lesioned mice to investigate, if acquired viscoelastic parameters are altered in affected areas: the SN, midbrain and hippocampus. Furthermore, we investigated, if changes in MRE parameters in the SN correlate with neurodegenerative and inflammatory processes and if we can confirm that MRE is feasible to selectively detect local pathological alterations in neurodegenerative diseases. This would add to the establishment of MRE as clinical evaluation tool.

Materials and Methods

Animal Treatment

All animal experiments were approved by the local animal ethics committee (Landesamt für Gesundheit und Soziales, Berlin, Germany) and carried out in accordance with the European Communities Council directive of 22 September 2010 (10/63/EU). In total, 35 female eight to ten weeks old C57Bl/6N mice were group-housed in a temperature- and humidity-controlled colony room with a light/dark cycle of 12/12 h and unrestricted access to food and water.

Animals were randomly divided into seven groups of $n = 5$. All animals, except the histological counterparts for the baseline measurement, were treated intraperitoneally with MPTP (Sigma Aldrich, Steinheim, Germany), dissolved in 0.9% NaCl, with a concentration of 20 mg/kg bodyweight on three consecutive days. One group ($n = 5$) underwent MRE-imaging the day before MPTP treatment started (-3 days post-injection (dpi)) as baseline and three, six, ten, 14 and 18 days after the last MPTP injection (3, 6, 10, 14, 18dpi). At each time point (six in total), animals of the corresponding histological group ($n = 5$ for each time point) were perfused. A timeline of the experimental procedure is given in [Fig 1](#) and [Table 1](#).

Perfusion and Tissue Preparation

At each time point of MRE measurement, the corresponding histological group of animals were deeply anaesthetized with Ketamine/Xylazine (10% Ketamine hydrochloride, WDT; 2% Rompun, Provet AG) and transcardially perfused with phosphate buffered saline (PBS) and 4% paraformaldehyde (PFA). Brains were dissected carefully, postfixed in 4% PFA for 24 h and dehydrated with 30% sucrose solution for 48 h. Then they were frozen in 2-methylbutane (Sigma-Aldrich, Steinheim, Germany) cooled with liquid nitrogen, sliced in 40 μm thick coronal sections using a Leica CM 1850 UV cryostat and stored in cryoprotectant solution until histological stainings were performed.

Immunohistochemistry

For immunohistochemistry, a well-established staining protocol was followed [23,24]. Briefly, a one-in-six free-floating brain section series of each mouse was pre-treated with 0.6% H_2O_2 and donkey serum-enriched PBS (PBS+) before being incubated with the first antibody anti-Tyrosinhydroxylase (TH; mouse 1:10000, Sigma-Aldrich) or anti-ionized calcium-binding adapter molecule 1 (Iba-1; rat 1:1000, Wako) at 4°C overnight. On the next day, brain sections were first pre-treated with PBS+ for background blocking and then incubated with the

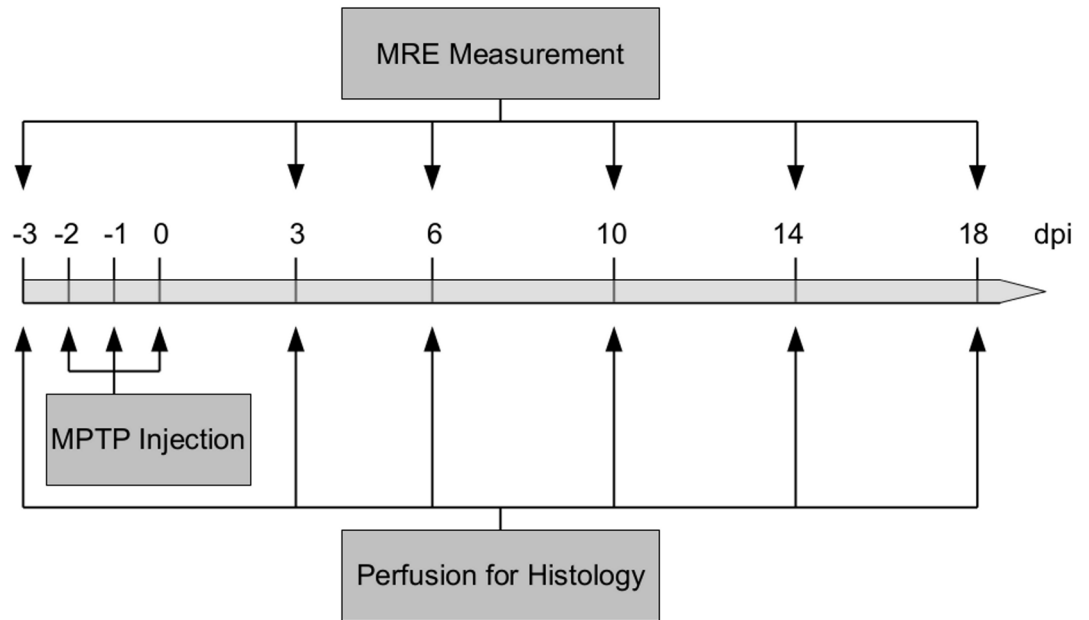


Fig 1. Timeline of the experimental procedure. The timeline of MPTP injections, time points of MRE measurement and brain perfusions for histological analyses.

doi:10.1371/journal.pone.0161179.g001

secondary biotinylated antibody (anti-mouse or anti-rat, 1:250, Dianova) at room temperature for two hours. Then, ABC solution (Vectastain Elite ABC Kit, Vector Laboratories) was applied, before the formed streptavidin-peroxidase complex was visualized by 3,3'-diaminobenzidine (DAB, Sigma-Aldrich)-nickel staining. Finally, stained sections were mounted on microscope slides and coverslipped.

To determine the total cell number in each region of interest (SN, midbrain and hippocampus), a separate one-in-twelve series of brain sections of two mice per group was stained with the fluorochrome 4',6-diamidino-2-phenylindole (DAPI), which binds to the DNA thereby labeling cell nuclei. Sections were incubated with PBS-diluted DAPI (1:1000, Thermo Scientific) for 7 min and afterwards mounted on microscope slides and coverslipped.

Cell Quantification

In total, four stained brain slices of each mouse were analyzed for TH+ cells in the SN, including pars compacta and pars reticulata. Cells were manually counted under the 40x objective of

Table 1. Experimental design.

Post-injection day	Performance
-3	MRE measurement or perfusion for histology
-2	MPTP injection
-1	MPTP injection
0	MPTP injection
3	MRE measurement or perfusion for histology
6	MRE measurement or perfusion for histology
10	MRE measurement or perfusion for histology
14	MRE measurement or perfusion for histology
18	MRE measurement or perfusion for histology

doi:10.1371/journal.pone.0161179.t001

an Axioskop HB50/AC light microscope (Zeiss, Germany) and multiplied by six to obtain an estimated absolute number of cells per SN.

For quantification of DAPI-stained cell nuclei in all regions of interest and Iba-1+ cells in the SN, the Stereo Investigator (MBF Bioscience) and a Leica DMRE microscope were used. The region of interest was defined with the 5x objective. Actual counting was done with the 40x oil objective. For quantification of DAPI-stained cell nuclei, two sections in an interval of twelve were counted by using a sampling grid size of 250x200 μm in the SN and 600x600 μm in the midbrain and hippocampus. Iba-1 positive cells were counted in four sections in an interval of six by using a sampling grid size of 150x120 μm . In all brain regions, a counting frame of 60x60 μm without guard dissector height was used. Cells were counted when cell bodies became sharp in their widest extent. The absolute number of cells per brain region was automatically calculated based on the counted cell number, slice interval, counting frame size, sampling grid size and slice thickness.

Magnetic Resonance Elastography (MRE)

All measurements were realized on a 7-Tesla MR Imaging (MRI) scanner (Bruker PharmaScan 70/16, Ettlingen, Germany) with a 20 mm diameter 1H-RF-quadrature mouse head coil and using ParaVision 4.0 software. As illustrated in Fig 2, shear waves into the mouse brain were induced by using a moveable bite bar transducer, linked with a carbon fiber piston to an electromagnetic coil as the source of vibration. During the MRE session, mice were anaesthetized with isoflurane/oxygen. The transducer was gimbaled through a rubber bearing and retaining bracket at the temperature-controlled mouse bed. This setup was held in the middle of the magnet bore of the MRI scanner by a plastic disc. Vibrations were induced by applying a sinusoidal electric current of 900 Hz frequency to an air-cooled Lorentz coil in the fringe area of the MRI scanner and were initialized by a trigger pulse from the control unit of the scanner, while the timing was defined by a customized FLASH sequence. Frequency, amplitude and number of sinusoidal oscillation cycles were controlled by an arbitrary function generator connected via an audio amplifier to the driving coil. The main polarization of the vibration was transverse to the principal axis of the magnet field, with amplitudes in the order of tens of micrometers.

The MRE data were acquired in one 2 mm transverse slice in which all regions of interests (ROI) could be analyzed. The imaging sequence was modified for MRE by sinusoidal motion sensitizing gradient (MSG) in the through-plane direction, as described elsewhere [16]. The MSG strength was 285 mT/m with a frequency of 900 Hz and nine periods. Phase difference images were calculated from two images differing in the sign of the MSG to compensate for static phase contributions. Additional imaging parameters were: a 128x128 matrix, 25 mm FoV, 14.3 ms echo time, 116.2 ms repetition time, eight dynamic scans over a vibration period and an acquisition time of 20 min.

Complex wave images according to the harmonic drive frequency were estimated by temporal Fourier transformation of the unfolded phase-difference images and filtered for suppressing noise and compression wave components [16,25]. An algebraic Helmholtz inversion was applied to the pre-processed 2D scalar wave fields calculating the complex shear modulus G^* [26]. Then, G^* was spatially averaged over the SN, midbrain and hippocampus of both hemispheres as ROIs, which were manually segmented by delineating its anatomical structure from T1w-MR images (Fig 3). Values of the averaged G^* contain the real part of G^* : storage modulus G' , and the imaginary part of G^* : loss modulus G'' , representing the elasticity and viscosity of tissue, respectively.

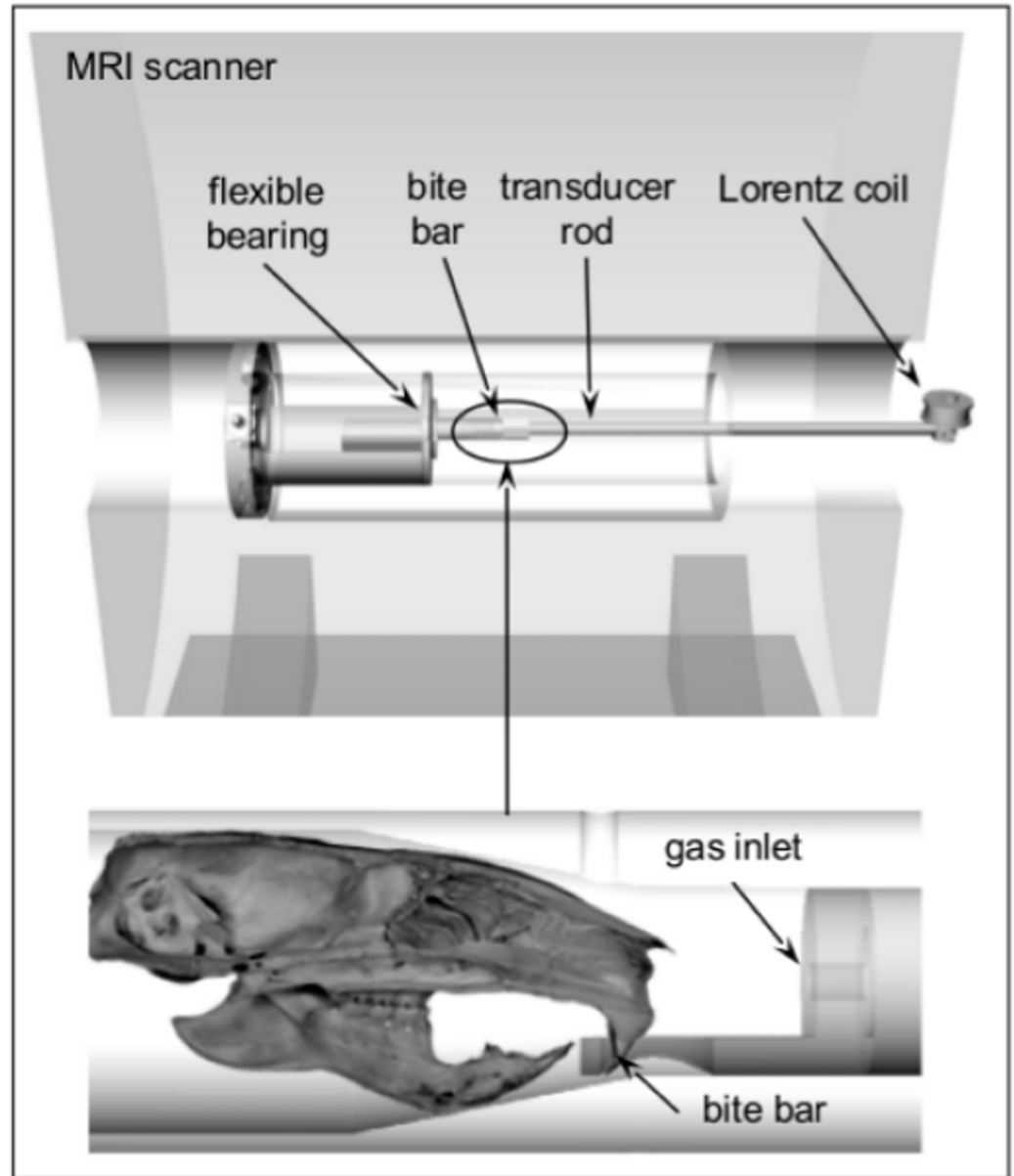


Fig 2. Schematic of the mouse MRE apparatus.

doi:10.1371/journal.pone.0161179.g002

Statistical Analysis

All statistical analyses were performed by using SPSS Statistics19 for Windows and GraphPad Prism 5. The homogeneity of variance was tested by Levene test. One-way ANOVA was performed the data from the quantification of TH+ and Iba1+ cells and one-way repeated measures (RM) ANOVA for MRE data. The data from the DAPI counts were not statistically evaluated, because only $n = 2$ per time point were quantified. Pairwise comparisons were done using the Bonferroni test in case of a significant ANOVA. The level of statistical significance was set at $p \leq 0.05$. All data are shown as mean values with standard error of the mean (SEM). Graphs were generated using GraphPad Prism 5.

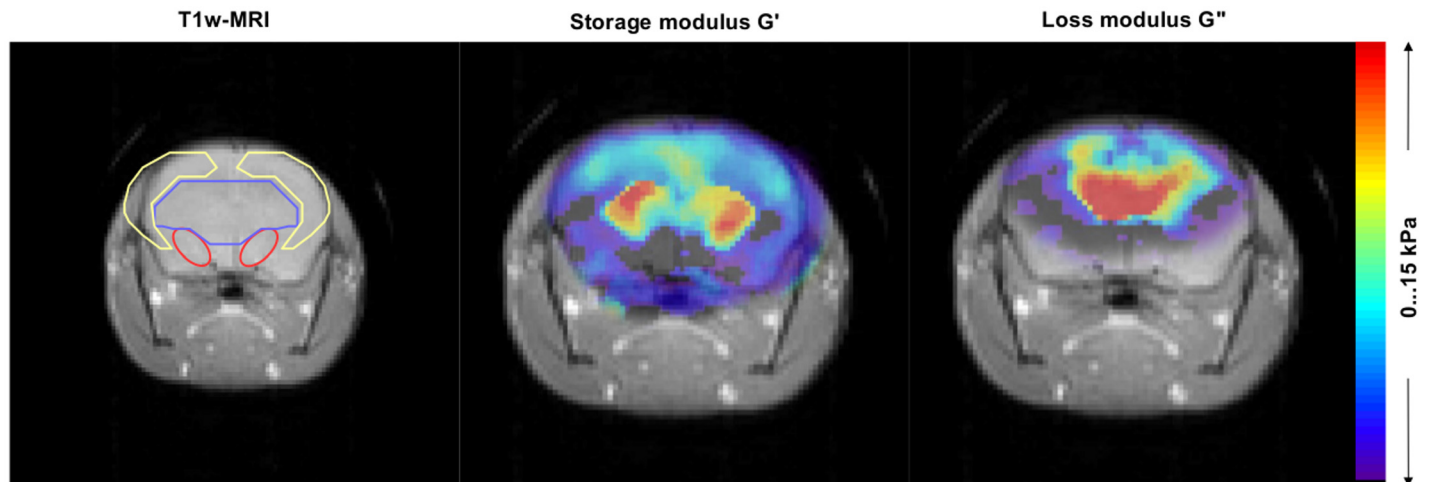


Fig 3. Representative images of MRI signal and complex modulus map of G' and G'' . Regions of interest: substantia nigra (red line), midbrain (blue line) and hippocampus (yellow line) were marked in T1w-MRI.

doi:10.1371/journal.pone.0161179.g003

Results

Initially, MRE measurement was performed the day before MPTP treatment started to generate baseline data of healthy brain tissue. Sessions were repeated three, six, ten, 14 and 18 days after the last MPTP injection and processed for the SN, midbrain and hippocampus. The MRE results are presented together with the results of the histological analysis of each brain region in Figs 4, 5 and 6.

One-way ANOVA of the MRE parameters at -3dpi revealed a significant difference in basic viscosity between the various brain areas ($F(2,14) = 5.396, p \leq 0.05$). Post-hoc pairwise comparison using the Bonferroni test showed a significant higher viscosity in the midbrain (1.836 ± 0.043 kPa) than in the hippocampus (1.426 ± 0.051 kPa) ($p \leq 0.05$).

MPTP induces a decrease of viscosity and elasticity in the SN

In the SN, MRE generated baseline values with mean (\pm SEM) of 5.012 (± 0.578) kPa and 1.627 (± 0.137) kPa for G' and G'' , respectively. A one-way RM ANOVA revealed a significant effect in the storage modulus G' ($F(5,29) = 4.274, p \leq 0.01$) and loss modulus G'' ($F(5,29) = 8.350, p \leq 0.001$) following MPTP treatment, which reflects alterations in the elastic and viscous properties of the SN. Post-hoc pairwise comparison using the Bonferroni test showed a significant decrease in G' (3dpi vs. 6dpi: $p \leq 0.05$) (Fig 4a) and G'' (-3dpi vs. 10dpi: $p \leq 0.05$, -3dpi vs. 18dpi: $p \leq 0.01$, -3dpi vs. 6dpi: $p \leq 0.001$) (Fig 4b), indicating a more reduced viscosity than elasticity in the SN following MPTP treatment with a slight restoration over time.

MPTP induces an increase of viscosity and elasticity in the midbrain

Mean values (\pm SEM) of G' and G'' were 5.397 (± 0.190) kPa and 1.836 (± 0.043) kPa in the midbrain at -3dpi. The one-way RM ANOVA revealed a significant effect of MPTP treatment on storage modulus G' ($F(5,29) = 6.702, p \leq 0.001$) and loss modulus G'' ($F(5,29) = 6.895, p \leq 0.001$) in the midbrain over time. A significant increase in G' (-3dpi vs. 14dpi: $p \leq 0.05$, -3dpi vs. 6dpi and 18dpi: $p \leq 0.01$) (Fig 5a) and G'' (-3dpi vs. 6dpi and 18dpi: $p \leq 0.01$) (Fig 5b) was observed as the post-hoc pairwise comparison showed. This indicates there tissue stiffening in the midbrain after MPTP treatment.

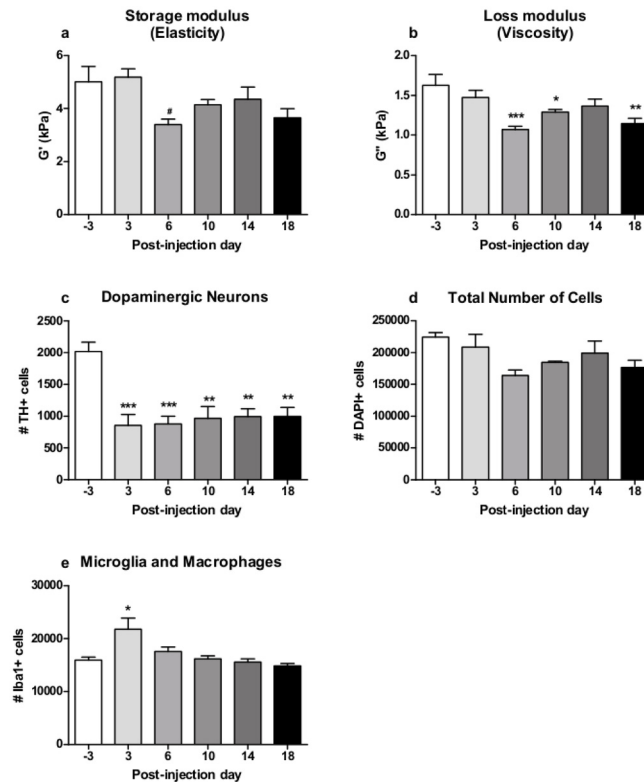


Fig 4. Results of MRE measurements and histological cell counts in the substantia nigra. MPTP induced a significant reduction in MRE elasticity (a) and viscosity (b) in the substantia nigra (mean±SEM, n (-3,3,6,10,14,18dpi) = 5). DAB-stained brain sections showed an immediate significant drop in TH+ dopaminergic neurons in the substantia nigra after MPTP treatment (c) (mean±SEM, n(-3dpi) = 4, n (3,6,10,14,18dpi) = 5). DAPI-stained cell amount was decreased by MPTP (d) (mean±SEM, n (-3,3,6,10,14,18dpi) = 2, no statistical analysis). Initially, the amount of Iba1+ microglia and macrophages was significantly raised after MPTP treatment, but ceased over time (e) (mean±SEM, n(-3dpi) = 4, n (3,6,10,14,18dpi) = 5). * vs. -3dpi, *p<0.05, **p<0.01, ***p<0.001. # vs. 3dpi, #p<0.05.

doi:10.1371/journal.pone.0161179.g004

MPTP induces a transient increase of viscosity and elasticity in the hippocampus

At baseline, mean values (±SEM) were 4.997 (±0.402) kPa and 1.426 (±0.52) kPa for G' and G'', respectively. The One-way RM ANOVA showed a significant effect of MPTP treatment on the storage modulus G' (F(5,29) = 11.75, p<0.001) and loss modulus G'' (F(5,29) = 8.075, p<0.001) in the hippocampus over time. Here, post-hoc pairwise comparison revealed a significant increase in G' (-3dpi vs. 6dpi: p<0.001) (Fig 6a) and G'' (-3dpi vs.6dpi: p<0.01) (Fig 6b), indicating a transient tissue stiffening in the hippocampus six days after treatment cessation.

MPTP induces dopaminergic neurodegeneration in the SN

A one-way ANOVA revealed a strong effect of MPTP treatment on the number of TH+ in the SN (F(5,28) = 7.499, p<0.001). Pairwise comparison showed that the number of TH+ dopaminergic neurons was decreased by MPTP at all time points in comparison to baseline level (-3dpi vs. 3dpi and 6dpi: p<0.001, -3dpi vs. 10dpi, 14dpi and 18dpi: p<0.01) (Fig 4c). The immediate reduction of TH+ dopaminergic neurons following MPTP treatment was approximately 57% with mean values declining from 2018 at -3dpi to 856 at 3dpi, respectively. The deficit of dopaminergic neurons persisted at least until the last time point at 18dpi investigated

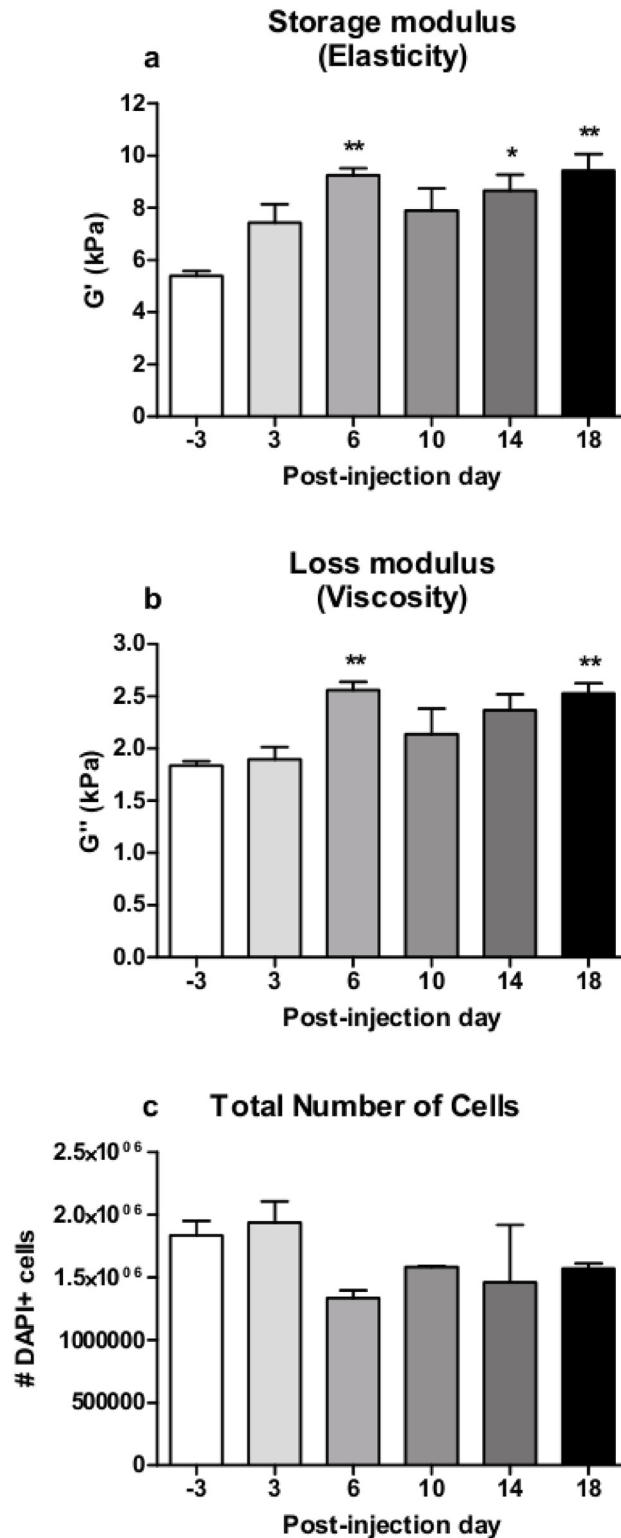


Fig 5. Results of MRE measurement and histological cell count in the midbrain. MPTP induced a significant increase of MRE elasticity (a) and viscosity (b) in the midbrain (mean±SEM, n (-3,3,6,10,14,18dpi) = 5). DAPI-stained brain sections showed a reduction following MPTP-treatment (c) (mean±SEM, n(-3,3,6,10,14,18dpi) = 2, no statistical analysis). * vs. -3dpi, *p<0.05, **p<0.01.

doi:10.1371/journal.pone.0161179.g005

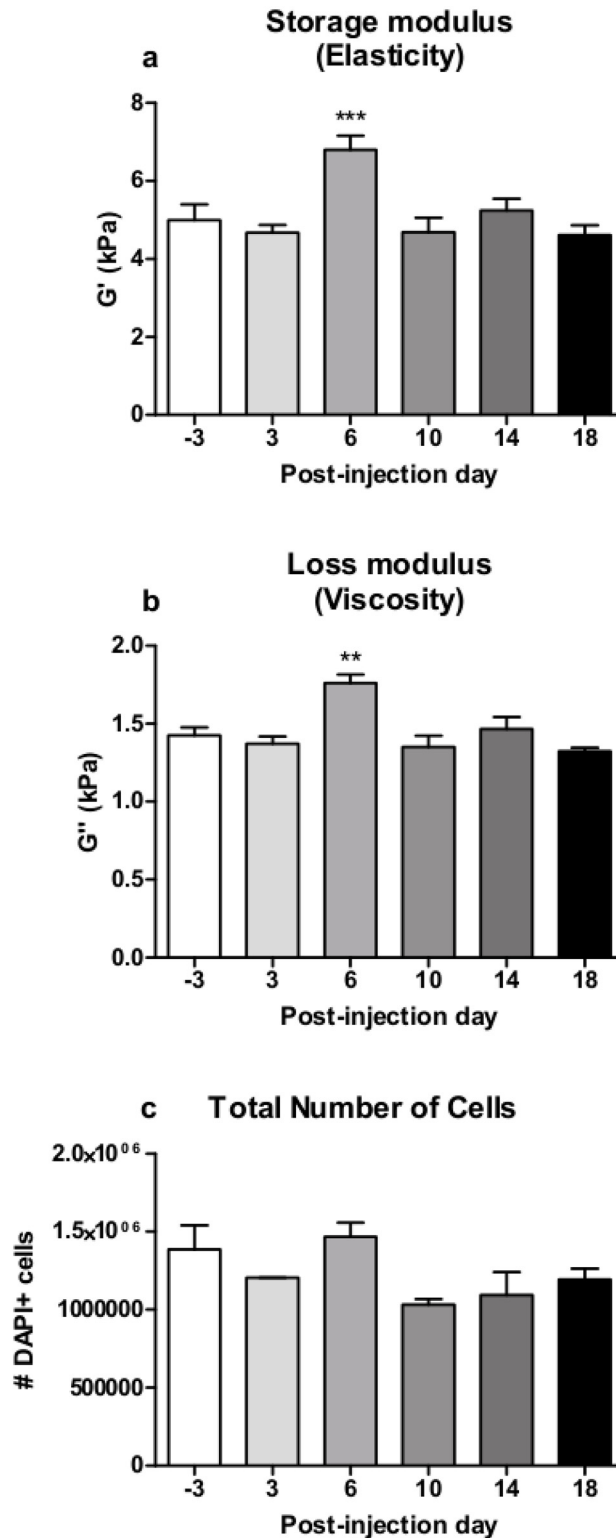


Fig 6. Results of MRE measurement and histological cell count in the hippocampus. MPTP induced a transient increase of elasticity (a) and viscosity (b) in the hippocampus at 6dpi (mean±SEM, n (-3,3,6,10,14,18dpi) = 5). Quantification of DAPI-stained cells showed an elevated amount at 6dpi (mean ±SEM, n(-3,3,6,10,14,18dpi) = 2, no statistical analysis). * vs. -3dpi, **p≤0.01, ***p≤0.001.

doi:10.1371/journal.pone.0161179.g006

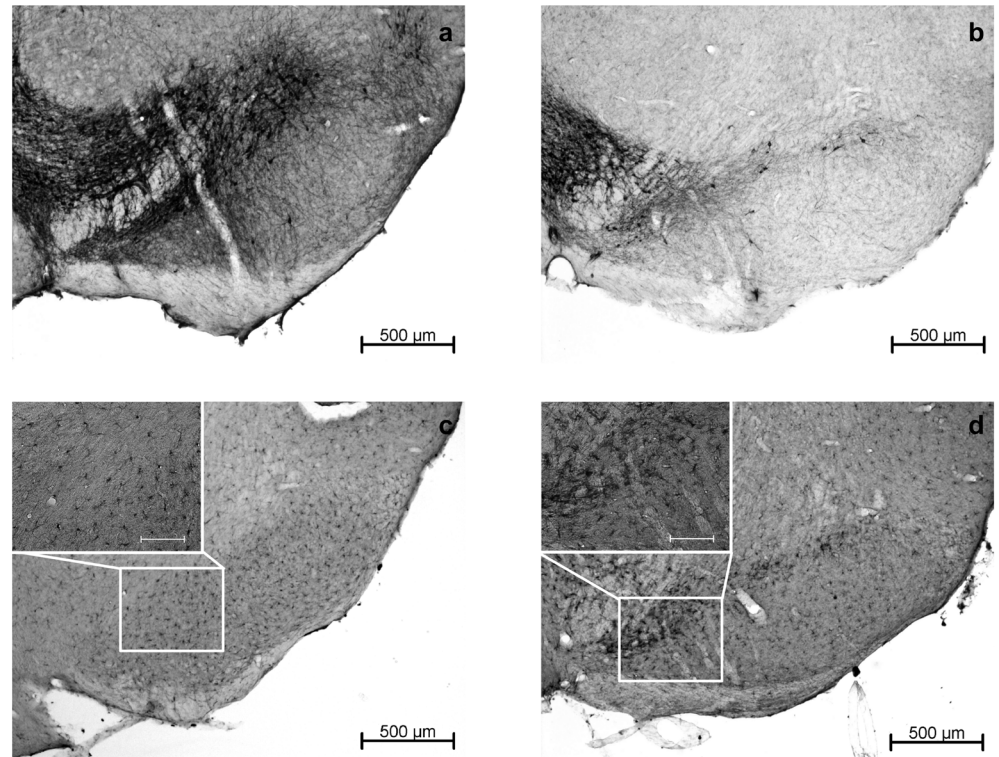


Fig 7. Representative images of DAB-stained brain slices showing the substantia nigra. TH+ cells at baseline at -3dpi (a) and directly after MPTP treatment at 3dpi (b) at 50x magnification, indicating a severe loss of dopaminergic neurons induced by MPTP. Iba-1+ at -3dpi (c) and 3dpi (d) at 50x magnification with detail in 200x magnification (scale bar 100 μ m), showing a reactive increase in the number of microglia and macrophages in the substantia nigra immediately after MPTP treatment.

doi:10.1371/journal.pone.0161179.g007

here. Representative images of TH+ cells before and after MPTP treatment are shown in [Fig 7a and 7b](#).

MPTP induces a reduction of total cell amount in the SN and midbrain and a transient rise in the hippocampus

In the SN, the quantification of DAPI+ cells ($n = 2$) revealed a decrease in the total amount of cells from 224700 (± 6967) cells at -3dpi to 164083 (± 8417) cells at 6dpi following MPTP-treatment. After that, a transient slight restoration over time can be observed ([Fig 4d](#)).

The DAPI+ cell count ($n = 2$) in the midbrain revealed a decrease in the total cell amount from 1834800 (± 116400) to 1333800 (± 60600) cells at -6dpi ([Fig 5c](#)).

In the hippocampus, the DAPI+ cell quantification ($n = 2$) revealed a total amount of 1385400 (± 155400) cells at -3dpi and a transient rise at 6dpi up to 1468200 (± 89400) cells ([Fig 6c](#)).

MPTP induces a transient increase of microglia and macrophages in the SN

The analysis of Iba1+ cell counts revealed a significant effect of MPTP treatment on the number of microglia and macrophages in the SN as a sign for a local inflammatory reaction ($F(5,28) = 5.706$, $p \leq 0.01$). Pairwise comparison showed that the amount of Iba+ cells directly after MPTP treatment (3dpi) was significantly higher than at baseline (-3dpi vs. 3dpi: $p \leq 0.05$), whereas no significant difference in the amount of Iba-1+ cells was observed between baseline

and later time points from 6dpi to the end of the study (Fig 4d). MPTP induced a transient inflammatory response, which is reflected here by increased numbers of microglia in the SN at 3dpi (21732 cells), that ceased over time until baseline levels (approximately 15000 cells) are reached again at 18dpi. Representative images of Iba+ cells before and after MPTP treatment are shown in Fig 7c and 7d.

Discussion

In this study, we demonstrate how viscosity and elasticity in various brain areas change in response to MPTP treatment and that the significant reduction of dopaminergic neurons in the SN in a mouse model for a neurodegenerative disease is reflected in the decrease of viscosity and—to a lesser extent—elasticity. Hence, the MRE setup is viable to detect viscous and elastic alterations even in small brain areas.

The neurotoxin MPTP primarily affects dopaminergic neurons and is therefore an established animal model for the histopathology seen in PD patients [19,20]. Besides the SN, the MPTP mouse model is also used for investigations in the midbrain [27] and hippocampus [24] to elucidate the effects of nigral dopaminergic neurodegeneration in other specific brain regions related to the pathology of PD. According to the fact that PD (and its animal model) includes the neurodegenerative affection of different areas in the brain, e.g. reduced neural precursor cells caused by dopamine denervation in the subgranular zone of the hippocampus [28], such extra-nigral histopathological changes were correlated to region specific changes in viscoelasticity detected by MRE [1].

In the SN, we observed a significant decrease in viscosity and—to a lesser extent—elasticity six days after treatment cessation followed by a slight but non-significant restoration over time. MPTP seem to primarily affect the geometry of the cellular network in the SN and secondarily the cell density. This is comprehensible considering the structure of the SN, with dopaminergic cell bodies and many cellular processes, which are substantially reduced after MPTP treatment (see Fig 7a and 7b for comparison). Our findings are in line with an observed tissue softening in other animal and human studies of pathological conditions [8,15,17].

Surprisingly, in contrast to the SN, calculated MRE parameters of the midbrain were significantly higher after treatment compared to healthy baseline values. This rather indicates an increase in tissue stiffness in response to MPTP. The decreased total amount of DAPI+ cells does not correlate with this finding. Up to now, it is known that MPTP treatment does not lead to dopaminergic neurodegeneration in the midbrain in contrast to the SN [27]. The biomechanical properties of tissue are not only determined by individual cell types and cellular density but also by the complexity of the cellular network, which depends on the degree of cross-linking and branching, and the interaction with the extracellular matrix [1–3]. The discrepancy between midbrain MRE and histology data may therefore be attributed to other processes following MPTP treatment than the ones examined here, as the midbrain is a larger and more complex area with several core regions and white matter tracts than the SN and hippocampus and cannot be narrowed down to only neuronal cells. Though MRE sensitively detects local tissue alterations, the specificity of the method is not yet established in detail.

Interestingly, a higher basic viscosity was observed in the midbrain compared to the hippocampus in healthy yet untreated mice at -3dpi. As mentioned above, the midbrain tissue exhibits its more complex network geometry with diverse core regions and white matter tracts. In humans, white matter has been shown to be stiffer than gray matter [29,30], which is in line with our observed higher viscosity in the midbrain.

In the hippocampus we observed a transient rise of the storage and loss modulus as described in our previous study [1]. In correlation to that, the total amount of cells was also

transiently elevated at 6dpi. This underlines the histological findings of Klein and colleagues, showing increased stiffness in the hippocampus following MPTP treatment. This was correlated to a higher percentage of newly generated neurons resulting from a reactively enhanced precursor cell proliferation [1].

The significant reduction of G' and G'' in the SN at 6dpi without full restoration over time is paralleled by the reduction of TH+ dopaminergic neurons. It is well-known that the neurotoxin MPTP damages dopaminergic neurons in the SN already shortly after application, which has been demonstrated by a reduced amount of TH+ cells [23,24,31]. In our study, we confirm the MPTP-induced decrease of TH activity in dopaminergic neurons of the SN. Although the amount of TH+ neurons is already significantly reduced three days after MPTP treatment, MRE parameters are changed not until 6dpi. Importantly, TH activity has been shown to decrease first, followed and paralleled by a “real” reduction in the number of neurons after MPTP treatment [32]. We confirm this observation by the quantified number of DAPI+ cells, which correlates with the changes in viscosity. This means that the changed loss and—to a lesser extent—storage modulus in our study are representative for the dopaminergic neurodegeneration in the SN. Moreover, our findings are in accordance with the hypothesis that a decrease of viscoelastic properties of the adult brain is mainly based on the reduced number of neuronal cells, which has first been investigated in a murine stroke model as an example of disturbed brain structure [17].

In line with a decreased brain stiffness in APP-PS1 mice, modelling AD [18], our results support the assumption that viscoelastic properties in neurodegenerative diseases decrease in the mainly affected area and can be correlated with histopathological changes in our animal model for PD. As investigated here, the neurotoxin MPTP leads to different viscous and elastic changes in adult mice depending on the studied brain area. Therefore, we conclude that alterations in MRE parameters following MPTP treatment are highly region-specific.

The size of the processed ROI in the SN is a relevant factor in our study. While in previous animal studies, MRE changes have been observed in the whole brain [16], in one hemisphere [17], in the hippocampus [1] or the cerebellum [15], we processed our MRE data from a smaller brain region. However, our correlating histological findings imply that the MRE setup is eligible to detect viscous and elastic alterations even in small brain areas such as the SN.

Besides dopamine depletion, MPTP provokes an inflammatory response. It has been shown, that the neurotoxin initially leads to a higher amount of microglia and oligodendrocytes in the SN and hippocampus, which diminishes over time after treatment cessation [1,21,23,33]. This course of inflammatory reaction in response to MPTP is also seen in our study. However, the initially elevated amount of Iba+ cells in the SN is not reflected in MRE parameters. Similar observations have been made before in the hippocampus by Klein et al. [1]. Thus, the present data suggest that MRE may not be suitable for detecting elevated amounts of microglia and macrophages or oligodendrocytes as a sign of a transient local inflammation at least with regard to particular structures as the SN and hippocampus. Therefore, the present data further support the hypothesis that neuronal cells likely constitute the mechanical backbone of the adult brain. However, the biomechanical properties of tissue not only depend on mere cell numbers of one neural cell type but also on other cell types, the network neural cells build by cross-linking and branching and their interaction with the extracellular matrix. Even though neuronal cells have been identified to playing a key role in viscoelasticity, important influence from other cell types, networks and interactions cannot be excluded.

In the present study, female mice were used. Human studies have revealed that female brains are stiffer than brains of age-matched male counterparts [7,9]. This raises the question, if the observed changes predominantly in the viscous properties of SN tissue following MPTP-induced neurodegeneration are stable across sex in mice or if differences as in the mentioned

human studies can be found. We have successfully established the MPTP mouse model in females to study the dopamine dependency of functional neurogenesis in the hippocampus and SN [23,24,34]. Thus, the present study can also be compared to our previous MRE study in MPTP-treated female mice [1].

In summary, we demonstrated the feasibility of MRE to sensitively detect viscoelastic changes in small and specific brain regions within an animal model for PD. Furthermore, we contribute to the investigation of the missing link between histopathological alterations and observed biomechanical constants in the SN, by demonstrating that changes in the amount of dopaminergic neurons in the SN of MPTP-lesioned mice are detectable by MRE. Thus, MRE is highly sensitive for the observation of local viscoelastic changes in particular brain regions adding to the understanding of how altered histopathological conditions influence biomechanical parameters of brain tissue that are changed under pathological conditions. This will help to establish MRE as a new potential instrument for clinical evaluation and diagnostics of neurodegenerative diseases.

Supporting Information

S1 Table. Results of MRE measurement in the substantia nigra, the midbrain and the hippocampus.

(PDF)

S2 Table. Results of histological cell count in the substantia nigra, the midbrain and the hippocampus.

(PDF)

Acknowledgments

We thank Jennifer Altschueler for technical assistance.

Author Contributions

Conceived and designed the experiments: EH CK KR IS BS.

Performed the experiments: EH CK TM KR SM.

Analyzed the data: EH CK JB IS.

Contributed reagents/materials/analysis tools: SM JB IS BS.

Wrote the paper: EH CK IS BS.

References

1. Klein C, Hain EG, Braun J, Riek K, Mueller S, Steiner B, et al. Enhanced adult neurogenesis increases brain stiffness: in vivo magnetic resonance elastography in a mouse model of dopamine depletion. *PLoS One* 2014; 9: e92582. doi: [10.1371/journal.pone.0092582](https://doi.org/10.1371/journal.pone.0092582) PMID: [24667730](https://pubmed.ncbi.nlm.nih.gov/24667730/)
2. Lu Y-B, Iandiev I, Hollborn M, Körber N, Ulbricht E, Hirrlinger PG, et al. Reactive glial cells: increased stiffness correlates with increased intermediate filament expression. *FASEB J*. 2011; 25: 624–631. doi: [10.1096/fj.10-163790](https://doi.org/10.1096/fj.10-163790) PMID: [20974670](https://pubmed.ncbi.nlm.nih.gov/20974670/)
3. Schregel K, Wuerfel E, Garteiser P, Gemeinhardt I, Prozorovski T, Aktas O, et al. Demyelination reduces brain parenchymal stiffness quantified in vivo by magnetic resonance elastography. *Proc Natl Acad Sci USA* 2012; 109: 6650–6655. doi: [10.1073/pnas.1200151109](https://doi.org/10.1073/pnas.1200151109) PMID: [22492966](https://pubmed.ncbi.nlm.nih.gov/22492966/)
4. Muthupillai R, Lomas DJ, Rossman PJ, Greenleaf JF, Manduca A, Ehman RL. Magnetic resonance elastography by direct visualization of propagating acoustic strain waves. *Science* 1995; 269: 1854–1857. PMID: [7569924](https://pubmed.ncbi.nlm.nih.gov/7569924/)

5. Mariappan YK, Glaser KJ, Ehman RL. Magnetic resonance elastography: a review. *Clin Anat*. 2010; 23: 497–511. doi: [10.1002/ca.21006](https://doi.org/10.1002/ca.21006) PMID: [20544947](https://pubmed.ncbi.nlm.nih.gov/20544947/)
6. Arani A, Murphy MC, Glaser KJ, Manduca A, Lake DS, Kruse SA, et al. Measuring the effects of aging and sex on regional brain stiffness with MR elastography in healthy older adults. *Neuroimage* 2015; 111: 59–64. doi: [10.1016/j.neuroimage.2015.02.016](https://doi.org/10.1016/j.neuroimage.2015.02.016) PMID: [25698157](https://pubmed.ncbi.nlm.nih.gov/25698157/)
7. Sack I, Beierbach B, Wuerfel J, Klatt D, Hamhaber U, Papazoglou S, et al. The impact of aging and gender on brain viscoelasticity. *Neuroimage* 2009; 46: 652–657. doi: [10.1016/j.neuroimage.2009.02.040](https://doi.org/10.1016/j.neuroimage.2009.02.040) PMID: [19281851](https://pubmed.ncbi.nlm.nih.gov/19281851/)
8. Streitberger KJ, Sack I, Krefting D, Pfueller C, Braun J, Paul F, et al. Brain viscoelasticity alteration in chronic-progressive multiple sclerosis. *PloS One* 2012; 7: e29888. doi: [10.1371/journal.pone.0029888](https://doi.org/10.1371/journal.pone.0029888) PMID: [22276134](https://pubmed.ncbi.nlm.nih.gov/22276134/)
9. Wuerfel J, Paul F, Beierbach B, Hamhaber U, Klatt D, Papazoglou S, et al. MR-elastography reveals degradation of tissue integrity in multiple sclerosis. *Neuroimage* 2010; 49: 2520–2525. doi: [10.1016/j.neuroimage.2009.06.018](https://doi.org/10.1016/j.neuroimage.2009.06.018) PMID: [19539039](https://pubmed.ncbi.nlm.nih.gov/19539039/)
10. Streitberger KJ, Wiener E, Hoffmann J, Freimann FB, Klatt D, Braun J, et al. In vivo viscoelastic properties of the brain in normal pressure hydrocephalus. *NMR Biomed*. 2011; 24: 385–392. doi: [10.1002/nbm.1602](https://doi.org/10.1002/nbm.1602) PMID: [20931563](https://pubmed.ncbi.nlm.nih.gov/20931563/)
11. Murphy MC, Huston J 3rd, Jack CR Jr, Glaser KJ, Manduca A, Felmlee JP, et al. Decreased brain stiffness in Alzheimer's disease determined by magnetic resonance elastography. *J Magn Reson Imaging* 2011; 34: 494–498. doi: [10.1002/jmri.22707](https://doi.org/10.1002/jmri.22707) PMID: [21751286](https://pubmed.ncbi.nlm.nih.gov/21751286/)
12. Huston J 3rd, Murphy MC, Boeve BF, Fattahi N, Arani A, Glaser KJ, et al. Magnetic resonance elastography of frontotemporal dementia. *J Magn Reson Imaging* 2016; 43: 474–478. doi: [10.1002/jmri.24977](https://doi.org/10.1002/jmri.24977) PMID: [26130216](https://pubmed.ncbi.nlm.nih.gov/26130216/)
13. Streitberger KJ, Reiss-Zimmermann M, Freimann FB, Bayerl S, Guo J, Arlt F, et al. High-resolution mechanical imaging of glioblastoma by multifrequency magnetic resonance elastography. *PloS One* 2014; 9: e110588. doi: [10.1371/journal.pone.0110588](https://doi.org/10.1371/journal.pone.0110588) PMID: [25338072](https://pubmed.ncbi.nlm.nih.gov/25338072/)
14. Lipp A, Trbojevic R, Paul F, Fehlner A, Hirsch S, Scheel M, et al. Cerebral magnetic resonance elastography in supranuclear palsy and idiopathic Parkinson's disease. *Neuroimage Clin*. 2013; 3: 381–387. doi: [10.1016/j.nicl.2013.09.006](https://doi.org/10.1016/j.nicl.2013.09.006) PMID: [24273721](https://pubmed.ncbi.nlm.nih.gov/24273721/)
15. Millward JM, Guo J, Berndt D, Braun J, Sack I, Infante-Duarte C. Tissue structure and inflammatory processes shape viscoelastic properties of the mouse brain. *NMR Biomed*. 2015; 28: 831–839. doi: [10.1002/nbm.3319](https://doi.org/10.1002/nbm.3319) PMID: [25963743](https://pubmed.ncbi.nlm.nih.gov/25963743/)
16. Riek K, Millward JM, Hamann I, Mueller S, Pfueller CF, Paul F, et al. Magnetic resonance elastography reveals altered brain viscoelasticity in experimental autoimmune encephalomyelitis. *Neuroimage Clin*. 2012; 1: 81–90. doi: [10.1016/j.nicl.2012.09.003](https://doi.org/10.1016/j.nicl.2012.09.003) PMID: [24179740](https://pubmed.ncbi.nlm.nih.gov/24179740/)
17. Freimann FB, Mueller S, Streitberger KJ, Guo J, Rot S, Ghori A, et al. MR elastography in a murine stroke model reveals correlation of macroscopic viscoelastic properties of the brain with neuronal density. *NMR Biomed*. 2013; 26: 1534–1539. doi: [10.1002/nbm.2987](https://doi.org/10.1002/nbm.2987) PMID: [23784982](https://pubmed.ncbi.nlm.nih.gov/23784982/)
18. Murphy MC, Curran GL, Glaser KJ, Rossman PJ, Huston J 3rd, Poduslo JF, et al. Magnetic resonance elastography of the brain in a mouse model of Alzheimer's disease: initial results. *Magn Reson Imaging* 2012; 30: 535–539. doi: [10.1016/j.mri.2011.12.019](https://doi.org/10.1016/j.mri.2011.12.019) PMID: [22326238](https://pubmed.ncbi.nlm.nih.gov/22326238/)
19. Hirsch E, Graybiel AM, Agid YA. Melanized dopaminergic neurons are differentially susceptible to degeneration in Parkinson's disease. *Nature* 1988; 334: 345–348. PMID: [2899295](https://pubmed.ncbi.nlm.nih.gov/2899295/)
20. Jackson-Lewis V, Przedborski S. Protocol for the MPTP mouse model of Parkinson's disease. *Nat Protoc*. 2007; 2: 141–151. PMID: [17401348](https://pubmed.ncbi.nlm.nih.gov/17401348/)
21. McGeer PL, McGeer EG. Glial reactions in Parkinson's disease. *Mov Disord*. 2008; 23: 474–483. PMID: [18044695](https://pubmed.ncbi.nlm.nih.gov/18044695/)
22. Przedborski S, Vila M. The 1-methyl-4-phenyl-1,2,3,6-tetrahydropyridine mouse model: a tool to explore the pathogenesis of Parkinson's disease. *Ann N Y Acad Sci*. 2003; 991: 189–198. PMID: [12846987](https://pubmed.ncbi.nlm.nih.gov/12846987/)
23. Klaisle P, Lesemann A, Huehnchen P, Hermann A, Storch A, Steiner B. Physical activity and environmental enrichment regulate the generation of neural precursors in the adult mouse substantia nigra in a dopamine-dependent manner. *BMC Neurosci*. 2012; 13: 132. doi: [10.1186/1471-2202-13-132](https://doi.org/10.1186/1471-2202-13-132) PMID: [23110504](https://pubmed.ncbi.nlm.nih.gov/23110504/)
24. Lesemann A, Reinel C, Huehnchen P, Pilhatsch M, Hellweg R, Klaisle P, et al. MPTP-induced hippocampal effects on serotonin, dopamine, neurotrophins, adult neurogenesis and depression-like behavior are partially influenced by fluoxetine in adult mice. *Brain Res*. 2012; 1457: 51–69. doi: [10.1016/j.brainres.2012.03.046](https://doi.org/10.1016/j.brainres.2012.03.046) PMID: [22520437](https://pubmed.ncbi.nlm.nih.gov/22520437/)

25. Clayton EH, Garbow JR, Bayly PV. Frequency-dependent viscoelastic parameters of mouse brain tissue estimated by MR elastography. *Phys Med Biol*. 2011; 56: 2391–2406. doi: [10.1088/0031-9155/56/8/005](https://doi.org/10.1088/0031-9155/56/8/005) PMID: [21427486](https://pubmed.ncbi.nlm.nih.gov/21427486/)
26. Papazoglou S, Hamhaber U, Braun J, Sack I. Algebraic Herlmholtz inversion in planar magnetic resonance elastography. *Phys Med Biol*. 2008; 53: 3147–3158. doi: [10.1088/0031-9155/53/12/005](https://doi.org/10.1088/0031-9155/53/12/005) PMID: [18495979](https://pubmed.ncbi.nlm.nih.gov/18495979/)
27. Phani S, Gonye G, Iacovitti L. VTA neurons show a potentially protective transcriptional response to MPTP. *Brain Res*. 2010; 343: 1–13.
28. Höglinger GU, Rizk P, Muriel MP, Duyckaerts C, Oertel WH, Caille I, et al. Dopamine depletion impairs precursor cell proliferation in Parkinson disease. *Nat Neurosci*. 2004; 7: 726–735. PMID: [15195095](https://pubmed.ncbi.nlm.nih.gov/15195095/)
29. Kruse SA, Rose GH, Glaser KJ, Manduca A, Felmlee P, Jack CR Jr, et al. Magnetic resonance elastography of the brain. *NeuroImage*. 2008; 39:231–237. PMID: [17913514](https://pubmed.ncbi.nlm.nih.gov/17913514/)
30. McCracken PJ, Manduca A, Felmlee J, Ehman RL. Mechanical transient-based magnetic resonance elastography. *Magn Reson Med*. 2005; 53:628–639. PMID: [15723406](https://pubmed.ncbi.nlm.nih.gov/15723406/)
31. Araki T, Mikami T, Tanji H, Matsubara M, Imai Y, Mizugaki M, et al. Biochemical and immunohistological changes in the brain of 1-methyl-4-phenyl-1,2,3,6-tetrahydropyridine (MPTP)-treated mouse. *Eur J Pharm Sci*. 2001; 12: 231–238. PMID: [11113642](https://pubmed.ncbi.nlm.nih.gov/11113642/)
32. Jackson-Lewis V, Jakowec M, Burke RE, Przedborski S. Time course and morphology of dopaminergic neuronal death caused by the neurotoxin 1-methyl-4-phenyl-1,2,3,6-tetrahydropyridine. *Neurodegeneration* 1995; 4: 257–269. PMID: [8581558](https://pubmed.ncbi.nlm.nih.gov/8581558/)
33. Annese V, Herrero MT, Di Pentima M, Gomez A, Lombardi L, Ros CM, et al. Metalloproteinase-9 contributes to inflammatory glia activation and nigro-striatal pathway degeneration in both mouse and monkey models of 1-methyl-4-phenyl-1,2,3,6-tetrahydropyridine (MPTP)-induced Parkinsonism. *Brain Struct Funct*. 2015; 220: 703–727. doi: [10.1007/s00429-014-0718-8](https://doi.org/10.1007/s00429-014-0718-8) PMID: [24558048](https://pubmed.ncbi.nlm.nih.gov/24558048/)
34. Klein C, Rasińska J, Empl L, Sparenberg M, Poshtiban A, Hain EG et al. Physical exercise counteracts MPTP-induced changes in neural precursor cell proliferation in the hippocampus and restores spatial learning but not memory performance in the water maze. *Behav Brain Res*. 2016; 307: 227–238. doi: [10.1016/j.bbr.2016.02.040](https://doi.org/10.1016/j.bbr.2016.02.040) PMID: [27012392](https://pubmed.ncbi.nlm.nih.gov/27012392/)

RESEARCH

Open Access



Indomethacin promotes survival of new neurons in the adult murine hippocampus accompanied by anti-inflammatory effects following MPTP-induced dopamine depletion

Elisabeth G. Hain^{1*} , Maria Sparenberg¹, Justyna Rasińska¹, Charlotte Klein¹, Levent Akyüz^{2,3} and Barbara Steiner¹

Abstract

Background: Parkinson's disease (PD) is characterized by dopaminergic cell loss and inflammation in the substantia nigra (SN) leading to motor deficits but also to hippocampus-associated non-motor symptoms such as spatial learning and memory deficits. The cognitive decline is correlated with impaired adult hippocampal neurogenesis resulting from dopamine deficit and inflammation, represented in the 1-methyl-4-phenyl-1,2,3,6-tetrahydropyridine hydrochloride (MPTP) mouse model of PD. In the inflammatory tissue, cyclooxygenase (COX) is upregulated leading to an ongoing inflammatory process such as prostaglandin-mediated increased cytokine levels. Therefore, inhibition of COX by indomethacin may prevent the inflammatory response and the impairment of adult hippocampal neurogenesis.

Methods: Wildtype C57Bl/6 and transgenic Nestin-GFP mice were treated with MPTP followed by short-term or long-term indomethacin treatment. Then, aspects of inflammation and neurogenesis were evaluated by cell counts using immunofluorescence and immunohistochemical stainings in the SN and dentate gyrus (DG). Furthermore, hippocampal mRNA expression of neurogenesis-related genes of the Notch, Wnt, and sonic hedgehog signaling pathways and neurogenic factors were assessed, and protein levels of serum cytokines were measured.

Results: Indomethacin restored the reduction of the survival rate of new mature neurons and reduced the amount of amoeboid CD68+ cells in the DG after MPTP treatment. Indomethacin downregulated genes of the Wnt and Notch signaling pathways and increased *neuroD6* expression. In the SN, indomethacin reduced the pro-inflammatory cellular response without reversing dopaminergic cell loss.

Conclusion: Indomethacin has a pro-neurogenic and thereby restorative effect and an anti-inflammatory effect on the cellular level in the DG following MPTP treatment. Therefore, COX inhibitors such as indomethacin may represent a therapeutic option to restore adult neurogenesis in PD.

Keywords: Neurogenesis, Inflammation, Neurodegeneration, Parkinson's disease, Indomethacin, MPTP, Hippocampus, Substantia nigra

* Correspondence: elisabeth-g.hain@charite.de

¹Charité – Universitätsmedizin Berlin, corporate member of Freie Universität Berlin, Humboldt – Universität zu Berlin and Berlin Institute of Health, Department of Neurology with Experimental Neurology, Charitéplatz 1, 10117 Berlin, Germany

Full list of author information is available at the end of the article



Background

The hallmark of Parkinson's disease (PD) is the dopaminergic cell loss in the substantia nigra (SN) leading to the characteristic motor deficits. Moreover, hippocampal non-motor functions such as spatial learning and memory are also impaired [1]. As nigral dopaminergic fibers project to the hippocampus, dopaminergic cell loss results in a deficit of the neurotransmitter dopamine in that brain area, affecting adult neurogenesis in the dentate gyrus (DG) of the hippocampus [2–5]. Animal models of PD have shown that this impaired neurogenesis following dopamine depletion correlates with PD-associated cognitive deficits [6–11]. These cognitive deficits together with a higher prevalence and earlier onset of PD are associated with the male gender [12, 13]. A commonly used animal model of the disease is the 1-methyl-4-phenyl-1,2,3,6-tetrahydropyridine hydrochloride (MPTP) mouse model. It represents the characteristic dopaminergic cell loss in the SN, determining the onset of PD [14, 15]. In this model, an impaired neurogenic process in the hippocampus and associated cognitive decline have also been reported [6–11]. In the SN, dopaminergic neurodegeneration leads to a release of soluble neuron-injury factors, which activate microglia [16, 17]. This results in the release of neurotoxic agents such as cytokines, reactive oxygen species, nitric oxide radicals, and prostaglandins (PG) and attracts lymphocytic infiltration of CD4+ and CD8+ T cells [17, 18]. All these events lead to a perpetuation of inflammation and neurodegeneration in the SN [17–21].

In the DG of the hippocampus of MPTP-treated mice, reactive microglia have also been observed [22, 23]. Microglial activation is known to alter the hippocampal microenvironment leading to a decreased survival of newly generated neurons in the DG [24–27]. The differentiation from newborn neural progenitor cells into functionally integrated neurons in the DG is a multistep process [28–30], which is highly vulnerable to pathological changes of the microenvironment such as inflammation [25, 27, 31]. Microglia-released pro-inflammatory cytokines such as interleukin (IL)-6 have been shown to be important factors between activated microglia and decreased hippocampal neurogenesis [27, 32]. In PD patients, pro-inflammatory cytokines are also elevated in the cerebrospinal fluid [33, 34], and microglial activation has been observed in the hippocampus of post-mortem brains [35, 36]. Thus, neurogenesis in the adult DG of PD patients might also be affected by inflammation in addition to the impaired homeostasis of the neurotransmitter dopamine.

The anti-inflammatory effect of the non-selective cyclooxygenase (COX) inhibitor indomethacin is based on a reduced PG production by inhibiting the basally expressed enzyme COX-1 and the inflammation-induced COX-2 [37, 38]. COX catalyzes the synthesis of PGH₂ in a

two-step process, which is accompanied by the production of neurotoxic free radicals [38, 39]. PGH₂ is converted into biologically active PG such as PGE₂, which leads to a rapid expression of COX-2 itself and other pro-inflammatory agents by activation of the PGE₂ receptor 2 [38, 40]. A decreased inflammation by indomethacin treatment leads to the protection against neural cell loss in the hippocampus in animal models of cranial irradiation or ischemia [27, 41–45]. However, some studies described a decreased proliferation of hippocampal neuronal cells by COX inhibition in healthy and ischemic brains [46, 47]. Serrano and colleagues suggested a potential early neuroprotective role and a delayed neurodegeneration by COX-2 signaling [48].

Interestingly, COX-2 is upregulated in the SN of PD patients and in the MPTP mouse model [49] and leads to higher dopaminergic cell loss than in COX-2-deficient mice [50]. COX inhibition has been shown to prevent microglial activation and dopaminergic cell loss in the SN [51–53], which implies that COX plays a role in dopaminergic neurodegeneration.

This suggests that a PG-mediated inflammation represents a potential target. Thus, treatment with the non-selective COX inhibitor indomethacin might be a therapeutic option against dopaminergic cell loss and inflammation in the SN and the DG. We investigated here if indomethacin shows an anti-inflammatory effect on the cellular level, thereby reducing the levels of circulating pro-inflammatory and elevating the levels of anti-inflammatory cytokines, respectively. Furthermore, we studied the influence of indomethacin on different stages of adult hippocampal neurogenesis after MPTP treatment to test whether a therapy with indomethacin could be a suitable strategy to restore adult neurogenesis in PD patients.

Methods

Animals and housing

In total, 6- to 12-week-old female wildtype C57Bl/6N mice ($n = 131$; Charles River, Sulzfeld, Germany) and transgenic C57Bl/6N mice, expressing the green fluorescent protein (GFP) under the *nestin* promoter (Nestin-GFP) to label neural progenitor cells ($n = 70$, Forschungseinrichtungen für Experimentelle Medizin, Berlin, Germany) with a median weight of 21.1 g, were used. They were group-housed in standard cages in a temperature- and humidity-controlled standard colony room with a light-dark cycle of 12 h (starting at 6 am) and free access to food and water. Even though estradiol has a pro-neurogenic effect, adult hippocampal neurogenesis is not influenced by the sex itself in C57Bl/6 mice at the age investigated here [54–56].

All experiments were approved by the local animal ethics committee (Landesamt für Gesundheit und Soziales, Berlin, Germany) and carried out in accordance with the European

Communities Council Directive of 22 September 2010 (10/63/EU).

Group design and experimental procedure

After 1 week of acclimatization, wildtype and Nestin-GFP mice were divided into two groups to receive either 2'-methyl-MPTP (further denoted as MPTP) or 0.9% saline as control (CTR) intraperitoneally (i.p.). Both groups were further assigned to short-term treatment (ST) groups and long-term treatment (LT) groups. Then, they were further divided to be treated either with indomethacin or 0.9% saline as vehicle i.p. over 6 consecutive days (ST) or every other day over 17 days (LT), starting after the last day of MPTP or saline injection. This results in eight groups with one control group (CTR + vehicle) in both time spans (ST and LT). All assignments into groups were performed pseudorandomly. After treatment cessation, mice were killed for histology and molecular analyses. A timeline of the experimental procedure is displayed in Fig. 1.

MPTP mouse model

MPTP (generous gift from Prof. Dr. Christian Klein, Medicinal Chemistry, Institute of Pharmacy and Molecular Biotechnology IPMB, Heidelberg University, Heidelberg, Germany) was dissolved in 0.9% saline and injected i.p. at a dose of 20 mg/kg body weight in the morning hours on three consecutive days. CTR mice received three injections of saline instead. During MPTP injections, mice were treated in an extra room of the animal housing facility and transferred into an isolation cage from the first day of MPTP treatment until 2 days after due to the excrements containing MPTP and its metabolites.

BrdU injections

5-Bromo-2'-deoxyuridine (BrdU, Sigma-Aldrich, Steinheim, Germany) was used for labeling proliferating cells. It was dissolved in 0.9% saline. All animals received BrdU i.p. at a dose of 50 mg/kg body weight in the morning hours on three consecutive days, starting at the last day of MPTP or saline, respectively.

Indomethacin treatment

Indomethacin (Liometacen, Promedica Chiesi, Parma, Italy) was dissolved in distilled water and administered i.p. at a concentration of 2.5 mg/kg body weight in the morning hours either over 6 consecutive days (ST) or every other day over 17 days (LT), starting after the last day of MPTP or saline. Animals receiving 0.9% saline injections instead of indomethacin served as controls for the drug treatment (vehicle).

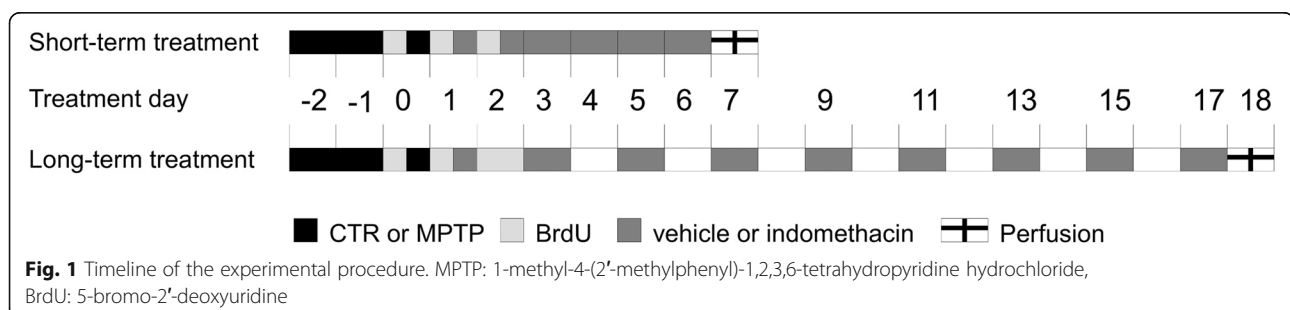
Perfusion and tissue preparation

Animals were deeply anesthetized with ketamine/xylazine (10% Ketamine hydrochloride, WDT; 2% Rompun, Provet AG) i.p. before being transcardially perfused with phosphate-buffered saline (PBS) and 4% paraformaldehyde (PFA). The brains were removed from the skull, post-fixed in 4% PFA at 4 °C overnight, dehydrated with 30% sucrose solution at 4 °C for 48 h, and frozen at -72 °C in 2-methylbutane (Sigma-Aldrich, Steinheim, Germany). Afterward, the brains were coronally sliced into 40- μ m-thick sections using a Leica CM1850 UV cryostat and stored in cryoprotectant solution at 4 °C until histological analysis was performed.

For collecting blood samples and fresh brain tissue for molecular analysis, the animals were as well deeply anesthetized with ketamine/xylazine. Then, the abdomen was opened, and the blood samples were taken from the inferior vena cava. Aprotinin (Sigma-Aldrich, St. Louis, USA; 1 μ l/1 ml blood sample) was added to the samples to prevent protein degradation. Samples were spun with an acceleration of 8000 \times g at 4 °C for 15 min, and sera were collected. After taking blood samples, the animals were transcardially perfused with PBS. Afterward, the brains were quickly removed from the skull and rapidly frozen on dry ice. The brains and serum samples were stored at -80 °C until further analysis.

Immunohistochemistry and cell quantification

For CD68 staining, antigen retrieval was performed on the brain sections using NaBH₃. To continue with the immunohistochemical staining, a well-established protocol was followed [9]. One-in-six free-floating brain section series were treated with 0.6% H₂O₂. Hereafter, the sections



for BrdU staining were also treated with 2 M HCl. After blocking with donkey serum-enriched PBS (PBS+), the sections were incubated overnight with the first antibody: anti-BrdU (rat, 1:500, AbD Serotec), anti-Iba-1 (rabbit, 1:1000, Wako), anti-CD68 (rat, 1:400, AbD Serotec), or anti-tyrosine hydroxylase (TH, mouse, 1:10,000, Sigma-Aldrich). The next day, the sections were incubated with the biotinylated secondary antibody (anti-rat, anti-rabbit, or anti-mouse, 1:250, dianova) at room temperature for 2 h. Afterward, an ABC solution to form a streptavidin-peroxidase complex (Vectastain ABC Elite Kit, Vector Laboratories) was applied, and the reaction was visualized by 3,3'-diaminobenzidine (DAB, Sigma-Aldrich)-nickel staining. Finally, the stained sections were mounted on microscope slides and coverslipped.

In total, the eight brain slices of the hippocampus (240 μm apart) of each mouse in the histological group were analyzed by manually counting BrdU-positive (BrdU+) cells in the subgranular zone and granular cell layer of the DG using the $\times 40$ objective. Total numbers of Iba-1-positive (Iba+) cells and CD68-positive (CD68+) cells were counted manually in the eight brain slices of the wildtype mice in the hilus and granular and molecular layer of the DG using the $\times 40$ objective. CD68+ cells were further subdivided into cells displaying an amoeboid or ramified shape. Amoeboid CD68+ cells are defined as cells with higher lysosomal activity, e.g., in microglia, macrophages, and to a lesser extent in dendritic cells, indicating a phagocytotic state [57]. Here, CD68+ cells were identified as amoeboid, if cell somas appear more round-shaped and more color-intense with no or only a few branches [58, 59]. In contrast, ramified CD68+ cells are characterized by a small cell body with thin processes [58, 59]. Numbers of amoeboid CD68+ cells were assessed by manual counting using the $\times 40$ objective. Numbers of ramified CD68+ cells were estimated by taking the difference between all CD68+ cells and amoeboid CD68+ cells. For manual cell counting in the SN, including pars compacta and pars reticulata, four stained brain slices (240 μm apart) in total were analyzed for amoeboid CD68+ cells in the SN of wildtype mice and TH-positive (TH+) cells of Nestin-GFP mice using the $\times 40$ objective. All manually assessed cell counts were done using an Axioskop HB50/AC light microscope (Zeiss, Germany) and multiplied by six to estimate the absolute cell numbers. A Stereo Investigator (MBF Bioscience) and a Leica DMRE microscope were used for quantification of the total numbers of Iba-1+ cells and CD68+ cells in the SN of wildtype mice. The region of interest was tracked with a $\times 5$ and $\times 4$ objective, respectively. Actual counting was done with a $\times 40$ oil and $\times 20$ objective, respectively, on four sections with a sampling grid size of $150 \times 120 \mu\text{m}$ and a counting frame of $60 \times 60 \mu\text{m}$ without guard disector height. Cells were counted when cells bodies

became sharp in their widest extent. The total amount of Iba-1+ and CD68+ cells was automatically estimated using the counted cell number, sampling grid size, counting frame size, slice interval, and slice thickness. The coefficient of error (Gundersen, $m = 1$) was ≤ 0.9 . The numbers of ramified CD68+ cells in the SN were estimated by taking the difference between all CD68+ cells and amoeboid CD68+ cells. All data were collected blinded to the treatment groups.

Immunofluorescence and cell quantification

For the characterization of newly generated BrdU+ cells in the DG following the stages of neuronal development in the adult DG [29] (Additional file 1: Figure S1), the brain slices were triple-stained for BrdU, Nestin, visualized by co-expressed GFP (Nestin-GFP), and doublecortin (DCX) in Nestin-GFP mice or BrdU, DCX, and neuronal nuclei (NeuN) in wildtype mice, following a well-established protocol [9]. Briefly, one-in-twelve free-floating brain sections (480 μm apart) were pre-treated with 2 M HCl and blocked with PBS+. Sections were then incubated with anti-BrdU (rat, 1:500, AbD Serotec), anti-GFP (rabbit, 1:200, Abcam), anti-DCX (goat, 1:100, Santa Cruz Biotechnology), and anti-NeuN (mouse, 1:1000, Abcam) at 4 $^{\circ}\text{C}$ overnight. The next day, the sections were incubated with fluorescent secondary antibodies RhodamineX (anti-rat, 1:250, dianova), Alexa488 (anti-rabbit or anti-mouse, 1:1000, invitrogen), and Alexa647 (anti-goat, 1:300, dianova) at room temperature for 4 h, mounted on microscope slides and coverslipped.

To evaluate the number of newly generated cells following the stages of neurogenesis (Additional file 1: Figure S1), 50 BrdU+ cells within the subgranular zone and the granule cell layer were detected using a confocal microscope (TCS SP2, Leica, Wetzlar, Germany) under a $\times 63$ objective and were analyzed for co-labeling with Nestin-GFP-positive (BrdU+/Nestin-GFP+) type 1 cells, triangular shaped cells with an apical process, and type 2a cells with short, tangentially orientated processes, Nestin-GFP-positive/DCX-positive (BrdU+/Nestin-GFP+/DCX+) type 2b cells, DCX-positive type 3 cells (BrdU+/DCX+) including immature neurons or NeuN-positive (BrdU+/NeuN+) mature neurons. Hereof, the absolute numbers were estimated by the ratio of co-labeled BrdU+ cells to all BrdU+ cells. All data were collected blinded to the treatment groups.

Measurement of cytokine concentration

To assess peripheral inflammatory processes following MPTP treatment, the protein levels of six representative cytokines were measured in the serum: interleukin (IL)-1 β , IL-6, IL-10, IL-17a, interferon (IFN)- γ , and tumor necrosis factor (TNF)- α . For the detection, a Bio-Plex Pro™ Mouse Cytokine Th17 Panel A 6-Plex Group 1 kit (Bio-Rad

Laboratories, Inc.) and a Bio-Plex[®] 200 System (Bio-Rad Laboratories, Inc.) plate reader were used. Serum samples were applied undiluted. The assay was processed following the manufacturer's protocol (Bio-Plex Pro™ Cytokine, Chemokine, and Growth Factor Assays Instruction Manual, Bio-Rad Laboratories, Inc.).

mRNA isolation and gene expression analysis

To investigate possible altered signaling pathways in neurogenesis, the expression of *gli1*, *hes5*, *lef1*, effector genes of the sonic hedgehog, Notch and Wnt signaling pathways, respectively, and of the pro-neurogenic factors *neuroD6* and *ngn1* in the hippocampus was assessed. Therefore, the samples (1 mm in diameter) were taken from the brain slices of the anterior hippocampus (Bregma -1.82 to -2.3 mm). Hippocampal total RNA was isolated with the Nucleospin RNA/Protein isolation kit (Macherey-Nagel, Düren, Germany) and reverse transcribed using the High Capacity RNA-to-cDNA kit (Applied Biosystems, CA, USA). cDNA corresponding to 1 ng of total RNA was used for gene expression analysis carried out with the StepOne real-time PCR instrument and software (Applied Biosystems, CA, USA). The amplification was performed with TaqMan assays (*gapdh*: Mm99999915_g1, *gli1*: Mm00494654_m1, *hes5*: Mm00439311_g1, *lef1*: Mm00550265_m1, *neuroD6*: Mm01326464_m1, *ngn1*: Mm00440466_s1) according to the TaqMan Fast Advanced Master Mix protocol (Applied Biosystems, CA, USA). Relative gene expression was calculated with the comparative C_t method ($\Delta\Delta C_t$) and *gapdh* as the reference gene. Data are displayed as fold change compared to CTR + vehicle.

Statistical analysis

Data of the ST and LT groups were analyzed separately by using IBM SPSS Statistics 25 for Windows and GraphPad Prism 7. A 2 × 2 factorial design with the between-subject factors neurotoxin (CTR vs. MPTP) and drug (vehicle vs. indomethacin) was used. The two-way between-subjects ANOVA was performed for histological, Multiplex ELISA, and real-time PCR data to test the main effects of the factors neurotoxin and drug and their interaction. Pairwise comparison using the Bonferroni test was done in case of a significant interaction. *P* values ≤ 0.05 were considered statistically significant. All histological data and real-time PCR data are displayed in box plots with a center line as median and whiskers indicating the minimum and maximum value. Multiplex ELISA data are given tabularly as mean ± SEM. Graphs were created using GraphPad Prism 7.

Results

Indomethacin prevents the MPTP-induced decrease in the number of new mature neurons in the DG

In the total cell count of BrdU⁺/NeuN⁺ mature granule cells in the LT group, a significant interaction ($F(1,26) =$

5.413) and a significant main effect of the factor drug ($F(1,26) = 7.658$) were observed. Pairwise comparison showed that MPTP treatment reduced the number of new mature neurons compared to CTR (CTR + vehicle vs. MPTP + vehicle, $p \leq 0.05$). Indomethacin treatment prevented this reduction (MPTP + vehicle vs. MPTP + indomethacin, $p \leq 0.01$) (Fig. 2a, Additional file 1: Figure S1). In CTR mice, the number of newly generated neurons was not altered by indomethacin (CTR + vehicle vs. CTR + indomethacin, $p \geq 0.05$).

Total number of proliferating cells is not affected by MPTP or indomethacin

At both time points, no significant alterations by the factors neurotoxin (ST: $F(1,28) = 0.086$; LT: $F(1,26) = 1.422$), drug (ST: $F(1,28) = 0.382$; LT: $F(1,26) = 0.511$), and their interaction (ST: $F(1,28) = 0.222$; LT: $F(1,26) = 0.005$) in the total number of BrdU⁺ cells were observed (Fig. 2b).

Neurotoxin treatment decreases the number of proliferating type 2a cells in the DG

A significant interaction of the factors neurotoxin and drug was detected in the number of BrdU⁺/Nestin-GFP⁺/DCX⁺ type 2b cells in the ST group ($F(1,26) = 4.325$) (Fig. 2c), but no relevant significant difference in the post hoc Bonferroni test. A significant main effect of the factor neurotoxin in the total number of newly generated BrdU⁺/Nestin-GFP⁺ type 2a cells was revealed in the LT group ($F(1,28) = 4.893$) (Fig. 2d). There were no effects of the factors neurotoxin and drug alone or in their interaction on the absolute numbers of BrdU⁺/Nestin-GFP⁺ type 1 cells, BrdU⁺/Nestin-GFP⁺ type 2a cells in the ST group and BrdU⁺/Nestin-GFP⁺/DCX⁺ type 2b cells in the LT group as well as BrdU⁺/DCX⁺ type 3 cells including immature neurons at both time points (Fig. 2c, d). Representative images of the different cells types are shown in Fig. 3a–e.

Indomethacin and MPTP transiently downregulate Wnt signaling, whereas drug treatment alone upregulates *neuroD6* expression in the hippocampus

In the ST group, there was a significant interaction ($F(1,16) = 7.067$) and a main effect of the factor drug ($F(1,16) = 5.275$) in the mRNA expression of *lef1*, an effector of the Wnt signaling pathway. Here, the pairwise comparison showed a reduced *lef1* expression by MPTP and indomethacin treatment compared to CTR mice (CTR + vehicle vs. MPTP + vehicle, $p \leq 0.05$; CTR + vehicle vs. CTR + indomethacin, $p \leq 0.01$) (Fig. 4a). These effects were no longer present in the LT group. The factor drug increased mRNA expression of the pro-neurogenic basic helix-loop-helix (bHLH) gene *neuroD6* in the ST group ($F(1,16) = 9.530$) and in the LT group ($F(1,16) = 13.548$). Significant main effects of the factor neurotoxin ($F(1,16) = 5.469$) and factor drug ($F(1,16) = 5.482$)

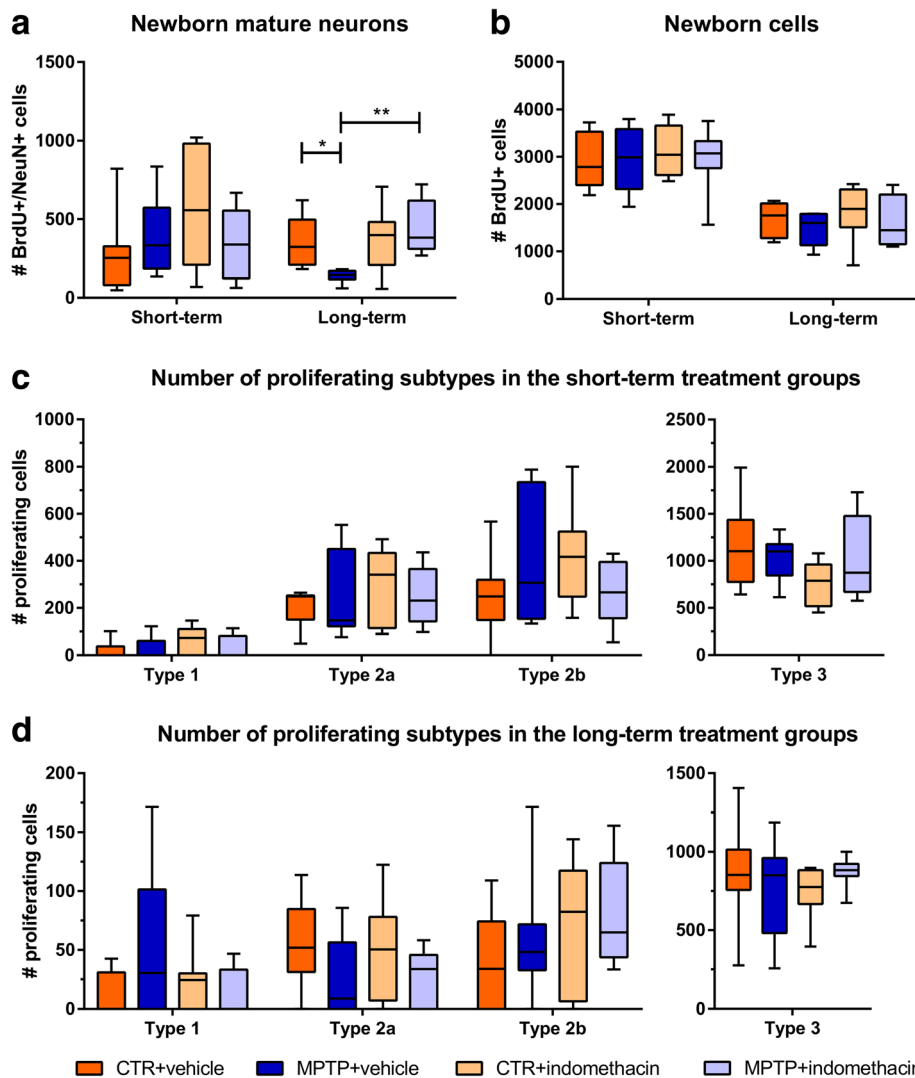


Fig. 2 Results of histological cell counts of proliferating cells in the dentate gyrus. Absolute numbers of newborn mature neurons (a) and all newborn cells (b), and subtypes of newborn progenitor cells in short-term- (c) and long-term-treated (d) mice in the dentate gyrus revealed by immunohistological and immunofluorescent analysis. $N=6-8$ /group. A two-way ANOVA with factors neurotoxin, drug, and their interaction was performed. A significant interaction was followed by a Bonferroni post hoc test with $*p \leq 0.05$, $**p \leq 0.01$. CTR: control; MPTP: 1-methyl-4-(2'-methylphenyl)-1,2,3,6-tetrahydropyridine hydrochloride

on mRNA expression of the anti-neurogenic bHLH repressor gene *hes5*, an effector of the Notch signaling pathway, were revealed in the ST group. These effects were no longer present in the LT group. No mRNA expression of the neurogenic factor *ngn1* could be measured in the ST group. No significant effects of the factors neurotoxin, drug, and their interaction were revealed on the mRNA expression of *ngn1* in the LT group and of *gli1*, an effector gene of the sonic hedgehog signaling pathway, at both time points. Data of mRNA levels are presented in Fig. 4 and in the supplementary material (Additional file 2: Table S1).

Reduced numbers of amoeboid CD68+ cells in the DG of MPTP mice following indomethacin treatment

There was a significant interaction of neurotoxin and drug in the total count of Iba-1+ microglia in the ST group ($F(1,28) = 4.497$). Post hoc analysis showed no significant differences (Fig. 5a). No significant main effects of the factors neurotoxin and drug or significant interaction on the total numbers of CD68+ cells were found (Fig. 5b). At both time points, the interaction of neurotoxin and drug led to significantly different amounts of amoeboid CD68+ cells (ST: $F(1,28) = 7.923$; LT: $F(1,26) = 5.860$). The pairwise comparison revealed a significantly

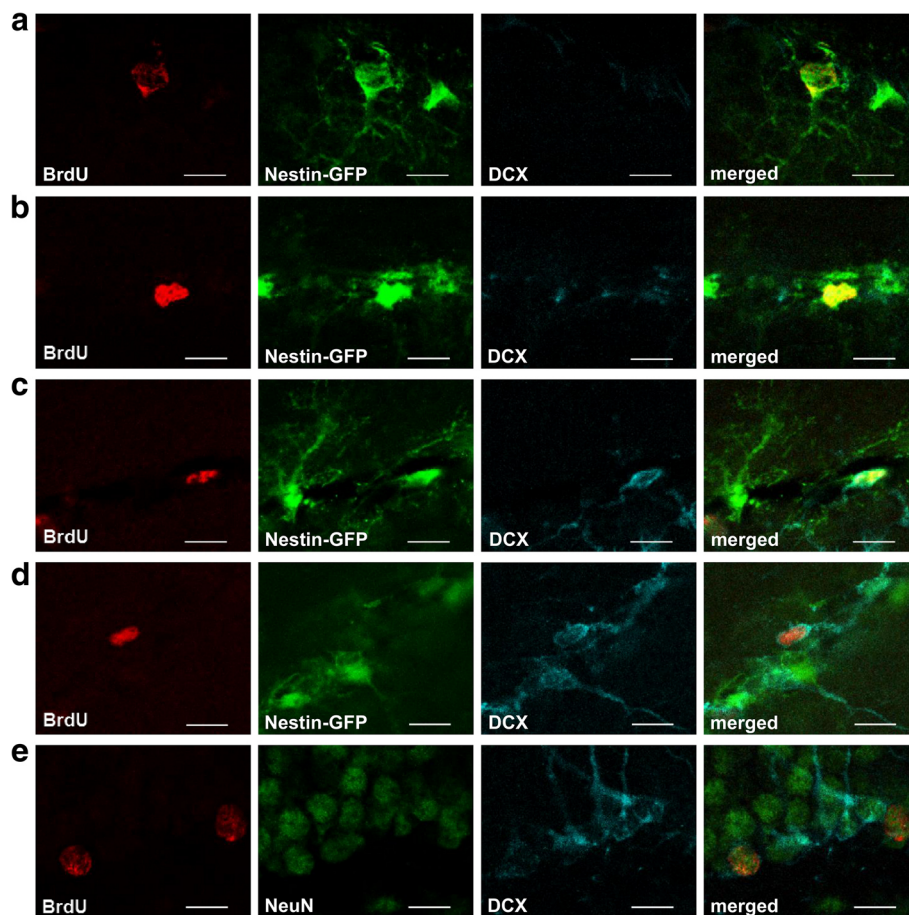


Fig. 3 Representative confocal images of the subtypes. Proliferating subtypes of neurogenesis in the dentate gyrus: progenitor cell type 1 (a), progenitor cell type 2a (b), progenitor cell type 2b (c), progenitor cell type 3 (d), and mature neuron (e). Scale bars indicate 10 μ m. BrdU: 5-bromo-2'-deoxyuridine; DCX: doublecortin; GFP: green fluorescent protein; NeuN: neuronal nuclei

higher cell count of amoeboid CD68+ cells in MPTP-treated mice compared to CTR mice at both time points (CTR + vehicle vs. MPTP + vehicle: ST $p \leq 0.001$; LT $p \leq 0.05$). Indomethacin prevented this in the ST group (MPTP + vehicle vs. MPTP + indomethacin, $p \leq 0.01$) (Fig. 5c). There were also significant main effects of the factor neurotoxin ($F(1,28) = 5.767$) and drug ($F(1,28) = 4.298$) on the amount of amoeboid CD68+ cells in the ST group. No significant main effects or interaction on the numbers of ramified CD68+ cells could be detected at both time points (Fig. 5d). Representative images of CD68+ cells are shown in Fig. 5e, f.

Long-term indomethacin treatment prevents MPTP-induced increase of IL-10 and IL-17a levels in serum

A significant interactive effect of the factors neurotoxin and drug was detected in the serum levels of IL-10 ($F(1,31) = 4.432$) and IL-17a ($F(1,29) = 7.825$) in the LT group. The pairwise comparison revealed a significantly higher serum concentration of the anti-inflammatory

cytokine IL-10 and the pro-inflammatory cytokine IL-17a in MPTP-treated mice compared to CTR mice (CTR + vehicle vs. MPTP + vehicle, $p \leq 0.05$ and $p \leq 0.01$, respectively). Treatment with indomethacin following MPTP prevented this increase (MPTP + vehicle vs. MPTP + indomethacin, $p \leq 0.01$). In the ST group, no significant effect of either the factors neurotoxin, drug, or their interaction was found. No significant change was revealed for the serum concentrations of the pro-inflammatory cytokines IL-1 β , IL-6, IFN- γ , and TNF- α at either time point (Table 1).

Indomethacin prevents MPTP-induced increase of Iba-1+ cell numbers, and drug treatment alone decreases the amount of CD68+ amoeboid cells in the SN

A two-way ANOVA revealed a significant main effect of the factor neurotoxin on the number of TH+ neurons at both time points (ST: $F(1,26) = 8.609$; LT: $F(1,33) = 11.303$), but no effect of drug (ST: $F(1,26) = 2.573$; LT: $F(1,33) = 3.189$) or interaction (ST: $F(1,26) = 3.821$; LT: $F(1,33) = 2.082$) (Fig. 6a). As dopaminergic cell loss by neurotoxic

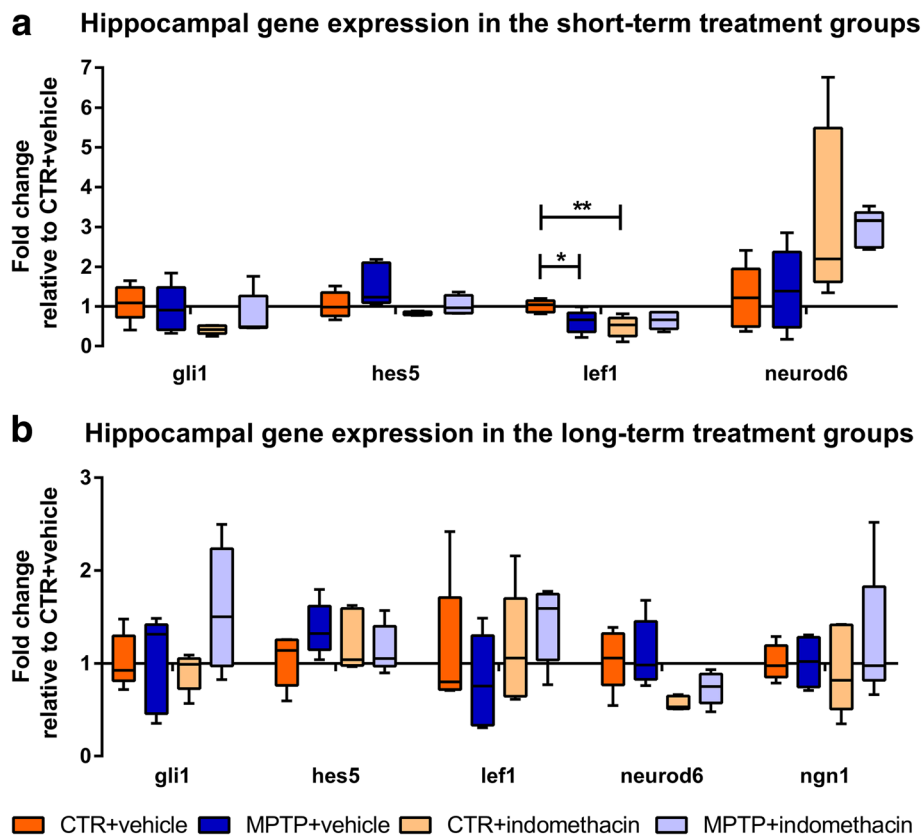


Fig. 4 Hippocampal gene expression analysis. Quantitative real-time PCR was performed for the effector genes *gli1*, *hes5*, and *lef1* of the sonic hedgehog, Notch, and Wnt signaling pathways, respectively, and for the neurogenic factors *neuroD6* and *ngn1* in short-term- (**a**) and long-term-treated (**b**) mice. Gene expression is displayed as fold changes of mRNA levels in relation to CTR + vehicle. $N = 5$ /group. A two-way ANOVA with factors neurotoxin, drug, and their interaction was performed. A significant interaction was followed by a Bonferroni post hoc test: * $p \leq 0.05$, ** $p \leq 0.01$. CTR: control; MPTP: 1-methyl-4-(2'-methylphenyl)-1,2,3,6-tetrahydropyridine hydrochloride

treatment was achieved, the here selected time points in this model represent the onset of PD. Representative images, displaying the reduction of TH+ cells after neurotoxic treatment, are represented in Fig. 6b, c.

A significant interaction of both factors in the amount of Iba-1+ cells was observed in the ST group ($F(1,28) = 7.715$) and LT group ($F(1,26) = 5.800$). At both time points, the pairwise comparison showed significantly higher numbers of Iba-1+ microglia in MPTP-treated mice than in CTR mice (CTR + vehicle vs. MPTP + vehicle: ST, $p \leq 0.01$; LT, $p \leq 0.05$). This was decreased following indomethacin treatment (MPTP + vehicle vs. MPTP + indomethacin: ST, $p \leq 0.001$; LT, $p \leq 0.05$) (Fig. 7a). A significant main effect of the factor drug was revealed in the amount of Iba-1+ cells in the ST group ($F(1,28) = 8.293$). On the numbers of all CD68+ cells, no significant effect of either the factors neurotoxin, drug, or their interaction was found (Fig. 7b). In the ST group, a significant main effect of the factor drug could be observed on the amount of amoeboid CD68+ cells ($F(1,28) = 14.753$) (Fig. 7c). No

significant main effects or interaction of both factors on the number of ramified CD68+ cells was observed at both time points (Fig. 7d). Representative images of Iba-1+ cells are presented in Fig. 7e, f.

Discussion

We here demonstrate that indomethacin is effective in preventing the impaired neurogenic process in the adult hippocampus following MPTP-induced dopamine depletion and has an anti-inflammatory effect by reducing the number of amoeboid CD68+ cells as one factor of inflammation. Both MPTP treatment and inflammation are known to decrease the survival of newly generated neurons in the DG [7, 9, 27, 60]. As MPTP treatment itself is also accompanied by inflammatory reactions on the cellular level in the hippocampus [22, 23], we suggest a pro-neurogenic effect by indomethacin treatment based on an anti-inflammatory effect on the cellular level.

According to previous studies, we observed a decreased number of new mature neurons, characterized by NeuN

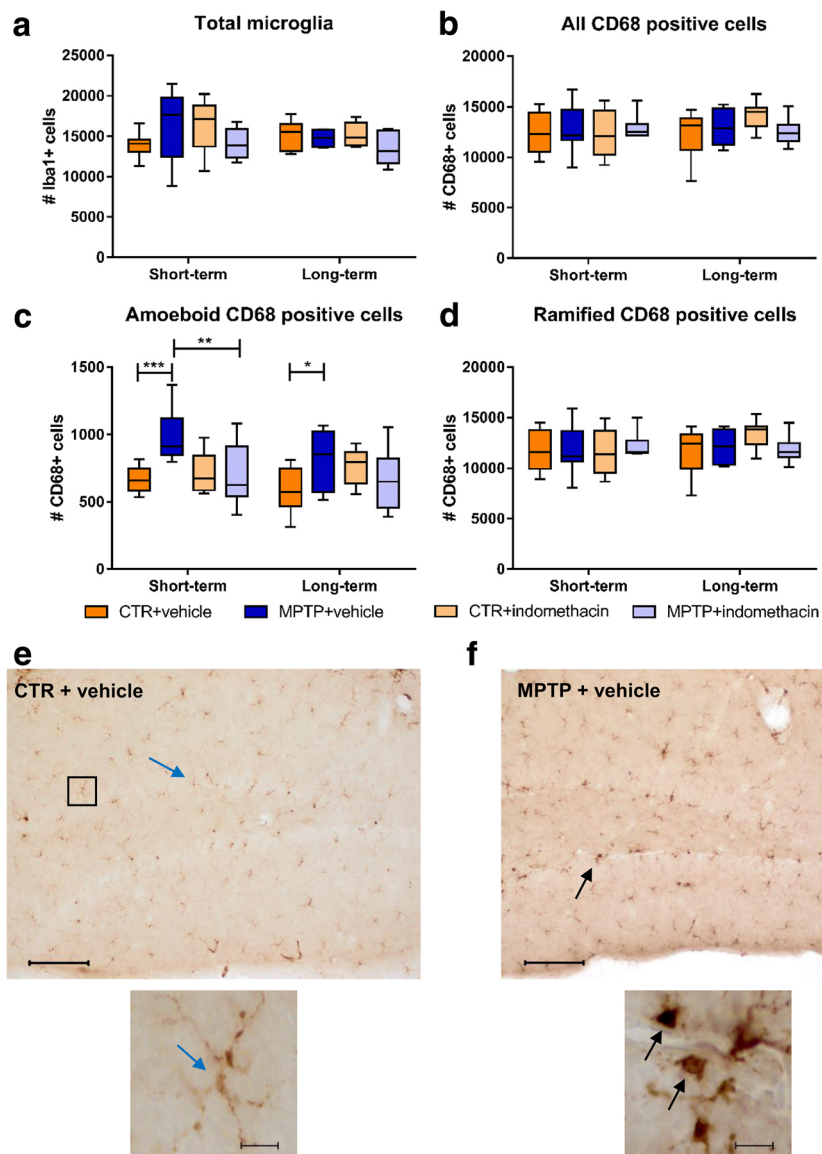


Fig. 5 Results of histological cell counts of cellular inflammation in the dentate gyrus. Absolute numbers of Iba-1-positive cells (**a**), CD68-positive cells (**b**), amoeboid CD68-positive cells (**c**), and ramified CD68-positive cells (**d**) and representative images of CD68-positive cells in CTR mice (**e**) and MPTP-treated mice (**f**). Black arrows indicate amoeboid CD68-positive cells, and blue arrows indicate ramified CD68-positive cells. In the short-term treatment group, indomethacin reduces the increased number of amoeboid CD68-positive cells after dopamine depletion. Scale bars indicate 100 and 10 μ m in the higher magnification. $N = 6-8$ /group. A two-way ANOVA with main factors neurotoxin, drug, and their interaction was performed. A significant interaction was followed by Bonferroni post hoc test with $*p \leq 0.05$, $**p \leq 0.01$, $***p \leq 0.001$. CTR: control; MPTP: 1-methyl-4-(2'-methylphenyl)-1,2,3,6-tetrahydropyridine hydrochloride

expression, in the DG after MPTP treatment [9, 60, 61]. We show that long-term indomethacin treatment in turn increased the survival of new mature neurons after MPTP treatment. Selective COX-2-inhibition is known to decrease the proliferation of hippocampal neuronal cells [46, 47], whereas the unselective COX-inhibition by indomethacin has been shown to restore the amount of new mature neurons after ischemia and irradiation associated with reduced microglial activation in the DG [27, 62]. We

additionally demonstrate the neurogenic potential of indomethacin on hippocampal neurogenesis in a principal model for neurodegeneration. In animal models of dopamine depletion as well as inflammation alone, impaired neurogenesis correlates with a decline of hippocampus-associated cognitive performances [6-11, 63, 64]. There is also a cellular pro-inflammatory reaction in the DG following dopamine depletion [22, 23], observed as a higher number of amoeboid CD68+ cells in this study.

Table 1 Serum protein levels of cytokines

		Cytokine					
		IL-1 β	IL-6	TNF- α	IL-17a	IFN- γ	IL-10
Short-term treatment	CTR + vehicle	123.7 \pm 65.7	9.9 \pm 1.8	481.2 \pm 93.0	22.0 \pm 4.8	26.4 \pm 4.7	61.4 \pm 11.2
	MPTP + vehicle	180.8 \pm 36.5	11.7 \pm 2.2	500.8 \pm 104.2	39.0 \pm 17.7	27.3 \pm 5.3	68.6 \pm 13.3
	CTR + indomethacin	255.2 \pm 30.2	11.6 \pm 2.0	537.2 \pm 91.4	27.1 \pm 4.4	29.9 \pm 5.1	76.4 \pm 12.1
	MPTP + indomethacin	157.5 \pm 76.5	9.1 \pm 1.3	442.8 \pm 91.5	22.8 \pm 2.1	26.2 \pm 1.8	70.4 \pm 4.3
Long-term treatment	CTR + vehicle	94.0 \pm 36.0	8.6 \pm 1.1	406.3 \pm 53.7	15.5 \pm 2.2	23.9 \pm 3.0	54.7 \pm 7.1
	MPTP + vehicle	151.4 \pm 29.6	11.5 \pm 1.9	569.5 \pm 82.3	38.2 \pm 6.4**	30.0 \pm 3.9	88.6 \pm 9.7*
	CTR + indomethacin	92.0 \pm 35.1	10.7 \pm 1.7	466.8 \pm 89.9	24.6 \pm 4.9	27.0 \pm 4.3	60.1 \pm 10.2
	MPTP + indomethacin	126.9 \pm 26.7	9.4 \pm 1.3	354.8 \pm 73.6	19.3 \pm 3.6**	24.8 \pm 4.2	52.5 \pm 9.9**

Multiplex ELISA was performed to evaluate the levels of pro-inflammatory IL-1 β , IL-6, TNF- α , IL-17a, and IFN- γ and anti-inflammatory IL-10 in serum of short-term and long-term groups. Values are expressed as mean \pm SEM in pg/ml, $n = 7-11$ /group. A two-way ANOVA with factors neurotoxin, drug, and their interaction was performed

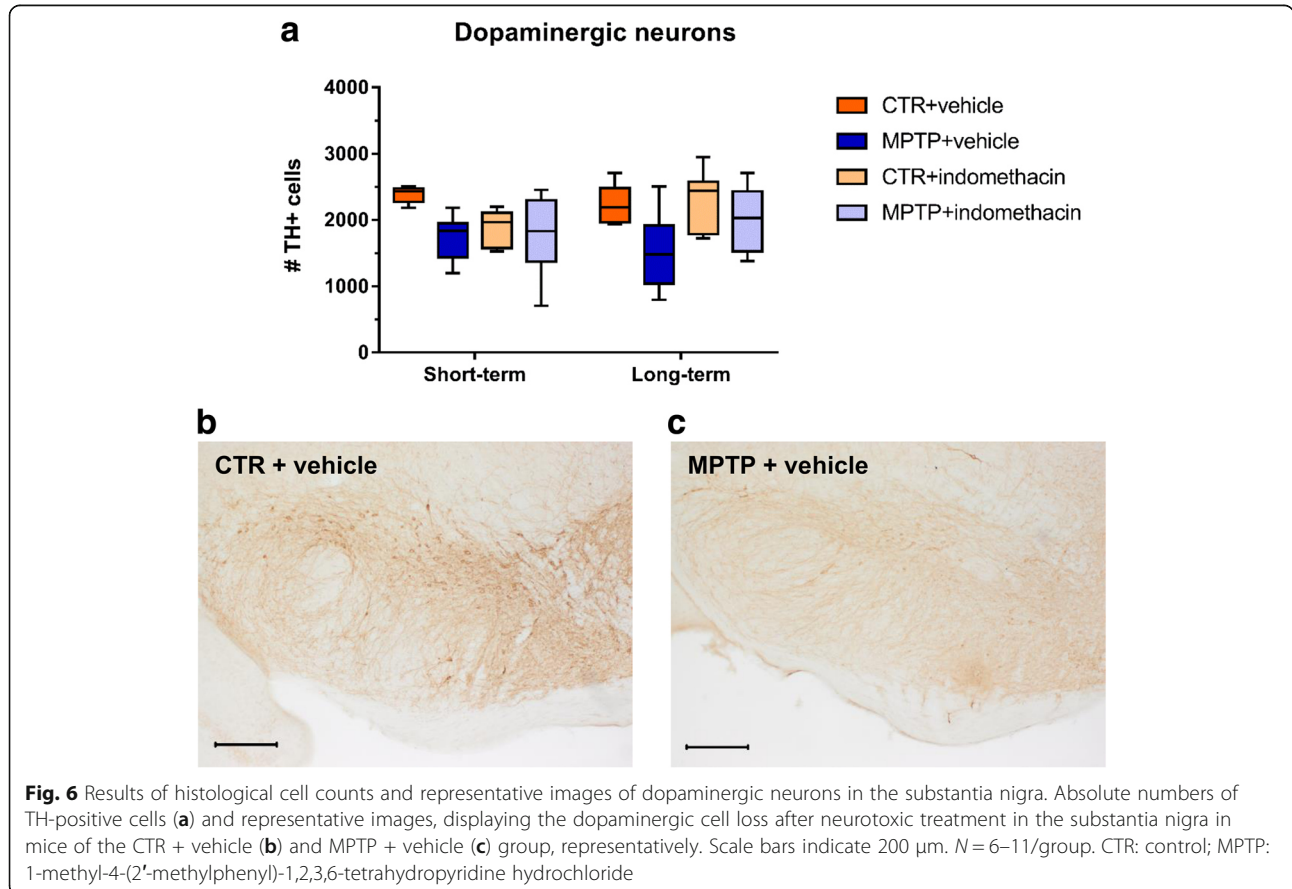
CTR control, MPTP 1-methyl-4-(2'-methylphenyl)-1,2,3,6-tetrahydropyridine hydrochloride

A significant interaction was followed by Bonferroni post hoc test: * $p \leq 0.05$, ** $p \leq 0.01$ compared to CTR + vehicle; ** $p \leq 0.01$ compared to MPTP + vehicle

Here, indomethacin shows an anti-inflammatory effect by reducing the number of amoeboid CD68+ cells. This is in line with previous studies, in which indomethacin treatment after irradiation or ischemia resulted in normalized numbers of activated microglia [27, 41, 44, 65, 66]. Thus, indomethacin treatment reduces the cellular inflammatory response in a model of PD thereby leading to a pro-neurogenic effect. Whether the anti-inflammatory

and neurogenesis-modulating effects of indomethacin may also improve cognitive performances, needs to be tested in future studies.

As the generation of mature neurons in the DG is a multistep process, we investigated if a specific stage of neuronal development in hippocampal neurogenesis is influenced by indomethacin. The total number of newly generated cells in the DG was not changed by MPTP or



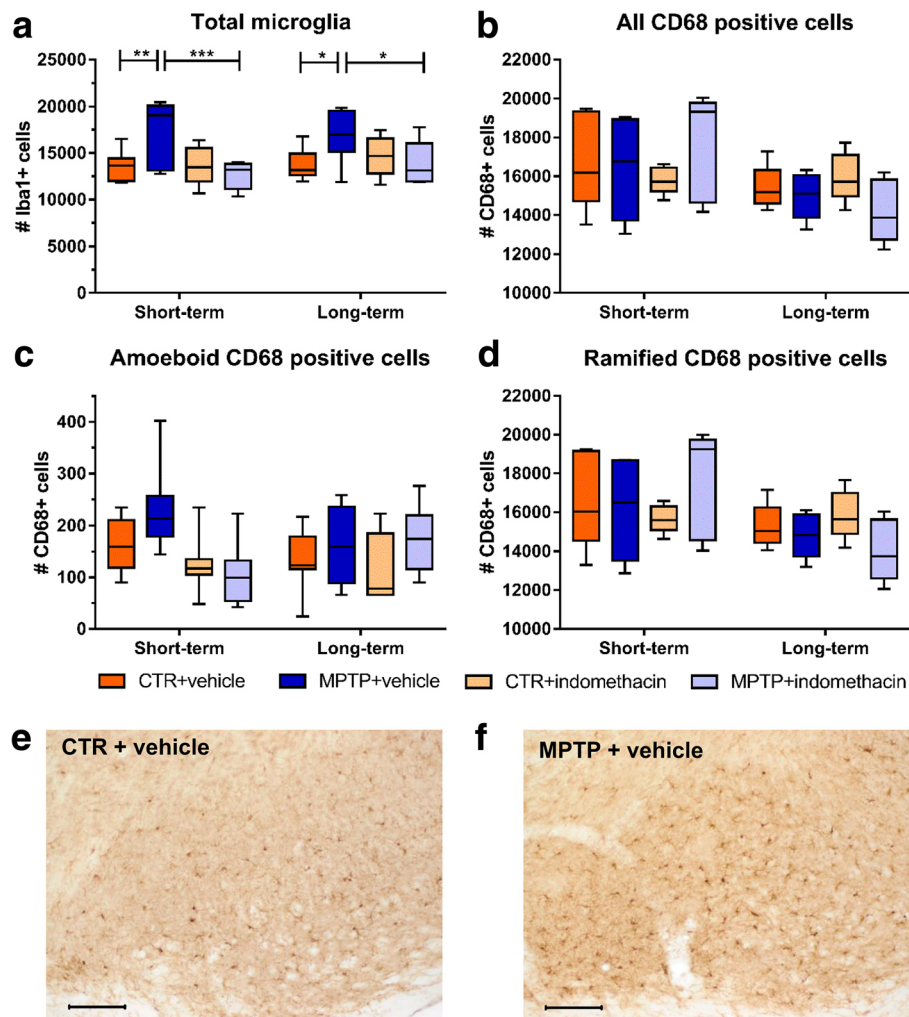


Fig. 7 Results of histological cell counts and representative images of cellular inflammation in the substantia nigra. Absolute numbers of Iba-1-positive cells (**a**), CD68-positive cells (**b**), amoeboid CD68-positive cells (**c**), and ramified CD68-positive cells (**d**) and representative images of Iba-1-positive cells in CTR mice (**e**) and MPTP-treated mice (**f**), displaying the higher amount of Iba-1-positive cells after dopamine depletion in the substantia nigra. Scale bars indicate 100 μ m. $N = 5-8$ /group. A two-way ANOVA with main factors neurotoxin, drug, and their interaction was performed. A significant interaction was followed by Bonferroni post hoc test with $*p \leq 0.05$, $**p \leq 0.01$, $***p \leq 0.001$. CTR: control; MPTP: 1-methyl-4-(2'-methylphenyl)-1,2,3,6-tetrahydropyridine hydrochloride

indomethacin treatment in our study. This is in line with previous studies, in which neither neurotoxin nor indomethacin treatment alone alters the general amount of proliferating cells [6, 7, 9, 23, 60, 67, 68]. We observed a decreased absolute number of newly generated type 2a cells by neurotoxin treatment regardless of drug treatment but found no change in the absolute numbers of proliferating type 1 progenitor cells by MPTP or indomethacin. We assume from our previous studies that, probably due to the here selected time points of analyses, the decreased number of newly generated type 2a cells results from a preceding reduction of type 1 cells after dopamine depletion [6]. As type 2a cells are glial progenitor cells, lineage determining to the later development of new neurons in the DG [29], their reduction may

contribute to an impaired neurogenesis following neurotoxin treatment despite drug treatment at later time points. Indomethacin itself seems to not influence the number of newly generated progenitor cells at these early stages of the neurogenic process. Thus, indomethacin has a pro-neurogenic effect, represented by normal neuronal differentiation and an increased amount of newly generated mature neurons after MPTP treatment.

To elucidate the underlying molecular mechanisms of an altered neurogenic process by MPTP and its restoration by indomethacin treatment, we investigated potentially involved downstream signaling pathways. We have previously shown in the experimental autoimmune encephalomyelitis murine model of the autoimmune disease multiple sclerosis as an inflammatory animal model with

subsequent neurodegeneration that the reduced differentiation into mature neurons in the DG is correlated with a reduced expression of pro-neurogenic genes [69]. Based on these findings, we investigated the expression of the target genes of the Notch, Wnt, and sonic hedgehog signaling pathways as well as of neurogenic factors in the hippocampus. The results indicate that the Wnt and Notch signaling pathways, and the neurogenic bHLH transcription factor *neuroD6* are indeed involved. The expression of *lefl*, a Wnt/ β -catenin effector gene, was decreased after MPTP treatment. This is in line with in vitro findings of decreased β -catenin in neuronal progenitor cells of the subventricular zone co-cultured with MPTP and microglia [70]. As a suppression of the Wnt signaling pathway results in a decreased number of newly generated type 3 cells and immature neurons [71], we suggest that downregulated Wnt signaling contributes to a reduced survival of newly generated mature neurons following MPTP treatment in the long term. Indomethacin had no significant influence on the expression of *lefl* after MPTP treatment. However, *lefl* was decreased in healthy mice by short-term indomethacin treatment. This was probably caused by a non-steroidal anti-inflammatory drugs' (NSAID) agonizing effect of the peroxisome proliferator-activated receptor-gamma [72–74]. Previous studies observed a downregulated Wnt signaling by indomethacin in cancer cells resulting in induced apoptosis and suppressed proliferation to prevent uncontrolled tumor growth [75, 76]. Here, the downregulated *lefl* expression in indomethacin-treated healthy mice did not affect adult neurogenesis. The expression of the neurogenic gene *neuroD6*, a member of the bHLH gene family and relevant in terminal neuronal differentiation [77], promotes neuronal survival as well as the cells' tolerance to oxidative stress by increasing mitochondrial biomass [78, 79]. Thus, indomethacin treatment regardless of neurotoxin treatment may promote the survival of newly generated neurons. In contrast to the ST group, *neuroD6* expression was downregulated by long-term indomethacin treatment regardless of neurotoxin treatment. This did not affect neuronal development within the time span observed here. *Hes5* is a primary Notch signaling pathway effector leading to impaired neurogenesis [80–82]. It is mainly expressed in putative progenitor cells type 1, 2a, and 2b, and increased Notch signaling as well as expression of the effector gene *hes5* inhibits the differentiation of these progenitor cells into mature neurons [83–86]. In the present study, the expression of *hes5* was transiently increased in neurotoxic-treated mice regardless of indomethacin treatment in the ST group. There could be consequential inhibition of further progenitor cell differentiation eventually leading to a reduced amount of mature neurons in the MPTP-treated mice in the LT group. Short-term drug administration

itself reduced *hes5* expression, which may have contributed to a differentiation into mature neurons in the indomethacin-treated mice of the LT group.

Subsequently, we assessed the serum concentration of the pro-inflammatory cytokines IL-1 β , IL-6, IL-17a, and TNF- α , which mainly disturb neurogenesis, as well as IFN- γ and the anti-inflammatory cytokine IL-10, which are both rather beneficial to the neurogenic process [32, 87–93]. These cytokines have been reported to be elevated in the cerebrospinal fluid as well as serum of PD patients [33, 34, 94–96]. As microglial response and T cell infiltration occur within a few days after MPTP injection [53, 96], we expected elevated cytokine levels in serum in the ST group. Instead, the serum levels of IL-17a and IL-10 were elevated in the LT group. As the majority of the pro-inflammatory and anti-neurogenic cytokines were unchanged but the anti-inflammatory and pro-neurogenic cytokine IL-10 was elevated in turn, we suggest an incipient recovery after MPTP treatment. Together with the observation by other research groups of increased cytokine concentration in the cerebrospinal fluid but not in serum after MPTP treatment [94, 97], it should be considered that there are higher cytokine concentrations altering the surrounding brain tissue after MPTP, reflected in highly expressed mRNA levels in the midbrain and striatum tissue [98–100], which is probably not detectable in C57Bl/6 mice peripherally. Here, the increased cytokine levels of IL-10 and IL-17a in the LT group may have resulted from an inflammatory response to MPTP in peripheral organs, such as the gut tissue, where macrophage infiltration and high levels of cytokines have been found for several days [101, 102].

As previously shown in the SN [103, 104], we also observed a reduction of dopaminergic neurons after neurotoxin treatment. Contrary to the DG, indomethacin treatment itself has no neuroprotective effect on dopaminergic neurons. This is in line with the investigation by Kurkowska-Jastrzebska and colleagues, where also no neuroprotective effect of indomethacin after MPTP treatment was observed [53]. In contrast, other studies have shown a prevention of dopaminergic cell loss by indomethacin or COX-2 inhibitors, when given before the MPTP treatment started [49, 51–53]. We also observed a transient pro-inflammatory reaction following MPTP, reflected by an increased total amount of microglia. Although indomethacin treatment with its anti-inflammatory effect normalized the cellular inflammatory response, it had no effect on dopaminergic cell numbers. This suggests that the neurodegeneration was caused by direct neurotoxicity of MPTP on dopaminergic cells [21]. In human studies, NSAIDs may reduce the risk of developing PD, whereas there is currently no evidence for a secondary prevention of PD [105]. Our results in the mouse model of dopamine depletion support this in part, as indomethacin given in higher total dosage or

adapted intervals may also prevent secondary inflammation-mediated dopaminergic cell loss. Nevertheless, hippocampal neurogenesis was restored correlating with reduced cellular inflammation, reflected by a decreased number of amoeboid CD68+ cells, despite dopaminergic cell loss. Thus, hippocampus-related deficits after dopamine depletion may result from inflammation-mediated reduced neurogenesis rather than from altered neurotransmitter homeostasis.

Conclusions

In summary, we demonstrated a pro-neurogenic and thereby restorative effect of indomethacin resulting in normal progenitor cell differentiation towards mature neurons despite a MPTP-induced neurotoxic and pro-inflammatory process. We suggest that the reduced level of pro-inflammation-associated cell types, the downregulated Notch signaling pathway, and the increased expression of *neuroD6* altogether contribute to the pro-neurogenic potential of indomethacin in the DG of MPTP-treated mice. Despite indomethacin treatment and its anti-inflammatory effect in the SN, there was a neurotoxin-induced dopaminergic cell loss. Regardless of that, indomethacin promoted the survival of new mature neurons in the DG. In conclusion, indomethacin might represent a therapeutic option to restore adult neurogenesis in the DG to improve hippocampus-associated deficits in neurodegenerative diseases such as PD.

Additional files

Additional file 1: Figure S1. Effects of dopamine depletion and indomethacin treatment on the stages of adult hippocampal neurogenesis. Neuronal development originates from a Nestin-positive, triangular-shaped stem cell (type 1). Then, neurogenesis progresses over the stages of the putative progenitor cells (type 2a, type 2b, and type 3) and ends in the NeuN-positive mature granule cell. Neurotoxic treatment leads to a decreased number of newly generated (type 2a cells) and mature neurons, whereas indomethacin treatment afterwards promotes the development towards mature neurons. MPTP: 1-methyl-4-(2'-methylphenyl)-1,2,3,6-tetrahydropyridine hydrochloride; NeuN: neuronal nuclei. (TIF 624 kb)

Additional file 2: Table S1. Hippocampal gene expression analysis. Quantitative real-time PCR was performed for the effector genes *gli1*, *hes5*, and *lef1* of the sonic hedgehog, Notch, and Wnt signaling pathway, respectively, and for the neurogenic factors *neuroD6* and *ngn1*. Gene expression is displayed as fold change of mRNA levels in relation to CTR + vehicle, $n = 5/\text{group}$. A two-way ANOVA with main factors neurotoxin, drug, and their interaction was performed. A significant interaction was followed by Bonferroni post hoc test: * $p \leq 0.05$, ** $p \leq 0.01$ compared to CTR + vehicle. CTR: control; 1-methyl-4-(2'-methylphenyl)-1,2,3,6-tetrahydropyridine hydrochloride. (DOCX 13 kb)

Abbreviations

bHLH: Basic helix-loop-helix; BrdU: 5-Bromo-2'-deoxyuridine; COX: Cyclooxygenase; CTR: Control; DAB: 3,3'-Diaminobenzidine; DCX: Doublecortin; DG: Dentate gyrus; GFP: Green fluorescent protein; i.p.: Intraperitoneally; IFN: Interferon; IL: Interleukin; LT: Long-term treatment; MPTP: 1-Methyl-4-phenyl-1,2,3,6-tetrahydropyridine hydrochloride, 1-methyl-4-(2'-methylphenyl)-1,2,3,6-tetrahydropyridine hydrochloride; NeuN: Neuronal nuclei; NSAID: Non-steroidal anti-inflammatory drug; PBS: Phosphate-buffered saline; PD: Parkinson's disease; PFA: Paraformaldehyde; PG: Prostaglandin;

SN: Substantia nigra; ST: Short-term treatment; TH: Tyrosine hydroxylase; TNF: Tumor necrosis factor

Acknowledgements

We would like to thank Prof. Dr. rer. nat. Christian Klein for the supply of 1-methyl-4-(2'-methylphenyl)-1,2,3,6-tetrahydropyridine hydrochloride and Jennifer Altschueler for the technical assistance. Furthermore, we acknowledge support from the German Research Foundation (DFG) and the Open Access Publication Fund of Charité-Universitätsmedizin Berlin.

Funding

This study was funded by the German Research Foundation (STE 1450/8) and Else Kröner-Fresenius-Foundation (P21/10//A141/09) to Barbara Steiner. The funder had no role in the study design, data collection and analysis, decision to publish, or preparation of the study.

Availability of data and materials

The datasets used and analyzed during the current study are available from the corresponding author on reasonable request.

Authors' contributions

EH contributed to the project design, animal handling, experimental procedures, statistical analysis, interpretation of data, and manuscript preparation. MS participated in the animal management and histological procedures. JR conducted the mRNA analysis. CK assisted with the project design, animal management, experimental procedures, interpretation of data, and manuscript preparation. LA participated in the ELISA analysis. BS conceived the project design and performed the interpretation of data and drafting and critical revision of the manuscript. All authors read and approved the final manuscript.

Ethics approval

All animal experiments were approved by the local animal ethics committee (Landesamt für Gesundheit und Soziales, Berlin, Germany) with approval number G0259/12 carried out in accordance with the European Communities Council directive of 22 September 2010 (10/63/EU).

Competing interests

The authors declare that they have no competing interests.

Publisher's Note

Springer Nature remains neutral with regard to jurisdictional claims in published maps and institutional affiliations.

Author details

¹Charité – Universitätsmedizin Berlin, corporate member of Freie Universität Berlin, Humboldt – Universität zu Berlin and Berlin Institute of Health, Department of Neurology with Experimental Neurology, Charitéplatz 1, 10117 Berlin, Germany. ²Charité – Universitätsmedizin Berlin, corporate member of Freie Universität Berlin, Humboldt – Universität zu Berlin, and Berlin Institute of Health, Institute for Medical Immunology, Augustenburger Platz 1, 13353 Berlin, Germany. ³Charité – Universitätsmedizin Berlin, corporate member of Freie Universität Berlin, Humboldt – Universität zu Berlin, and Berlin Institute of Health, Berlin-Brandenburg Center for Regenerative Therapies (BCRT), Augustenburger Platz 1, 13353 Berlin, Germany.

Received: 15 April 2018 Accepted: 25 April 2018

Published online: 26 May 2018

References

- Pillon B, Dubois B, Bonnet AM, Esteguy M, Guimaraes J, Vigouret JM, et al. Cognitive slowing in Parkinson's disease fails to respond to levodopa treatment: the 15-objects test. *Neurology*. 1989;39:762–8.
- Höglinger GU, Airas-Carrión O, Ipach B, Oertel WH. Origin of the dopaminergic innervation of adult neurogenic areas. *J Comp Neurol*. 2014; 522:2336–48.
- Höglinger GU, Rizk P, Muriel MP, Duyckaerts C, Oertel WH, Caille I, Hirsch EC. Dopamine depletion impairs precursor cell proliferation in Parkinson's disease. *Nat Neurosci*. 2004;7:726–35.

4. Gassbari A, Sulli A, Packard MG. The dopaminergic mesencephalic projections to the hippocampal formation in the rat. *Prog Neuro-Psychopharmacol Biol Psychiatry*. 1997;21:1–22.
5. Gasbarri A, Verney C, Innocenzi R, Campana E, Pacitti C. Mesolimbic dopaminergic neurons innervating the hippocampal formation in the rat: a combined retrograde tracing and immunohistochemical study. *Brain Res*. 1994;668:71–9.
6. Klein C, Rasińska J, Empl L, Sparenberg M, Poshtiban A, Hain EG, et al. Physical exercise counteracts MPTP-induced changes in neural precursor cell proliferation in the hippocampus and restores spatial learning but not memory performance in the water maze. *Behav Brain Res*. 2016;307:227–38.
7. Sung YH. Effects of treadmill exercise on hippocampal neurogenesis in an MPTP/probenecid-induced Parkinson's disease mouse model. *J Phys Ther Sci*. 2015;27:3203–6.
8. Das NR, Gangwal RP, Damre MV, Sangamwar AT, Sharma SS. A PPAR- β/δ agonist is neuroprotective and decreases cognitive impairment in a rodent model of Parkinson's disease. *Curr Neurovasc Res*. 2014;11:114–24.
9. Lesemann A, Reinel C, Hühnchen P, Pilhatsch M, Hellweg R, Klaisle P, et al. MPTP-induced hippocampal effects on serotonin, dopamine, neurotrophins, adult neurogenesis and depression-like behavior are partially influenced by fluoxetine in adult mice. *Brain Res*. 2012;1457:51–69.
10. Deguil J, Chavant F, Lafay-Chebassier C, Péralut-Pochat MC, Fauconneau B, Pain S. Neuroprotective effect of PACAP on translational control alteration and cognitive decline in MPTP parkinsonian mice. *Neurotox Res*. 2010;17:142–55.
11. Pothakos K, Kurz MJ, Lau YS. Restorative effect of endurance exercise on behavioral deficits in the chronic mouse model of Parkinson's disease with severe neurodegeneration. *BMC Neurosci*. 2009;10:6.
12. Miller IN, Cronin-Golomb A. Gender differences in Parkinson's disease: clinical characteristics and cognition. *Mov Disord*. 2010;25:2695–703.
13. Heller J, Dogan I, Schulz JB, Reetz K. Evidence for gender differences in cognition, emotion and quality of life in Parkinson's disease? *Aging Dis*. 2013;5:63–75.
14. Kalia LV, Lang AE. Parkinson's disease. *Lancet*. 2015;386:896–912.
15. Jackson-Lewis V, Jakowec M, Burke RE, Przedborski S. Time course and morphology of dopaminergic neuronal death caused by the neurotoxin 1-methyl-4-phenyl-1,2,3,6-tetrahydropyridine. *Neurodegeneration*. 1995;4:257–69.
16. Levesque S, Wilson B, Gregoria V, Thorpe LB, Dallas S, Polikov VS, et al. Reactive microgliosis: extracellular micro-calpain and microglia-mediated dopaminergic neurotoxicity. *Brain*. 2010;133:808–21.
17. Lull ME, Block ML. Reactive microgliosis: extracellular micro-calpain and microglia-mediated dopaminergic neurotoxicity. *Neurotherapeutics*. 2010;7:354–65.
18. Brochard V, Combadière B, Prigent A, Laouar Y, Perrin A, Beray-Berthet V, et al. Infiltration of CD4+ lymphocytes into the brain contributes to neurodegeneration in a mouse model of Parkinson disease. *J Clin Invest*. 2009;119:182–92.
19. Hirsch EC, Vyas S, Hunot S. Neuroinflammation in Parkinson's disease. *Parkinsonism Relat Disord*. 2012;18(Suppl 1):S210–2.
20. McGeer PL, EG MG. Glial reactions in Parkinson's disease. *Mov Disord*. 2008;23:474–83.
21. Przedborski S, Vila M. The 1-methyl-4-phenyl-1,2,3,6-tetrahydropyridine mouse model: a tool to explore the pathogenesis of Parkinson's disease. *Ann N Y Acad Sci*. 2003;991:189–98.
22. Costa G, Simola N, Morelli M. MDMA administration during adolescence exacerbates MPTP-induced cognitive impairment and neuroinflammation in the hippocampus and prefrontal cortex. *Psychopharmacology*. 2014;231:4007–18.
23. Klein C, Hain EG, Braun J, Riek K, Mueller S, Steiner B, Sack I. Enhanced adult neurogenesis increases brain stiffness: in vivo magnetic resonance elastography in a mouse model of dopamine depletion. *PLoS One*. 2014;9:e92582.
24. Wang B, Jin K. Current perspectives on the link between neuroinflammation and neurogenesis. *Metab Brain Dis*. 2015;30:355–65.
25. Ekdahl CT. Microglial activation—tuning and pruning adult neurogenesis. *Front Pharmacol*. 2012;3:41.
26. Ming GL, Song H. Adult neurogenesis in the mammalian brain: significant answers and significant questions. *Neuron*. 2011;70:687–702.
27. Monje ML, Toda H, Palmer TD. Inflammatory blockade restores adult hippocampal neurogenesis. *Science*. 2003;302:1760–5.
28. Ehninger D, Kempermann G. Neurogenesis in the adult hippocampus. *Cell Tissue Res*. 2008;331:243–50.
29. Kempermann G, Jessberger S, Steiner B, Kronenberg G. Milestones of neuronal development in the adult hippocampus. *Trends Neurosci*. 2004;27:447–52.
30. van Praag H, Schinder AF, Christie BR, Toni N, Palmer TD, Gage FH. Functional neurogenesis in the adult hippocampus. *Nature*. 2002;415:1030–4.
31. Ekdahl CT, Kokaia Z, Lindvall O. Brain inflammation and adult neurogenesis: the dual role of microglia. *Neuroscience*. 2009;158:1021–9.
32. Belarbi K, Rosi S. Modulation of adult-born neurons in the inflamed hippocampus. *Front Cell Neurosci*. 2013;7:145.
33. Mogi M, Harada M, Narabayashi H, Inagaki H, Minami M, Nagatsu T. Interleukin (IL)-1 beta, IL-2, IL-4, IL-6 and transforming growth factor-alpha levels are elevated in ventricular cerebrospinal fluid in juvenile parkinsonism and Parkinson's disease. *Neurosci Lett*. 1996;211:13–6.
34. Blum-Degen D, Müller T, Kuhn W, Gerlach M, Przuntek H, Riederer P. Interleukin-1 beta and interleukin-6 are elevated in the cerebrospinal fluid of Alzheimer's and de novo Parkinson's disease patients. *Neurosci Lett*. 1995;202:17–20.
35. Doorn KJ, Drukarch B, van Dam AM, Lucassen PJ. Hippocampal proliferation is increased in presymptomatic Parkinson's disease and due to microglia. *Neural Plast*. 2014;2014:959154.
36. Imamura K, Hishikawa N, Sawada M, Nagatsu T, Yoshida M, Hashizume Y. Distribution of major histocompatibility complex class II-positive microglia and cytokine profile of Parkinson's disease brains. *Acta Neuropathol*. 2003;106:518–26.
37. Lucas S. The pharmacology of indomethacin. *Headache*. 2016;56:436–46.
38. Ajmone-Cat MA, Bernardo A, Greco A, Minghetti L. Non-steroidal anti-inflammatory drugs and brain inflammation: effects on microglial functions. *Pharmaceuticals (Basel)*. 2010;3:1949–65.
39. Bartels AL, Leenders KL. Cyclooxygenase and neuroinflammation in Parkinson's disease neurodegeneration. *Curr Neuropharmacol*. 2010;8:62–8.
40. Quan Y, Jiang J, Dingleline R. EP2 receptor signaling pathways regulate classical activation of microglia. *J Biol Chem*. 2013;288:9293–302.
41. Yang Y, Zhang M, Kang X, Jiang C, Zhang H, Wang P, Li J. Thrombin-induced microglial activation impairs hippocampal neurogenesis and spatial memory ability in mice. *Behav Brain Funct*. 2015;11:30.
42. Sandu RE, Uzoni A, Coman C, Popa-Wagner A. Cerebral ischemia in the aged. Limited anti-inflammatory efficacy of the indomethacin treatment. *Romanian J Morphol Embryol*. 2015;56:1111–7.
43. Covey MV, Loporchio D, Buono KD, Levison SW. Opposite effect of inflammation on subventricular zone versus hippocampal precursors in brain injury. *Ann Neurol*. 2011;70:616–26.
44. Hoehn BD, Palmer TD, Steinberg GK. Neurogenesis in rats after focal cerebral ischemia is enhanced by indomethacin. *Stroke*. 2005;36:2718–24.
45. Sasaki T, Nakagomi T, Kirino T, Tamura A, Noguchi M, Saito I, Takakura K. Indomethacin ameliorates ischemic neuronal damage in the gerbil hippocampal CA1 sector. *Stroke*. 1988;19:1399–403.
46. Nam SM, Kim JW, Yoo DY, Choi JH, Kim W, Jung HY, et al. Comparison of pharmacological and genetic inhibition of cyclooxygenase-2: effects on adult neurogenesis in the hippocampal dentate gyrus. *J Vet Sci*. 2015;16:245–51.
47. Sasaki T, Kitagawa K, Sugiura S, Omura-Matsuoka E, Tanaka S, Yagita Y, et al. Implication of cyclooxygenase-2 on enhanced proliferation of neural progenitor cells in the adult mouse hippocampus after ischemia. *J Neurosci Res*. 2003;72:41–71.
48. Serrano GE, Lelutiu N, Rojas A, Cochi S, Shaw R, Makinson CD, et al. Ablation of cyclooxygenase-2 in forebrain neurons is neuroprotective and dampens brain inflammation after status epilepticus. *J Neurosci*. 2011;31:14850–60.
49. Teismann P, Tieu K, Choi DK, Wu DC, Naini A, Hunot S, et al. Cyclooxygenase-2 is instrumental in Parkinson's disease neurodegeneration. *Proc Natl Acad Sci U S A*. 2003;100:5473–8.
50. Feng ZH, Wang TG, Li DD, Fung P, Wilson BC, Liu B, et al. Cyclooxygenase-2-deficient mice are resistant to 1-methyl-4-phenyl-1, 2, 3, 6-tetrahydropyridine-induced damage of dopaminergic neurons in the substantia nigra. *Neurosci Lett*. 2002;329:354–8.
51. L'Episcopo F, Tirolo C, Caniglia S, Testa N, Serra PA, Impagnatiello F, et al. Combining nitric oxide release with anti-inflammatory activity preserves nigrostriatal dopaminergic innervation and prevents motor impairment in a 1-methyl-4-phenyl-1,2,3,6-tetrahydropyridine model of Parkinson's disease. *J Neuroinflammation*. 2010;7:83.
52. Vijitruth R, Liu M, Choi DY, Nguyen XV, Hunter RL, Bing G. Cyclooxygenase-2 mediates microglial activation and secondary dopaminergic cell death in the mouse MPTP model of Parkinson's disease. *J Neuroinflammation*. 2006;3:6.

53. Kurkowska-Jastrzebska I, Babiuch M, Joniec I, Przybylkowski A, Czlonkowska A, Czlonkowska A. Indomethacin protects against neurodegeneration caused by MPTP intoxication in mice. *Int Immunopharmacol.* 2002;2:1213–8.
54. Marques AA, Bevilacqua MC, da Fonseca AM, Nardi AE, Thuret S, Dias GP. Gender differences in the neurobiology of anxiety: focus on adult hippocampal neurogenesis. *Neural Plast.* 2016;2016:5026713.
55. Roughton K, Kalm M, Blomgren K. Sex-dependent differences in behavior and hippocampal neurogenesis after irradiation to the young mouse brain. *Eur J Neurosci.* 2012;36:2763–72.
56. Lagace DC, Fischer SJ, Eisch AJ. Gender and endogenous levels of estradiol do not influence adult hippocampal neurogenesis in mice. *Hippocampus.* 2007;17(3):175–80.
57. Fu R, Shen Q, Xu P, Luo JJ, Tang Y. Phagocytosis of microglia in the central nervous system diseases. *Mol Neurobiol.* 2014;49:1422–34.
58. Doorn KJ, Goudriaan A, Blits-Huizinga C, Bol JG, Rozemuller AJ, Hoogland PV, et al. Increased amoeboid microglial density in the olfactory bulb of Parkinson's and Alzheimer's patients. *Brain Pathol.* 2014;24:152–65.
59. Doorn KJ, Moors T, Drukarch B, de Berg WDJ v, Lucassen PJ, van Dam AM. Microglial phenotypes and toll-like receptor 2 in the substantia nigra and hippocampus of incidental Lewy body disease cases and Parkinson's disease patients. *Acta Neuropathol Commun.* 2014;2:90.
60. Schlachetzki JC, Grimm T, Schlachetzki Z, Ben Abdallah NM, Ettle B, Vöhringer P, et al. Dopaminergic lesioning impairs adult hippocampal neurogenesis by distinct modification of α -synuclein. *J Neurosci Res.* 2016;94:62–73.
61. Chiu WH, Depboylu C, Hermann G, Maurer L, Windolph A, Oertel WH, et al. Long-term treatment with L-DOPA or pramipexole affects adult neurogenesis and corresponding non-motor behavior in a mouse model of Parkinson's disease. *Neuropharmacology.* 2015;95:367–76.
62. Kluska MM, Witte OW, Bolz J, Redecker C. Neurogenesis in the adult dentate gyrus after cortical infarcts: effects of infarct location, N-methyl-D-aspartate receptor blockade and anti-inflammatory treatment. *Neuroscience.* 2005;135:723–35.
63. He W, Wang C, Chen Y, He Y, Cai Z. Berberine attenuates cognitive impairment and ameliorates tau hyperphosphorylation by limiting the self-perpetuating pathogenic cycle between NF- κ B signaling, oxidative stress and neuroinflammation. *Pharmacol Rep.* 2017;69:1341–8.
64. Wadhwa M, Prabhakar A, Ray K, Roy K, Kumari P, Jha PK, et al. Inhibiting the microglia activation improves the spatial memory and adult neurogenesis in rat hippocampus during 48 h of sleep deprivation. *J Neuroinflammation.* 2017;14:222.
65. Lopes RS, Cardoso MM, Sampaio AO, Barbosa MS Jr, Souza CC, DA Silva MC, et al. Indomethacin treatment reduces microglia activation and increases numbers of neuroblasts in the subventricular zone and ischaemic striatum after focal ischaemia. *J Biosci.* 2016;41:381–94.
66. Bok S, Wang T, Lee C, Jeon S, Kim Y, Kim J, et al. In vivo imaging of activated microglia in a mouse model of focal cerebral ischemia by two-photon microscopy. *Biomed Opt Express.* 2015;6:3303–2.
67. Boehme M, Guenther M, Stahr A, Liebmann M, Jaenisch N, Witte OW, Frahm C. Impact of indomethacin on neuroinflammation and hippocampal neurogenesis in aged mice. *Neurosci Lett.* 2014;572:7–12.
68. Ho N, Brookshire BR, Clark JE, Lucki I. Indomethacin reverses decreased hippocampal cell proliferation in streptozotocin-induced diabetic mice. *Metab Brain Dis.* 2015;30(2):555–62.
69. Huehnchen P, Prozorovski T, Klaisle P, Lesemann A, Ingwersen J, Wolf SA, et al. Modulation of adult hippocampal neurogenesis during myelin-directed autoimmune neuroinflammation. *Glia.* 2011;59:132–42.
70. L'Episcopo F, Tirolo C, Testa N, Caniglia S, Morale MC, Deleidi M, et al. Plasticity of subventricular zone neuroprogenitors in MPTP (1-methyl-4-phenyl-1,2,3,6-tetrahydropyridine) mouse model of Parkinson's disease involves cross talk between inflammatory and Wnt/ β -catenin signaling pathways: functional consequences for neuroprotection and repair. *J Neurosci.* 2012;32:2062–85.
71. Lie DC, Colamarino SA, Song HJ, Désiré L, Mira H, Consiglio A, et al. Wnt signalling regulates adult hippocampal neurogenesis. *Nature.* 2005;437:1370–5.
72. Vallée A, Lecarpentier Y. Alzheimer disease: crosstalk between the canonical Wnt/ β -catenin pathway and PPARs alpha and gamma. *Front Neurosci.* 2016;10:459.
73. Puhl AC, Milton FA, Cvoro A, Sieglaff DH, Campos JC, Bernardes A, et al. Mechanisms of peroxisome proliferator activated receptor γ regulation by non-steroidal anti-inflammatory drugs. *Nucl Recept Signal.* 2015;13:e004.
74. Liu J, Wang H, Zuo Y, Farmer SR. Functional interaction between peroxisome proliferator-activated receptor gamma and beta-catenin. *Mol Cell Biol.* 2006;26:5827–37.
75. Zheng Q, Zhang Y, Ren Y, Wu Y, Yang S, Zhang Y, et al. Antiproliferative and apoptotic effects of indomethacin on human retinoblastoma cell line Y79 and the involvement of β -catenin, nuclear factor- κ B and Akt signaling pathways. *Ophthalmic Res.* 2014;51:109–15.
76. Dihlmann S, Siermann A, von Knebel Doeberitz M. The nonsteroidal anti-inflammatory drugs aspirin and indomethacin attenuate beta-catenin/TCF-4 signaling. *Oncogene.* 2001;20:645–53.
77. Schwab MH, Bartholomae A, Heimrich B, Feldmeyer D, Druffel-Augustin S, Goebbels S, et al. Neuronal basic helix-loop-helix proteins (NEX and BETA2/neuro D) regulate terminal granule cell differentiation in the hippocampus. *J Neurosci.* 2000;20:3714–24.
78. Uittenbogaard M, Baxter KK, Chiamarello A. The neurogenic basic helix-loop-helix transcription factor NeuroD6 confers tolerance to oxidative stress by triggering an antioxidant response and sustaining the mitochondrial biomass. *ASN Neuro.* 2010;2:e00034.
79. Uittenbogaard M, Chiamarello A. The basic helix-loop-helix transcription factor Nex-1/Math-2 promotes neuronal survival of PC12 cells by modulating the dynamic expression of anti-apoptotic and cell cycle regulators. *J Neurochem.* 2005;92:585–96.
80. Kageyama R, Ohtsuka T, Kobayashi T. The Hes gene family: repressors and oscillators that orchestrate embryogenesis. *Development.* 2007;134:1243–51.
81. Ohtsuka T, Sakamoto M, Guillemot F, Kageyama R. Roles of the basic helix-loop-helix genes Hes1 and Hes5 in expansion of neural stem cells of the developing brain. *J Biol Chem.* 2001;276:30467–74.
82. Ohtsuka T, Ishibashi M, Gradwohl G, Nakanishi S, Guillemot F, Kageyama R. Hes1 and Hes5 as notch effectors in mammalian neuronal differentiation. *EMBO J.* 1999;18(8):2196–207.
83. Mathieu P, Adami PV, Morelli L. Notch signaling in the pathologic adult brain. *Biomol Concepts.* 2013;4:465–76.
84. Matsuda S, Kuwako K, Okano HJ, Tsutsumi S, Aburatani H, Saga Y, et al. Sox21 promotes hippocampal adult neurogenesis via the transcriptional repression of the Hes5 gene. *J Neurosci.* 2012;32:12543–57.
85. Lugert S, Basak O, Knuckles P, Haussler U, Fabel K, Götz M, et al. Quiescent and active hippocampal neural stem cells with distinct morphologies respond selectively to physiological and pathological stimuli and aging. *Cell Stem Cell.* 2010;6:445–56.
86. Grandbarbe L, Bouissac J, Rand M, Hrabé de Angelis M, Artavanis-Tsakonas S, Mohier E. Delta-Notch signaling controls the generation of neurons/glia from neural stem cells in a stepwise process. *Development.* 2003;130:1391–402.
87. O'Leime CS, Cryan JF, Nolan YM. Nuclear deterrents: intrinsic regulators of IL-1 β -induced effects on hippocampal neurogenesis. *Brain Behav Immun.* 2017;66:394–412.
88. Chesnokova V, Pechnick RN, Wawrowsky K. Chronic peripheral inflammation, hippocampal neurogenesis, and behavior. *Brain Behav Immun.* 2016;58:1–8.
89. Borsini A, Zunszaín PA, Thuret S, Pariante CM. The role of inflammatory cytokines as key modulators of neurogenesis. *Trends Neurosci.* 2015;38:145–57.
90. Sierra A, Beccari S, Diaz-Aparicio I, Encinas JM, Comeau S, Tremblay ME. Surveillance, phagocytosis, and inflammation: how never-resting microglia influence adult hippocampal neurogenesis. *Neural Plast.* 2014;2014:610343.
91. Dooley D, Vidal P, Hendrix S. Immunopharmacological intervention for successful neural stem cell therapy: new perspectives in CNS neurogenesis and repair. *Pharmacol Ther.* 2014;141(1):21–31.
92. Liu Q, Xin W, He P, Turner D, Yin J, Gan Y, et al. Interleukin-17 inhibits adult hippocampal neurogenesis. *Sci Rep.* 2014;4:7554.
93. Kiyota T, Ingraham KL, Swan RH, Jacobsen MT, Andres SJ, Ikezu T. AAV serotype 2/1-mediated gene delivery of anti-inflammatory interleukin-10 enhances neurogenesis and cognitive function in APP+PS1 mice. *Gene Ther.* 2012;19:724–33.
94. Manocha GD, Floden AM, Puing KL, Nagamoto-Combs K, Scherzer CR, Combs CK. Defining the contribution of neuroinflammation to Parkinson's disease in humanized immune system mice. *Mol Neurodegener.* 2017;12:17.
95. Reale M, Iarlori C, Thomas A, Gambi D, Perfetti B, Di Nicola M, Onofri M. Peripheral cytokines profile in Parkinson's disease. *Brain Behav Immun.* 2009;23:55–63.
96. Hirsch EC, Hunot S. Neuroinflammation in Parkinson's disease: a target for neuroprotection? *Lancet Neurol.* 2009;8:382–97.

97. Yasuda Y, Shimoda T, Uno K, Tateishi N, Furuya S, Yagi K, et al. The effects of MPTP on the activation of microglia/astrocytes and cytokine/chemokine levels in different mice strains. *J Neuroimmunol.* 2008;204:43–51.
98. Guan J, Yang B, Fan Y, Zhang J. GPER agonist G1 attenuates neuroinflammation and dopaminergic neurodegeneration in Parkinson disease. *Neuroimmunomodulation.* 2017;24:60–6.
99. Ren Y, Ye M, Chen S, Ding J. CD200 inhibits inflammatory response by promoting KATP channel opening in microglia cells in Parkinson's disease. *Med Sci Monit.* 2016;22:1733–41.
100. Ciesielska A, Joniec I, Przybyłkowski A, Gromadzka G, Kurkowska-Jastrzebska I, Członkowska A, Członkowski A. Dynamics of expression of the mRNA for cytokines and inducible nitric synthase in a murine model of the Parkinson's disease. *Acta Neurobiol Exp (Wars).* 2003;63:117–26.
101. Côté M, Poirier AA, Aubé B, Jobin C, Lacroix S, Soulet D. Partial depletion of the proinflammatory monocyte population is neuroprotective in the myenteric plexus but not in the basal ganglia in a MPTP mouse model of Parkinson's disease. *Brain Behav Immun.* 2015;46:154–67.
102. Côté M, Drouin-Ouellet J, Cicchetti F, Soulet D. The critical role of the MyD88-dependent pathway in non-CNS MPTP-mediated toxicity. *Brain Behav Immun.* 2011;25:1143–52.
103. Hain EG, Klein C, Munder T, Braun J, Riek K, Mueller S, et al. Dopaminergic neurodegeneration in the mouse is associated with decrease of viscoelasticity of substantia nigra tissue. *PLoS One.* 2016;11:e0161179.
104. Klaisle P, Lesemann A, Huehnchen P, Hermann A, Storch A, Steiner B. Physical activity and environmental enrichment regulate the generation of neural precursors in the adult mouse substantia nigra in a dopamine-dependent manner. *BMC Neurosci.* 2012;13:132.
105. Rees K, Stowe R, Patel S, Ives N, Breen K, Clarke CE, Ben-Shlomo Y. Non-steroidal anti-inflammatory drugs as disease-modifying agents for Parkinson's disease: evidence from observational studies. *Cochrane Database Syst Rev.* 2011;11:CD008454.

Ready to submit your research? Choose BMC and benefit from:

- fast, convenient online submission
- thorough peer review by experienced researchers in your field
- rapid publication on acceptance
- support for research data, including large and complex data types
- gold Open Access which fosters wider collaboration and increased citations
- maximum visibility for your research: over 100M website views per year

At BMC, research is always in progress.

Learn more biomedcentral.com/submissions



Lebenslauf

Mein Lebenslauf wird aus datenschutzrechtlichen Gründen in der elektronischen Version meiner Arbeit nicht veröffentlicht.

Komplette Publikationsliste

1. Klein C, Hain EG, Braun J, Riek K, Mueller S, Steiner B, Sack I. Enhanced adult neurogenesis increases brain stiffness: in vivo magnetic resonance elastography in a mouse model of dopamine depletion. *PLoS One*. 2014 Mar 25;9(3):e92582.
Impact Factor (2017): 2,766
2. Klein C, Rasińska J, Empl L, Sparenberg M, Poshtiban A, Hain EG, Iggena D, Rivalan M, Winter Y, Steiner B. Physical exercise counteracts MPTP-induced changes in neural precursor cell proliferation in the hippocampus and restores spatial learning but not memory performance in the water maze. *Behav Brain Res*. 2016 Jul 1;307:227-38. doi: 10.1016/j.bbr.2016.02.040. Epub 2016 Mar 21.
Impact Factor (2017): 3,173
3. Hain EG, Klein C, Munder T, Braun J, Riek K, Mueller S, Sack I, Steiner B. Dopaminergic Neurodegeneration in the Mouse Is Associated with Decrease of Viscoelasticity of Substantia Nigra Tissue. *PLoS One*. 2016 Aug 15;11(8):e0161179.
Impact Factor (2017): 2,766
4. Hain EG, Sparenberg M, Rasińska J, Klein C, Akyüz L, Steiner B. Indomethacin promotes survival of new neurons in the adult murine hippocampus accompanied by anti-inflammatory effects following MPTP-induced dopamine depletion. *J Neuroinflammation*. 2018 May 26;15(1):162.
Impact Factor (2017): 5,193

Danksagung

Zuerst möchte ich mich herzlichst bei meiner Doktormutter Frau PD Dr. med. Barbara Steiner für die freundliche sowie intensive wissenschaftliche Betreuung und für die Überlassung des Themas bedanken.

Weiterhin danke ich den aktuellen und ehemaligen Mitgliedern der Arbeitsgruppe, insbesondere Charlotte Klein für ihre unermüdliche Geduld und Engagement mich in das wissenschaftliche Arbeiten einzuführen, Justyna Rasińska, Tonia Munder, Anna Pfeiffer, Stefanie Schreyer, Deetje Iggena und Maria Sparenberg für die stets freundschaftliche als auch kollegiale Zusammenarbeit.

Ein großer Dank geht an meine Familie und Freunde, vor allem meinen Eltern Katrin und Peter, die mich auf dem Weg durch das Studium und der Promotion begleitet und unterstützt haben.

Zuletzt widme ich meinem Lebenspartner Philipp für die unendliche Kraft mir zugehört, mich in tieferen Zeiten aufgebaut und immer motiviert zu haben den größten Dank.